(12) FG.

THE UNIVERSITY OF TEXAS AT AUSTIN

ARL-TR-76-14
6 April 1976

Copy No. 49

INITIAL PHASE OF A STUDY OF BOTTOM INTERACTION OF LOW FREQUENCY UNDERWATER SOUND

Final Report under Contract N00039-75-C-0171
1 December 1974 - 30 November 1975

Kenneth E. Hawker, Aubrey L. Anderson,
Karl C Focke, Terry L Foreman

NAVAL ELECTRONIC SYSTEMS COMMAND
Contract N00039-75-C-0171

UNCLASSIFIED

SECURITY CLASSIFICATION OF THIS PAGE *(When Data Entered)*

REPORT DOCUMENTATION PAGE

READ INSTRUCTIONS BEFORE COMPLETING FORM

1. REPORT NUMBER: ARL-TR-76-14	2. GOVT ACCESSION NO.
3. RECIPIENT'S CATALOG NUMBER	
4. TITLE *(and Subtitle)*: INITIAL PHASE OF A STUDY OF BOTTOM INTERACTION OF LOW FREQUENCY UNDERWATER SOUND	5. TYPE OF REPORT & PERIOD COVERED: FINAL 1 Dec 74 — 30 Nov 75
	6. PERFORMING ORG. REPORT NUMBER
7. AUTHOR(s): Kenneth E. Hawker, Aubrey L. Anderson, Karl C. Focke, Terry L. Foreman	8. CONTRACT OR GRANT NUMBER(s): N00039-75-C-0171 NEW
9. PERFORMING ORGANIZATION NAME AND ADDRESS: Applied Research Laboratories, The University of Texas at Austin, Austin, Texas 78712	10. PROGRAM ELEMENT, PROJECT, TASK AREA & WORK UNIT NUMBERS
11. CONTROLLING OFFICE NAME AND ADDRESS: NAVAL ELECTRONIC SYSTEMS COMMAND, Department of the Navy, Washington, D.C. 20362	12. REPORT DATE: 6 April 1976
	13. NUMBER OF PAGES: 184
14. MONITORING AGENCY NAME & ADDRESS *(If different from Controlling Office)* 184p.	15. SECURITY CLASS. *(of this report)*: UNCLASSIFIED
	15a. DECLASSIFICATION/DOWNGRADING SCHEDULE

16. DISTRIBUTION STATEMENT *(of this Report)*

Approved for public release; distribution unlimited.

17. DISTRIBUTION STATEMENT *(of the abstract entered in Block 20, if different from Report)*

18. SUPPLEMENTARY NOTES

19. KEY WORDS *(Continue on reverse side if necessary and identify by block number)*

underwater sound propagation
bottom interaction
propagation models
bottom loss models
sensitivity

20. ABSTRACT *(Continue on reverse side if necessary and identify by block number)*

Bottom interaction is recognized as an important and only partially understood component of low frequency underwater sound propagation. Several phases of this complex problem have been investigated during the first year of a planned multiple year study. This report describes several aspects of the study including sensitivity of propagation loss to bottom loss variations, sensitivity of bottom loss to variations in ocean bottom physical parameters, bottom roughness effects, and propagation over a sloping bottom. (U)

DD FORM 1 JAN 73 1473 EDITION OF 1 NOV 65 IS OBSOLETE

UNCLASSIFIED

SECURITY CLASSIFICATION OF THIS PAGE *(When Data Entered)*

404 434

ARL-TR-76-14
6 April 1976

INITIAL PHASE OF A STUDY OF BOTTOM INTERACTION OF LOW FREQUENCY UNDERWATER SOUND

Final Report under Contract N00039-75-C-0171
1 December 1974 - 30 November 1975

Kenneth E. Hawker, Aubrey L. Anderson,
Karl C. Focke, Terry L. Foreman

NAVAL ELECTRONIC SYSTEMS COMMAND
Contract N00039-75-C-0171

APPLIED RESEARCH LABORATORIES
THE UNIVERSITY OF TEXAS AT AUSTIN
AUSTIN, TEXAS 78712

ABSTRACT

Bottom interaction is recognized as an important and only partially understood component of low frequency underwater sound propagation. Several phases of this complex problem have been investigated during the first year of a planned multiple year study. This report describes several aspects of the study including sensitivity of propagation loss to bottom loss variations, sensitivity of bottom loss to variations in ocean bottom physical parameters, bottom roughness effects, and propagation over a sloping bottom.

ACKNOWLEDGEMENTS

The problem of bottom interaction of low frequency underwater sound is complex. Several groups have made progress in understanding different facets of the problem in past work as well as in ongoing programs. The work described in this report has benefitted from discussions with several of these groups. The people involved include Halcyon Morris, Homer Bucker, Ed Hamilton, and Mel Pederson of the Naval Undersea Center, San Diego, California; Fred DiNapoli, Sal Santaniello, and Roy Deavenport of the Naval Underwater Systems Center, New London, Connecticut; Bert Hurdle of the Naval Research Laboratory, Washington, D. C.; Brackett Hersey, the Deputy Assistant Oceanographer for Ocean Science, ONR; John Hanna of the Acoustic Environmental Support Detachment of ONR; Alick Kibblewhite of The University of Auckland, Auckland, New Zealand; Dave Stickler of ARL, Pennsylvania State University, Pennsylvania; and Bob Winokur, Ron Dicus, Maurice Schulkin, Ken MacKenzie, Wil Geddes, and Bob Christensen of the Naval Oceanographic Office. Also, several people in addition to the authors have worked directly on some aspects of the work reported: Dr. Claude Horton, Sr., of The University of Texas at Austin, Dr. A. O. Williams of Brown University, and Jan Draeger of the Federal Republic of Germany.

TABLE OF CONTENTS

TABLE OF CONTENTS (Cont'd)

I. INTRODUCTION AND SUMMARY

This report describes some of the results of the first year of a planned multiple-year investigation of sea bottom interaction of propagating low frequency underwater sound. Because much of the work is still in progress, the report pictures an investigation and is not conclusions of a completed study. As different phases of the work are completed, beginning in the second year, technical reports are to be issued that present conclusions.

The background for the study is described in the introduction, followed by a summary of the report. The subsequent chapters (II, III, IV, and V) are written to each give a description of separate aspects of the ongoing program. Chapter II deals with studies of sensitivity of propagation loss to variations in the bottom loss, whereas chapter III describes studies of the sensitivity of bottom loss to variations of the geoacoustic description of the bottom material. The investigation of the effect of bottom roughness on propagation is described in chapter IV and the study of propagation over a sloping bottom is described in chapter V. The subject of each chapter is also the subject of a task of the overall bottom interaction program. Although these subjects are all related, in this report they are treated separately because they are now being separately studied.

A. Introduction

Underwater sound energy propagates between a source and receiver by one or more of several paths: direct (refracted-refracted, R'R'), surface reflected-refracted (R'SR), bottom reflected-refracted (R'BR), and surface reflected-bottom reflected (SRBR or simply RR) being the conventional designations of the more important multipaths (surface duct and leakage or diffraction multipaths being significant in some cases). The relative

amount of sound energy arriving via the various paths (the partitioning of energy among the multipaths) is a function of the propagation geometry (source depth, receiver depth, bottom depth, and topography), of the form of the sound speed profile and of other parameters such as frequency of the sound and loss associated with phenomena occurring along a given path (e.g., surface reflection loss).

The question of the relative importance of bottom interaction in the propagation process is complex. In some circumstances, underwater sound propagation is dominated by non-bottom-interacting energy regardless of the bottom reflection coefficient. In other circumstances, the details of the bottom interaction strongly determine the propagation loss. For long range propagation in some geometries multiple interactions with the bottom will result in extreme sensitivity of propagation loss to small changes in the reflection coefficient. This sensitivity can be such that single bounce reflection measurements cannot be made with sufficient accuracy to allow accurate estimation of propagation loss (i.e., if bottom interacting multipaths dominate the propagation, an error of 1 dB in the bottom loss would result in a 10 dB error in the propagation loss estimate for ranges such that ten bottom interactions occur).

Another complexity in the bottom interaction problem involves a question of the adequacy of characterizing the bottom interaction process with a plane wave reflection coefficient. Underwater sound energy impinging on the sea bottom is partially reflected back into the water and partially transmitted into the bottom material. At sufficiently high frequencies, the bottom interaction has been successfully represented by a reflection coefficient. As frequencies of interest decrease, more and more bottom penetrating energy is returned to the water column. This bottom penetrating energy reflects from subbottom layers and is refracted by the usually observed positive gradient of sound speed with depth in the bottom. At some low frequency, below a few kilohertz and above the frequencies used in seismic subbottom profiling, the relative amount of energy in the subbottom returns becomes so large that it cannot be ignored

in the bottom interaction process. The frequency regime requiring treatment of the bottom as a coupled propagation domain will, of course, be dependent on the propagation geometry and the geoacoustic description of the water and bottom in the area of interest. Additional complexity is introduced into the bottom interaction problem by a range changing geoacoustic description of the water or bottom as well as by topographic variations on scales varying from a sloping to a rough bottom.

If either reflection at the sea bottom interface or propagation through the subbottom is required to accurately model a given propagation situation, then an important question must be answered: how much detail and accuracy is required in the input geophysical description of the bottom?

In the present investigation, various features of the bottom interaction are studied individually to develop a quantitative understanding of their importance. For example, the question of when variations in bottom loss are significant to low frequency propagation is being investigated for a horizontally stratified ocean by runs of propagation models such as FACT. The bottom loss versus grazing angle input to the model is varied and the resulting variation of propagation loss is computed for various sound speed profiles, propagation geometries, bottom depths and frequencies. This results in a quantitative description of propagation sensitivity to variations of bottom loss. To relate bottom loss to variations in the bottom material, the changes in bottom loss associated with various geoacoustical descriptions of the bottom are calculated with bottom loss models. The result is a quantitative description of bottom loss sensitivity to varying sea bottom material. Considerable progress has been made in this study as described in the following chapters. A detailed presentation of the results of this part of the work is to be made in a separate technical report.

If the bottom interaction is characterized by a reflection coefficient (or bottom loss), then a pertinent concern is the degree of bottom loss

introduced by bottom interface roughness. Part of the present study examines the usefulness of existing scattering theory to answer this question.

Another task is the investigation of propagation in a region with a sloping bottom. Several questions are of interest. How well do predictions using existing techniques compare with ocean propagation data and with exact solutions in simplified sloping bottom regions? What are the sensitivities of this type of propagation to changes in source/receiver geometry, sound speed profile, frequency and bottom description (for various segments of the propagation path)? What approaches are promising for improving prediction capability?

All of these studies are designed to elucidate our present prediction capabilities for bottom interacting multipaths, to suggest lines of approach where prediction deficiencies exist, to determine the minimum amount of information required for adequate predictions, and to determine our existing bottom description data base and techniques for filling in the gaps.

B. Summary

Four aspects of a study of bottom interaction of low frequency sound are described separately in Chapters II through V. The four aspects, also to be considered separately in this summary, are: sensitivity of propagation loss to bottom loss variations, sensitivity of bottom loss to variations in the geoacoustic description of the bottom, rough interface effects, and propagation over a sloping bottom. Progress has been achieved in each task area in problem identification and development of tools and methods, and in obtaining initial results with these tools and methods.

1. Sensitivity of Propagation to Bottom Loss

The propagation parameter being studied is propagation loss. The propagation loss has been shown to be very sensitive to variations of

bottom loss for some propagation geometries and sound speed profiles, whereas it is relatively insensitive for other combinations of these parameters. This seemingly trivial result is important because the degree of sensitivity is being quantified for different combinations of parameters: this is a significant step beyond reliance on intuition to define sensitive and insensitive propagation geometries. One of the first goals of this phase of the work has been identified. It is to determine those combinations of propagation parameters (source depth, receiver depth, profile form, bottom depth) showing only small sensitivity to bottom effects (and quantifying what is meant by "small"). This excludes a domain of parameter combinations from the more complete examination of detailed aspects of the importance of bottom loss variations. For those combinations of parameters not thus excluded, detailed investigations are under way to determine which grazing angle segments (of the bottom loss versus grazing angle curve) are important and what the quantitative sensitivity is. In chapter II, some examples are given for approaches being examined, using range averages of propagation loss, to identify insensitive combinations of parameters. Such averaging techniques must, of course, be used with caution and details of the actual propagation loss versus range curves must be examined to verify any domains identified as "insensitive." Also described in chapter II are some of the detailed examinations being conducted in sensitive portions of the water column (e.g., near the bottom) to quantify the sensitivity (x change in bottom loss produces y change in propagation loss) and the grazing angle segments controlling the sensitivity. A technical report detailing the results of these studies is in preparation.

2. Sensitivity of Bottom Loss to the Geoacoustic Description of the Bottom

One primary goal of this work has been identified as a determination of the "hidden depth." This is the depth below which the geoacoustic description of the bottom material does not affect the calculation of bottom loss. That is, below this depth the bottom material can be clay, sand, rock, or clathrate and the resulting bottom loss will be the same. This depth defines the maximum depth to which one must describe the bottom

material to accurately calculate bottom loss (or interpret bottom loss measurements). The results will obviously be frequency dependent, and will probably also depend on such parameters as absorption and gradients of sound speed in the bottom material. Initial results from this study suggest that the hidden depth (for a ray incident at a given bottom grazing angle) lies within a few wavelengths of the turning depth of the ray in the bottom.

Another question is, for depths shallower than the hidden depth, how much precision is needed in the geoacoustical description of the bottom? That is, how accurate must geoacoustic descriptions or measurements be (and what is the required resolution) to produce bottom loss results within acceptable bounds?

To answer these questions, various bottom loss models are being used. These include a Rayleigh reflection coefficient model, an implementation of the Morris pseudolinear gradient model (with shear waves added to the lowest layer), and a numerical integration model developed at ARL. The last model was developed to overcome the difficulties of using the pseudolinear gradient model for very thick layers, as must be done to address the hidden depths question. Other models will be used in this study as they become available.

The ARL numerical integration bottom loss model makes it possible to investigate the influence of density gradients on the bottom loss. Density gradients used were within the observed bounds reported by Hamilton (ref. 14 of chapter III). The change of bottom loss resulting from introduction of the density gradient (versus constant density calculations) was found to exceed 1 or 2 dB only rarely, with more common values on the order of a few tenths of a decibel.

The effects of shear waves in the underlying basement rock were also studied. They were found normally to be important only for steep angles of incidence on the bottom. However, for some combinations of

parameters, especially for clay and silt overburdens, shear waves in the basement rock can cause large changes in bottom loss at low angles. This is potentially significant because it occurs in a grazing angle segment identified as important for low frequency propagation.

3. Rough Interface Effects

Various available techniques were examined for including roughness in bottom interaction calculations. The reflection coefficient method accounts for rough interface scattering in a propagation problem by multiplying the ordinary bottom reflection coefficient (for a flat bottom) by a scattering coefficient determined from the topographic properties of the rough bottom. The resulting product is then used in propagation calculations as a modified reflection coefficient for the bottom. Available conventional scattering theory for a penetrable rough interface has been examined, necessitating the writing of a computer program to examine the predicted degree of sensitivity of the modified reflection coefficient to rough bottom parameters such as the rms surface slope. The large sensitivity to this parameter, predicted by the theory, is interpreted to be a result of shadowing corrections and a single scattering assumption introduced in the development of the theory.

A potentially more useful approach, that of Lysanov (ref. 4 of chapter IV), replaces the exact boundary condition on the rough surface by an approximate boundary condition on the mean plane of the bottom. This perturbation approach is potentially valuable for the present study because it sets out from the beginning to specify a boundary condition for a propagation problem. It is anticipated that the continuing work on rough interface effects will be along the lines initiated by Lysanov, and more recently pursued by Kuperman (refs. 5 and 7, chapter IV).

4. Propagation over a Sloping Bottom

Two numerical models capable of propagation calculations in a range changing environment were implemented at ARL. They are the NRL ray

model TRIMAIN and the AESD parabolic equation model PE. Although the ability of these models to treat bottom interacting energy has some limitations, the models have been found useful for slope enhancement calculations. The slope enhancement shown by some recent data sets can be approximated by calculations with these models. The enhancement was found to be related in a complex manner to source and receiver depths, sound speed profile, angular slope of the bottom, and bottom loss on the slope. Quantifying these relationships is the goal of ongoing sensitivity studies.

To test the validity of some of these calculations, various theoretical approaches to calculation of propagation over a sloping bottom are being examined. These include a dual integral equation approach and mode-mode coupling.

II. SENSITIVITY OF PROPAGATION TO BOTTOM LOSS

A. Introduction

The impact of variations in the geoacoustical description of the bottom on propagation is being investigated at ARL by studies of propagation loss sensitivity to bottom loss variations and of bottom loss sensitivity to variations of the bottom geoacoustics. Later studies will directly investigate propagation loss sensitivity to variations of bottom geoacoustics without the intermediate calculation of bottom loss.

The challenge of the present study is to determine techniques for measuring and describing these sensitivities in a concise manner. The brute force approach would involve a very large number of computer model runs and subsequent publication of a catalog of results. This would not be very useful. Therefore, our approach is to make a few test computer runs, extend hypotheses of sensitivities based on these results and a knowledge of the propagation processes and then test these hypotheses with additional runs. In this way an understanding of bottom interaction is developed. Our present challenge, in addition to continued development of this understanding, is the development of techniques for conveying the understanding without requiring a person to go through the entire process as we have. Intermediate results of propagation loss sensitivity are described below.

The sensitivity of propagation loss to bottom loss has been studied using FACT model runs. In order to simplify the problem, certain parameters were held fixed for most of the model runs. These parameters were source depth (500 ft), frequency (100 Hz), and the sound speed profile, shown in Fig. II.1. This profile, which is a simplification of a North Pacific profile, was used in these initial studies to allow controlled variation of its characteristics. The profile is representative of many regions of the subtropical oceans and has a well developed deep sound channel.

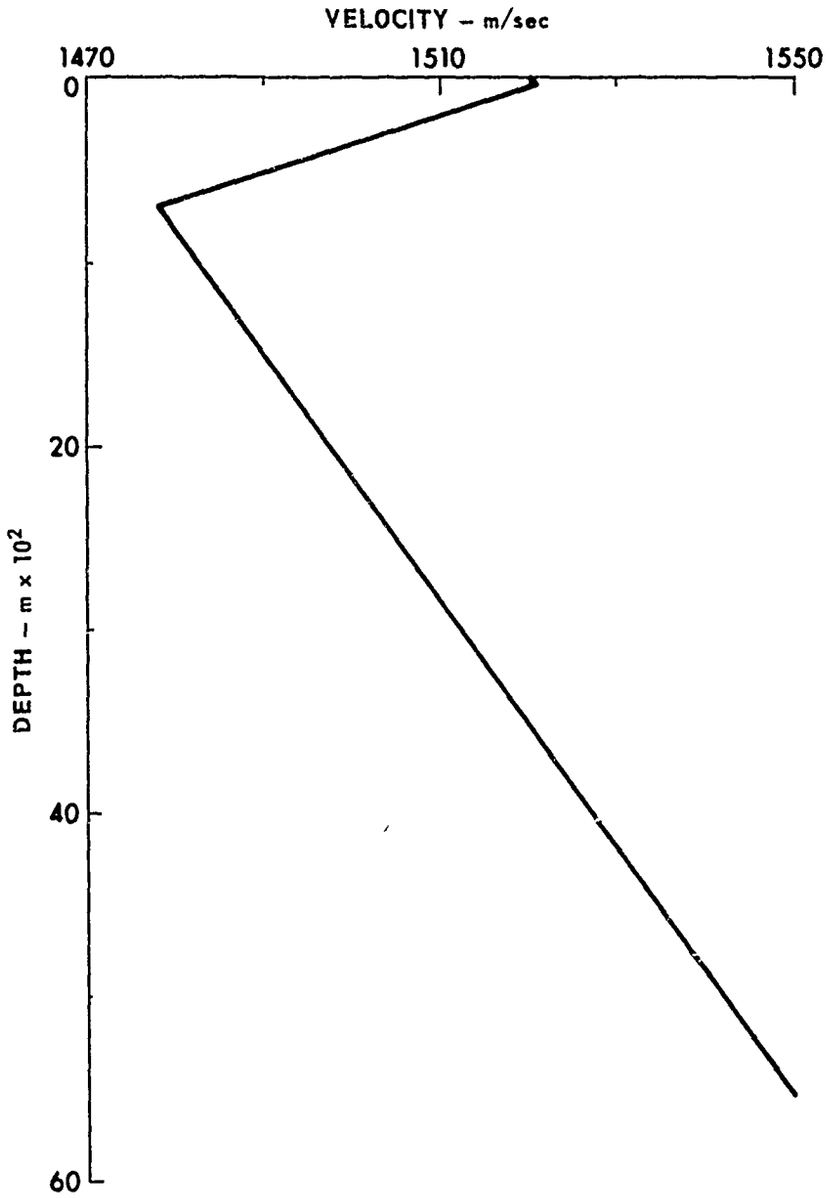

FIGURE II-1
4-POINT PROFILE USED IN FACT RUNS

ARL - UT
AS-76-132
KCF - DR
2 - 12 - 76

With source depth, frequency and profile fixed, parameters that varied were receiver depth, bottom depth, and bottom loss versus grazing angle. The receiver depths studied were the channel axis (700 m), the critical depth when it existed (3600 m) and 30 m off the bottom. Five bottom depths were used. They produced a depth deficiency of 100 m and depth excesses of 60 m, 670 m, 1280 m, and 1400 m. The bottom loss versus grazing angle curves which were used are shown in Fig. II.2 and are those designated as types 1, 3, and 5 in the FACT program. The bottom type 1 is a low loss bottom, exhibiting no loss below a critical angle of 19°. Bottom type 3 is of intermediate loss and bottom type 5 is high loss, having some loss at all grazing angles.

The propagation loss for each of the runs was calculated at 120 range points out to 480 nm range. Since direct comparisons between runs at individual range points have little real meaning, averages of the dB propagation loss over approximately 100 nm intervals were calculated for each run. Comparisons between these averages were performed to determine the magnitude of the bottom effects.

B. Bottom Depth Dependence

The averages of propagation loss for three receiver depths are presented in Tables II.1 through II.3 as a function of the bottom depth. Within each range interval column comparisons can be made to determine bottom depth dependence.

The bottom depth dependence for either the axis depth or critical depth receiver is dependent on bottom type: for bottom type 1, loss decreases with decreasing bottom depth; for bottom type 3 only small variation is shown with no consistent bottom dependence; and for bottom type 5, loss increases with decreasing bottom depth. Furthermore, for these two receiver depths and bottom type 5, the effect of a 600 m change in bottom depth was greater for a shallower initial bottom depth. A 600 m decrease in depth from 5900 m resulted in about 0.6 dB increase in

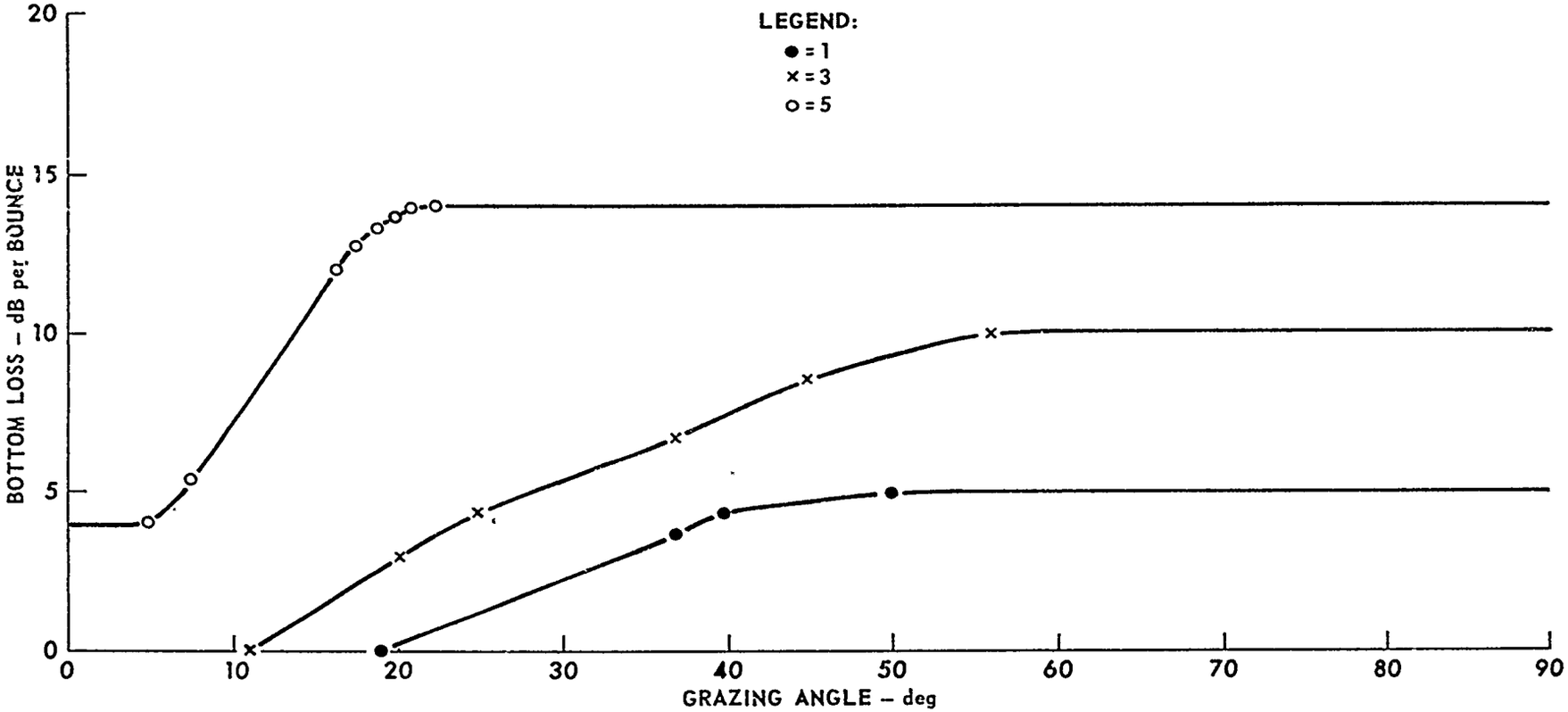

FIGURE II-2
BOTTOM LOSS CURVES FOR FACT BOTTOM
TYPE 1, 3, 5

ARL - UT
AS-76-129
KCF - DR
2 - 12 - 76

TABLE II-1

AVERAGE PROPAGATION LOSS FOR FIXED RECEIVER DEPTH OF 700 m
(SOURCE DEPTH 152 m)
frequency 100 Hz

Bottom Depth (m)	100 to 200 nm			200 to 300 nm			300 to 400 nm		← Range Interval
	1	3	5	1	3	5	1	3	5 ← Bottom Type
3500	93.82	96.17	102.68	95.99	98.27	102.52	97.48	99.82	104.01
3660	93.97	96.21	101.18	96.19	98.38	102.11	97.81	100.07	103.80
4270	94.55	96.39	99.81	96.64	98.37	100.96	98.38	100.23	102.85
4880	94.88	96.47	98.54	96.91	98.40	100.16	98.71	100.33	102.03
5000	94.92	96.45	98.43	96.89	98.34	100.08	98.64	100.16	101.87

TABLE II-2

AVERAGE PROPAGATION LOSS FOR FIXED RECEIVER DEPTH OF 3600 m (CRITICAL DEPTH)

(SOURCE DEPTH 152 m)

frequency 100 Hz

Bottom Depth (m)	100 to 200 nm			200 to 300 nm			300 to 400 nm ← Range Interval		
	1	3	5	1	3	5	1	3	5 ←Bottom Type
3660	92.23	94.72	116.96	94.81	97.47	141.06	96.44	99.12	180.90
4270	92.82	94.87	109.88	94.82	96.80	120.66	96.86	98.84	125.21
4880	94.03	96.02	103.19	96.04	97.82	100.30	97.23	98.89	101.13
5000	93.98	95.83	101.73	96.04	97.68	100.21	97.12	98.60	100.74

TABLE II-3

AVERAGE PROPAGATION LOSS FOR A RECEIVER 30 m OFF THE BOTTOM
(SOURCE DEPTH 152 m)

Bottom Depth (m)	100 to 200 nm			200 to 300 nm			300 to 400 nm ← Range Interval		
	1	3	5	1	3	5	1	3	5 ← Bottom Type
3500	91.70	94.04	113.99	93.98	96.29	123.48	95.71	98.05	136.70
3660	92.10	94.55	116.90	94.42	96.86	132.37	96.25	98.83	177.66
4270	93.30	95.66	118.85	95.58	97.95	143.98	97.21	99.59	159.61
4880	94.72	97.48	123.41	96.94	99.91	139.99	98.59	101.59	160.88
5000	94.70	97.30	122.75	97.07	99.83	146.19	98.63	101.47	163.73

propagation loss at the axis receiver. The same depth change from an initial bottom depth of 4300 m resulted in a 1.2 dB increase. The effects of the change in bottom depth from 5000 m to 3660 m for a type 5 bottom were range dependent. For the axis receiver the effect of this change in bottom depth was 2.7 dB in the 100 to 200 nm interval and only 1.9 dB in the 300 to 400 nm interval. For the critical depth receiver this effect for the same two range intervals was respectively, 15.2 dB and over 80 dB.

For all bottom types the propagation loss to a receiver 30 m off the bottom decreased as the bottom depth decreased. When the bottom depth decreased from 5000 m to 3500 m, the propagation loss for a type 1 bottom decreased by 3 dB, while for a type 3 bottom, it decreased by 3.5 dB. For this same change in bottom depth, the decrease in propagation loss for the type 5 bottom was between 9 and 30 dB; the decrease being range dependent with larger effects at greater ranges.

Two competing factors produce the observed results. (1) As the bottom depth is decreased, more energy interacts with the bottom and the bottom interaction angles are steeper (which factors tend to increase the average propagation loss). (2) The reduced bottom depth reduces the total volume over which the propagating energy is spread (which factor tends to reduce the average propagation loss).

The relative importance of these factors is modified for the different bottom types according to the value of the critical angle and the bottom loss below the critical angle. Bottom types 1 and 3 are perfect reflectors at grazing angles less than their critical angle. As the bottom depth decreases, additional bottom interactions above critical angle will result in additional losses but this is counteracted by rays intersecting the bottom below the critical angle and being redistributed over a smaller depth interval. For the sound speed profile of this study, redistribution of the low grazing angle energy dominated the additional loss of energy at higher angles. The effects of moving the bottom up the water column

were independent of range for these two bottom types. This indicates that beyond 100 nm range the bottom interactions above the critical angle become insignificant in FACT's calculations of propagation loss.

The critical angle is much smaller for bottom type 5 and there is a finite loss below the critical angle. When the bottom depth is decreased, the additional bottom interactions result in a significant additional loss. This loss is sufficient to cause an overall increase in propagation loss with decreasing bottom depth for the sound channel axis and critical depth receivers.

The results in Table II.3 indicate that the amount of energy reaching the receiver 30 m off the bottom increases as the bottom depth decreases, independent of the bottom loss characteristics. These results obtained with the ray theory model FACT are being compared with results from the wave theory model PE.

C. Receiver Depth Dependence

Table II.4 presents the average propagation loss for a series of receiver depths in 5000 m of water (also for the profile in Fig. II-1). Results are shown for receivers at axis depth, at critical depth, and at receivers spaced about 300 m apart between critical depth and the bottom.

Receiver depth dependence is small and follows a similar pattern for either type 1 or 3 bottoms. The average propagation loss decreases about 1 dB between the axis depth and critical depth. Below critical depth, the loss in general increases with receiver depth.

For the type 5 bottom, the loss in general increases with receiver depth at all depths. The increase in propagation loss with depth change

TABLE II-4

AVERAGE PROPAGATION LOSS FOR A FIXED BOTTOM DEPTH OF 5000 m
(SOURCE DEPTH 152 m)

Receiver Depth (m)	100 to 200 nm			200 to 300 nm			300 to 400 nm			← Range Interval
	1	3	5	1	3	5	1	3	5	← Bottom Type
700	94.92	96.45	98.43	96.89	98.34	100.08	98.64	100.16	101.87	
3600	93.98	95.83	101.73	96.04	97.68	100.21	97.12	98.60	100.74	
3810	94.13	96.16	103.55	95.45	97.08	99.81	97.43	99.10	101.60	
4115	94.50	96.77	108.59	96.87	99.06	109.44	98.39	100.50	105.48	
4420	94.14	96.31	111.22	96.38	98.57	115.56	97.90	100.02	110.77	
4970	94.70	97.30	127.75	97.07	99.83	146.19	98.63	101.47	163.73	

was greatest between 4420 and 4970 m depth. Near the bottom, small changes in the receiver depth led to large changes in the average propagation loss.

D. Bottom Loss Dependence

Comparisons were made between average propagation loss for the various bottom types in the discussions of Tables II.1 through II.3. Differences were described as being the result of change in the critical angle and as the effect of the variation of bottom loss below critical angle.

Comparison shows that differences in average loss associated with changes between the types 1 and 3 bottom are independent of the range; this is due to the perfect reflection below the critical angle. The differences between the calculations for these two bottom types increase with receiver depth. The differences are generally less than 2 dB.

Two additional test cases were run. For these the bottom loss below the critical angle was varied to examine the sensitivity to the low grazing angle losses. The receiver in both cases was 30 m off the bottom. For the first case, the profile of Fig. II.1 was used together with an initial bottom loss curve which was similar to a type 1 bottom. Below the critical angle, constant bottom loss values of 0, 1, 2, and 3 dB were used for the separate runs (see Fig. II.3).

The resulting four propagation loss curves are shown in Fig. II.4. With a perfect reflector below the critical angle, the propagation falls off with only an inverse range dependence (no convergence zones are apparent). When a 1 dB loss is introduced below critical angle, an additional decibel of loss is incurred for each bottom interaction. There are approximately 15 convergence zones out to 400 nm, which accounts for most of the 19 dB difference between the 0 dB and 1 dB

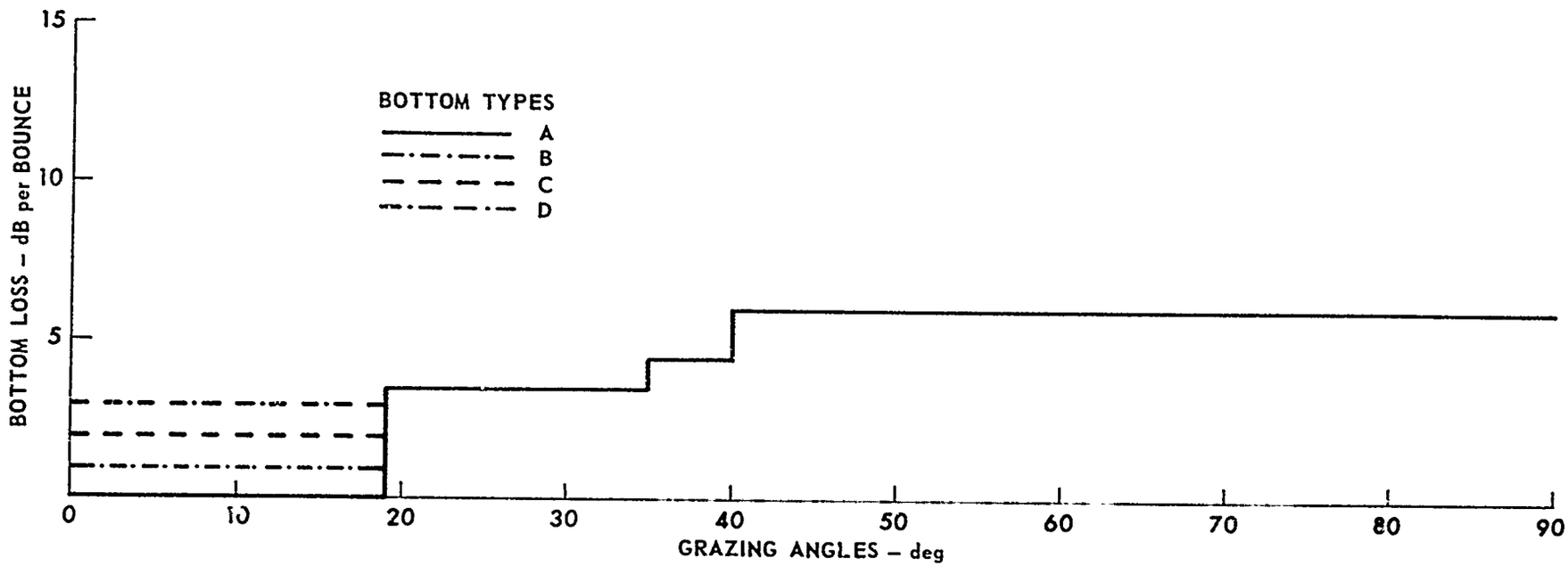

FIGURE II-3
4 BOTTOM LOSS CURVES
LOSSES VARYING BELOW THE CRITICAL ANGLE

ARL - UT
AS-76-134
KCF - DR
2 - 12 - 76

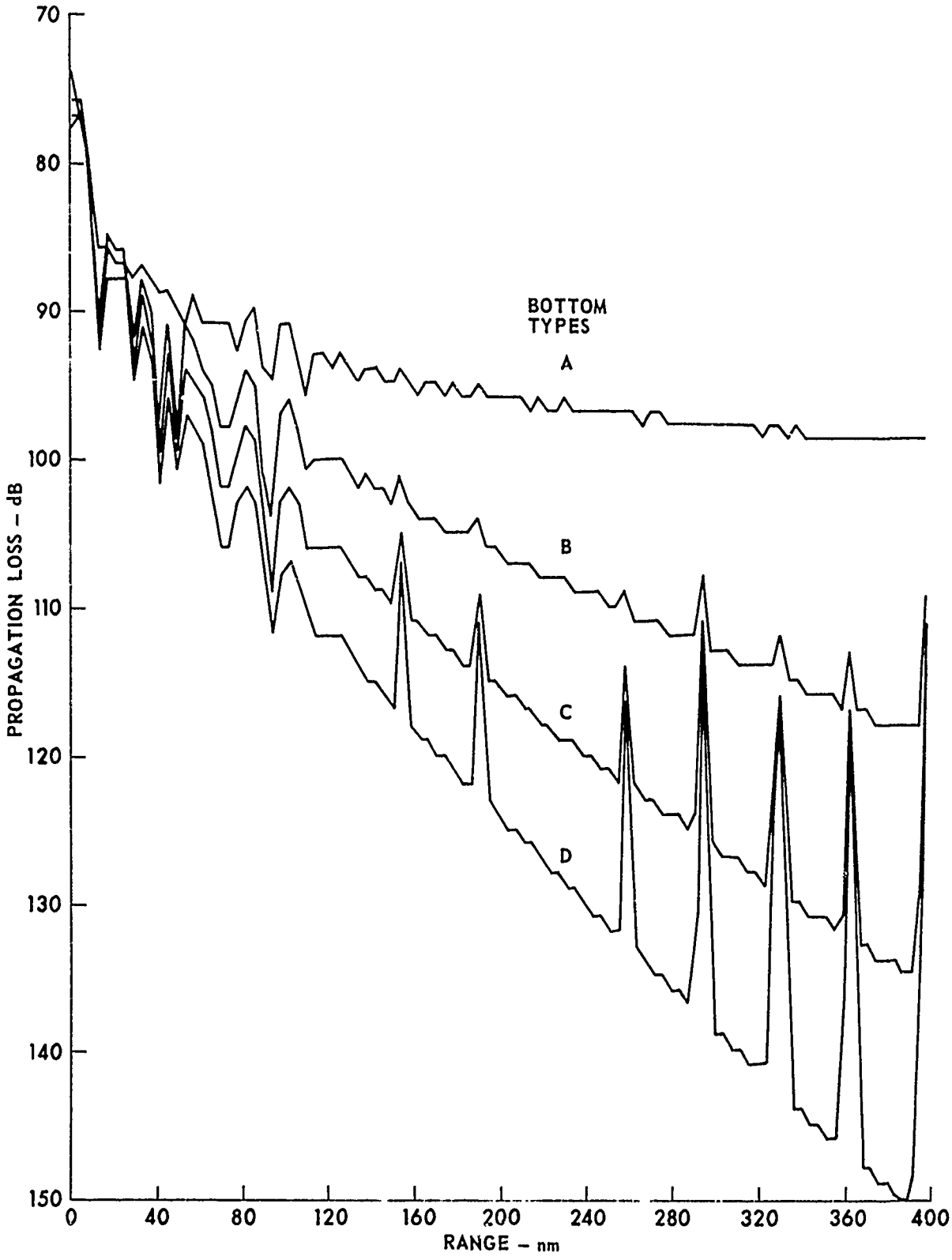

FIGURE II-4
PROPAGATION LOSS CURVES FOR VARYING BOTTOM LOSSES BELOW CRITICAL ANGLE

ARL - UT
AS-76-130
KCF - DR
2 - 12 - 76

loss runs at 400 nm. Similarly, the 16 dB difference between the 1 dB and 2 dB runs and the 15 dB difference between the 2 dB and 3 dB runs can be accounted for by the additional losses below the critical angle. As the energy reflected from the bottom decreases in runs with successively higher loss below critical angle, the bottom reflected energy does not dominate the received signal and convergence zones appear.

To examine the influence of a smaller segment of bottom grazing angles, a second set of runs was made. In the second case a measured profile was used. The bottom loss used in this case varied only in the 0 to 1° grazing angle segment (Fig. II.5). For one run, the loss was 1 dB, and for the other, 2 dB for grazing angles below 1°. The two propagation runs for case 2 appear in Fig. II.6. In this case the two curves also separate about 1 dB per convergence zone.

The bottom bounce energy at long range falls off at the same rate for the 1° critical angle and the 19° critical angle (compare Figs. II-4 and II-6). This is true because, for this near bottom receiver, at the long ranges, only very low grazing angles are important; this is further illustrated by the arrival angle structure shown in Fig. II.7. The higher angles will affect the falloff only at the shorter ranges.

These are but a few examples of the propagation loss sensitivity studies which are underway. They show that in some cases great sensitivity to bottom loss is exhibited by propagation loss model runs, while in other cases the propagation loss is relatively insensitive to the bottom. Systematizing and quantifying these observations is continuing. One of the present efforts is delineating those propagation geometries exhibiting minimal sensitivity to bottom interactions. Another effort is delineating the details of the relationship when bottom interaction is a significant component of the propagation.

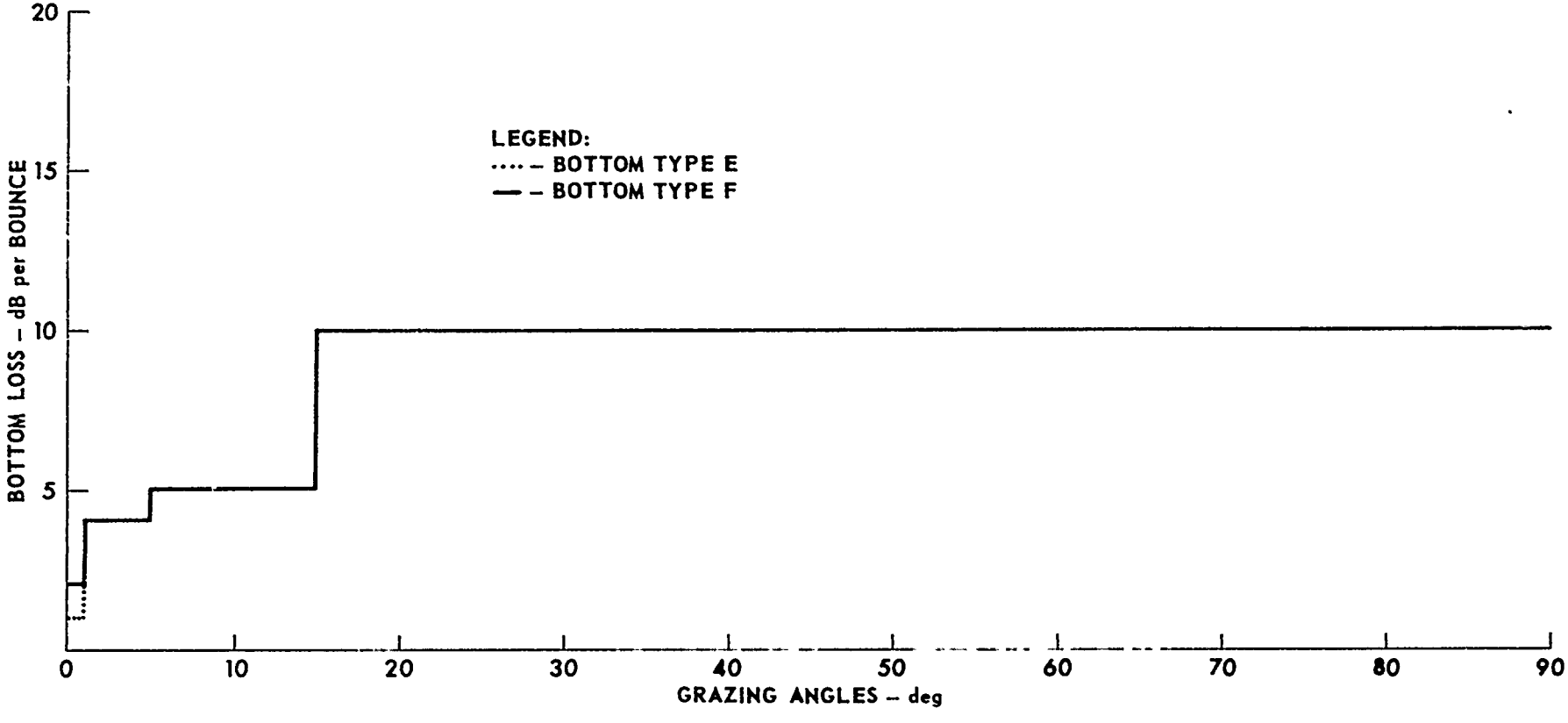

FIGURE II-5
BOTTOM LOSS CURVES
VARYING BELOW 1° GRAZING ANGLE

ARL - UT
AS-76-135
KCF - DR
2 - 12 - 76

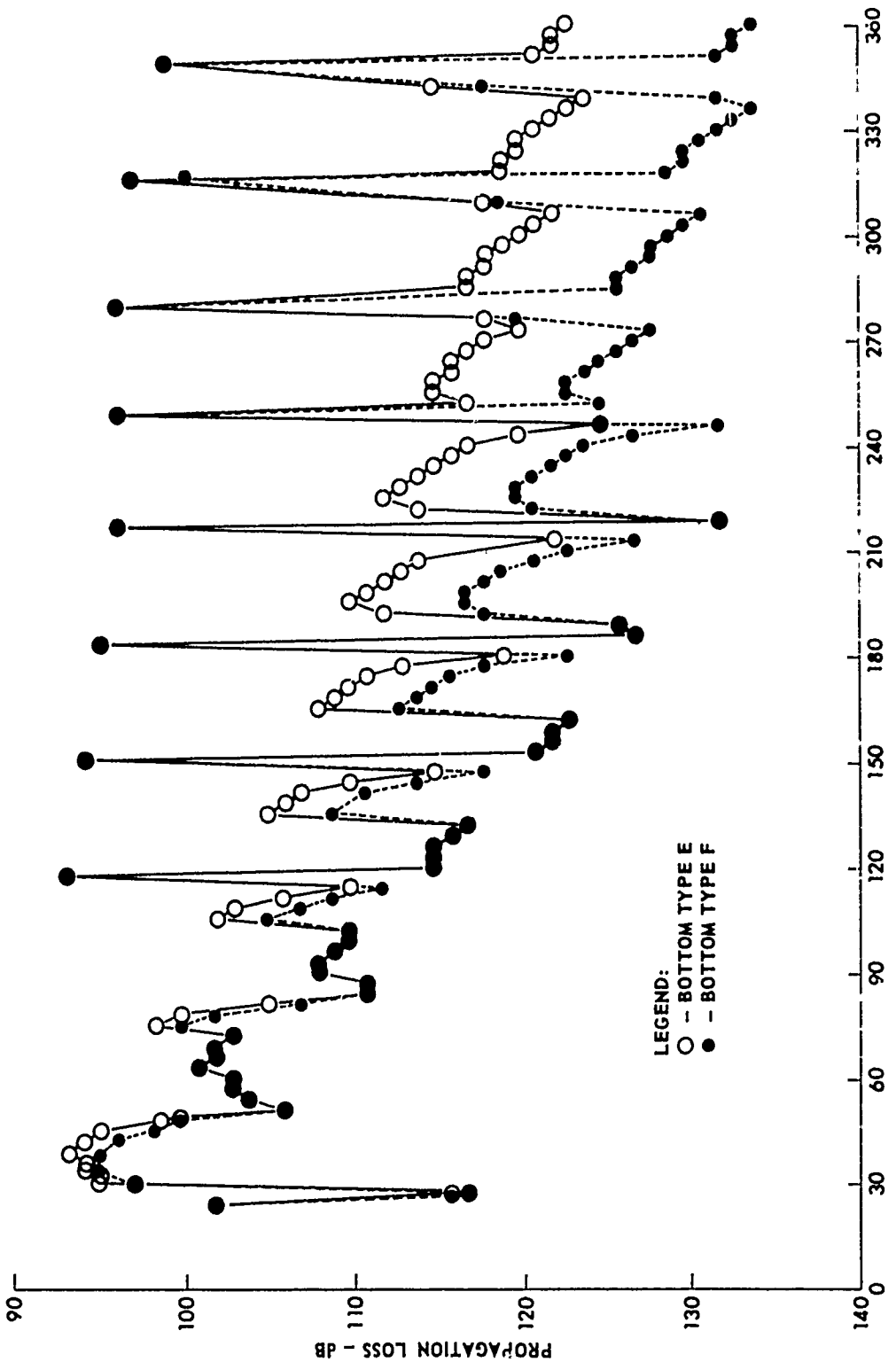

FIGURE II-6
PROPAGATION LOSS CURVES FOR VARYING BOTTOM LOSSES BELOW 1° GRAZING ANGLE

ARL - UT
AS-76-133
KCF - DR
2 - 12 - 76

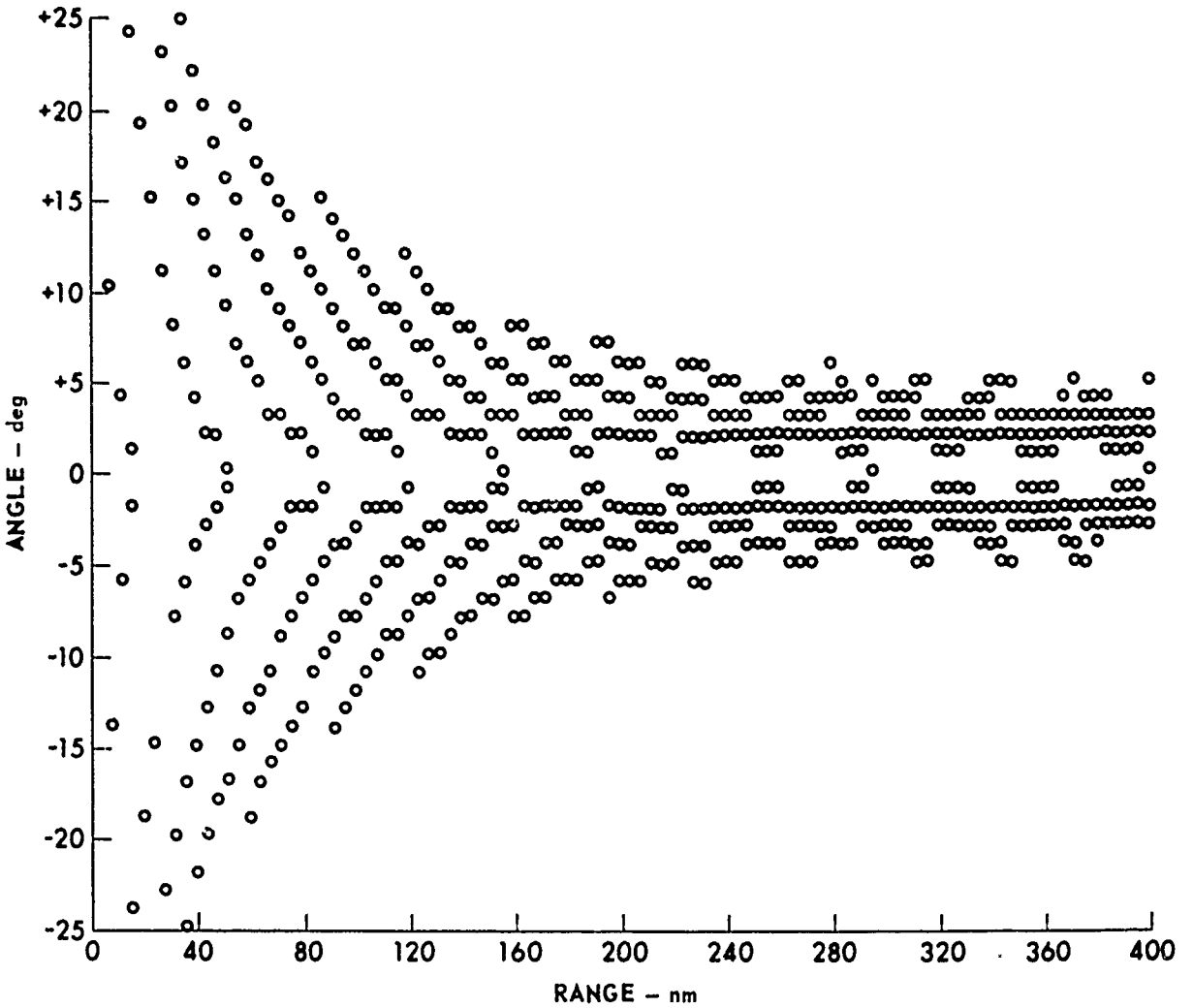

FIGURE II-7
ARRIVAL ANGLE VERSUS RANGE FOR A RECEIVER 30 m OFF THE BOTTOM
(BOTTOM DEPTH 5000 m)

ARL - UT
AS-76-131
KCF - DR
2 - 12 - 76

III. SENSITIVITY OF BOTTOM LOSS TO THE GEOACOUSTIC DESCRIPTION OF THE BOTTOM

A. Introduction

A relatively complete geoacoustic description of the bottom is required for prediction of some propagation phenomena at very low frequencies. However, many models used for predicting underwater sound propagation treat the bottom as a reflecting interface which can be characterized by a plane wave reflection coefficient (or bottom loss). Given such a description, it is then reasonable to ask, independent of any propagation situation or model, about the sensitivity of the reflection coefficient (bottom loss) to changes in any of the physical parameters characterizing the bottom.

Of course, if a particular propagation situation is not specified it is not possible to restrict the angular range over which such questions are to be answered. Although we shall usually have in mind long range acoustic propagation paths for which the bottom loss at low grazing angles dominate, the study will not be restricted to such angles. For shorter ranges or severe bottom depth deficiencies, the higher grazing angles will also be important.

Given a bottom loss model of multilayered horizontally stratified sediments overlying a rock substrate, the number of physical parameters and layering configurations required for an exhaustive sensitivity study is quite large. In this report application of models is restricted to the simplest and most obvious questions, such as the importance of shear waves, sound speed gradient, density gradient, etc.

In addition to sensitivity of bottom loss to changes in a specific parameter, there is the generic problem of determining the depth below which nothing needs to be known about the sediment or substrate. These depths, the hidden depths, will of course depend on the propagation configuration (range of bottom grazing angles) as well as sediment type, sound speed gradient, absorption, and frequency. Although there is not a final answer to the hidden depths question considerable progress has been made.

B. Development of Bottom Loss Models

1. Preliminaries

Given the wide scope of this task, it is clear that a reasonably sophisticated bottom loss model will be required. Since we are at present treating the rough surface problem separately, it is reasonable to assume a model which is completely horizontally stratified. Beyond this it is not immediately clear, without prejudging the outcome, what other aspects of the general case might be ignored. One simplification is achieved by restricting the sediments to fluids. It may be that shear waves provide a nontrivial loss mechanism in some subbottom sediment layers. However, the additional complexity introduced by including them is not justified in the initial part of the study. The shear wave speed in unconsolidated sediments is usually less than 10% of the compressional wave speed. However, in the underlying basement rock it is no longer reasonable to ignore shear waves because the shear wave speed can be on the order of 50% of the compressional wave speed and can therefore provide a significant acoustic path.

We are left then with a class of bottom loss models based on a series of horizontally stratified fluid layers overlying a semiinfinite solid layer. Two other significant points are the variation of sound speed and density with depth within any given sediment layer. The

simplest case, constant sound speed and constant density, has been adequately treated in the literature. The generally observed linear increase of sound speed with depth should be incorporated in any model used in the sensitivity study. Estimates of the importance of variable density are to be made in a later phase of the work.

2. Early Attempts

By ignoring for the moment the possibility of a continuously variable density, the mathematical problem can be very simply stated. The field (velocity potential) in the water is written as

$$\varphi_\omega = e^{ik_o \sin\theta z} + R\, e^{-ik_o z \sin\theta} ,$$

where $k_o = \omega/c_o$ and R is the reflection coefficient. In each sediment layer we must solve

$$\frac{\varphi^2 \varphi_i}{\varphi z^2} + \left(k_i^2(z) - k_o^2 \cos^2\theta \right) \varphi_i = 0 ,$$

where $k_i^2(z) = \omega^2/c_i^2(z)$ and $c_i(z)$ is the sound speed in the ith layer. At each sediment-sediment (or sediment-water) interface the fields must satisfy the usual conditions of continuity of φ_i' and $\rho_i \varphi_i$. At the sediment-rock interface the conditions are more complicated and will be discussed later.

The only difficult part of the problem is, for given $\{c_i(z)\}$, to solve the one-dimensional wave equation in each layer. There are several ways in which this question may be approached:

a) analytical methods - choose $c_i(z)$ such that the equation is solvable,

b) asymptotic techniques - for example the WKB method.

c) perturbation - variational methods, and

d) numerical methods - a numerical integration of the wave equation itself.

Since our primary object is to study bottom effects rather than to develop models, the straightforward approach was to investigate first an analytically solvable model. Previous applicable work has been published by Morris.[1-3] Her work has been extensively applied to predict and correlate experimental bottom loss data from various areas. This model is based upon the pseudolinear sound speed model, $c(z)=c/\sqrt{1+\beta z}$, which for small βz becomes $c(z)\cong c[1-1/2(\beta z)]$ representing a linear increase (or decrease) of sound speed with depth.

From both theoretical and experimental considerations one expects that the sound speed in a sediment layer will in fact increase approximately linearly with depth. Consequently, this model is attractive since it is exactly solvable in terms of Airy functions which may be evaluated numerically on a computer.

The first attempt at assembling a bottom loss model for use in the sensitivity study was therefore based on an implementation of Morris' model. A program was written to evaluate the reflection coefficient in the Morris formulation using a preexisting ARL subroutine to compute the Airy functions. The program was checked both internally and by comparison with Morris' results and was found to be operating properly.

Originally, Morris' model was composed of a series of fluid sediment layers overlying a fluid half space, also containing a pseudolinear variation of sound speed with depth. In the ARL version of this model the number of sediment layers was restricted to two and these overlay a solid half-space containing no sound speed gradient. The inclusion of shear waves in the underlying half space was the only significant extension of Morris' original model.

Although this model has proved useful for some aspects of the sensitivity study, it has drawbacks when used to address the hidden depths question. The most important requirements for a model which can provide answers to the hidden depth question are (1) an adequate treatment of the increase of sound speed with depth, and (2) the capacity to compute the bottom loss for thick sediment layers.

There are, however, difficulties in using the pseudolinear model for thick layers. One difficulty is that $c(z)=c/\sqrt{1+\beta z}$ will approximate a linear increase of sound speed with depth for $(\beta z)\ll 1$ only. When this inequality is not satisfied, a different physical model is implied. More seriously, since $\beta<0$, there will be a depth at which the sound speed becomes unbounded. This has no physical meaning, but if there is appreciable sound energy at this depth, it cannot be ignored since it is built into the mathematical model.

Some of these aspects of the pseudolinear model are discussed in a recent paper by A. O. Williams, Jr.[4] Williams also discusses some aspects of an alternative reflection coefficient based on an exponential profile $k^2(z)=k^2+\eta^2 e^{-z}$. Such a profile avoids both the singularity in the sound speed of a pseudolinear model and the unbounded increase in $c(z)$ as $z\to\infty$ of a true linear model. Some estimates using this model are given, but no extensive calculations have yet been carried out.

In any event, the pseudolinear model will always have an ultimate hidden depth at $z=\beta^{-1}$ since below this depth the sound field vanishes exponentially in all cases. The "barrier" thus formed can exhibit tunneling and the highly upward refracting profile can cause odd diffraction behavior, especially for large angle reflection. These are again artifacts of the mathematical model. Even in only moderately thick layers, when the sound speed is finite everywhere, the "anomalous" upward refraction (relative to a true linear model) can lead to a desensitization of the reflection coefficient to changes in the physical description of the subbottom.

Thus, the pseudolinear model is primarily useful for its originally stated purpose of calculating reflection loss from bottoms composed of thin layers. It is not useful for investigating the hidden depths problem because the nature of the question involves thick layers.

An obvious direction to go in improving the existing models is to use a linearly increasing sound speed, which is the same condition as the actual physical situation being modeled. The one-dimensional wave equation with $k^2(z)=\omega^2/c^2(1+\beta z)^{-2}$ can be solved in terms of Bessel functions. The solution can conveniently be taken to be

$$\varphi = A\sqrt{1+\beta z}\;\frac{H^{(1)}}{\sqrt{1/4 - k^2/\beta^2}}\left(\frac{ik_o \cos\theta}{\beta}[1+\beta z]\right)$$

$$+ B\sqrt{1+\beta z}\;\frac{H^{(2)}}{\sqrt{1/4 - k^2/\beta^2}}\left(\frac{ik_o \cos\theta}{\beta}[1+\beta z]\right) \quad ,$$

where $H^{(1)}_{\sqrt{\cdot}}(\omega)$ and $H^{(2)}_{\sqrt{\cdot}}(\omega)$ are Hankel functions. At 100 Hz and a sound speed gradient of 1 sec^{-1}, $|k^2/\beta^2| \cong 4\times10^5$; hence we are dealing with Hankel functions of large order and, generally, large argument as well. Since $k/\beta \gg 1/2$, the solution is essentially $H_2^{(1)/(2)}[\nu w]$ where $w=k_o \cos/k_1(1+\beta z)$ and $\nu \cong ik_1/\beta$. The appropriate expansions to use in evaluating such Bessel functions are the uniform asymptotic expansions (see Abramowitz and Stegun,[5] or Olver[6]). For example,

$$H_\nu^{(1)}(\nu w) = 2e^{i\pi/3}\left(\frac{4\zeta}{1-w^2}\right)^{1/4}\left\{\frac{A_i(e^{2\pi i/3}\,\nu^{2/3}\,\zeta)}{\nu^{1/3}}\left[1+\frac{a_i(\zeta)}{\nu^2}+\ldots\right]\right.$$

$$\left. + e^{2\pi i/3}\,\frac{A_i'(e^{2\pi i/3}\,\nu^{2/3}\,\zeta)}{\nu^{5/3}}\left[\frac{b_i(\zeta)}{\nu^2}+\ldots\right]\right\} \quad .$$

where $\zeta^{3/2}=3/2\left[\ln[(1+1-z^2)z] - 1 - z^2\right]$, and Ai(u) is the Airy function. The functions $a_i(\ )$ and $b_i(\ )$ are tabulated and for low orders are not themselves prohibitively complicated. Since the argument of Ai(u) and Ai'(u) will generally be very large, the asymptotic evaluation of these functions is appropriate. There is, however, a problem due to the presence of the factors of $e^{i2\pi/3}$ in the arguments of the Airy functions.. In the absence of absorption this would require evaluation of Ai(u) for $|u|\gg 1$ and $\arg(u)=\pm 2\pi/3$, a region of the complex plane where great difficulties are found in evaluation of Re[Ai(u)] and Im[Ai(u)] together. Furthermore, the acoustic frequency and sediment layer thickness enter in such a fashion as to frequently lead to exponential function overflow in computer calculations. Another approach was felt to be warranted, in view of the numerical difficulties encountered in evaluating these Bessel functions in the region of interest. This view was strengthened by two additional points: (1) incorporation of a continuously variable density would further increase the difficulties, and (2) for thick sediment layers it might be necessary to use a model in which the sound speed gradient was not constant but decreased toward the bottom (and perhaps the top) of the layer. For these various reasons work on the analytical solution of linear sound speed models was also terminated and alternate approaches were investigated.

3. A Numerical Approach to Bottom Loss Models

After briefly considering an approach involving asymptotic expressions for the solution of the wave equation (WKB solution would be an example) it was decided to construct a model based entirely on numerical integration of the differential equation. This approach has the important advantage of being applicable to essentially arbitrary sound speed profiles as well as allowing a continuously variable density to be included in a straightforward manner. Variable density modifications to the usual linear wave equation are discussed by Bergmann.[7]

A direct numerical solution of the depth separated wave equation on an interval (0,H) requires specification of initial values of the velocity potential and its derivative $\varphi(H)$, $\Phi'(H)$. This can be accomplished simply by letting the incident wave have an arbitrary intensity rather than the unit intensity assumed in conventional formulations of plane wave reflection coefficients. In this formulation, the incident intensity is that corresponding to a unit amplitude in the substrate just below the lowest sediment interface. The value of $\varphi'(H)$ is then obtained by realizing that in the substrate the velocity potential is $\varphi(z)=Ae^{iHz}$ and hence $\varphi'=iH\varphi$ which yields $\varphi'(H)=iH\varphi(H)=iu$ with $\varphi(H)=1$, and u is a wavenumber appropriate to the substrate. The usual continuity conditions yield values of φ and φ' in the sediment just above the sediment-substrate interface and a numerical integration of the "initial value" problem is then possible. The inclusion of shear waves in the substrate modifies the fluid-fluid conditions as described by Brekhovshikh.[8]

Once the initial values of the field $\varphi(H)$ and $\varphi'(H)$ are known, a direct numerical integration of the depth separated wave equation, $\varphi'' + (k^2(z) - k_o^2 \cos^2 G)\varphi = 0$, becomes possible. As described in Appendix B, a computer program has been written to implement this approach. In the program a Runge-Kutta scheme was employed in the numerical integration (see Shampise and Allen).[9] The overall global error of this integration process is unknown but controlled since the local error (per integration step) is specified as a program input. Extensive comparison with constant sound speed (Rayleigh) models as well as with the pseudolinear model has shown that the numerical model is operating correctly and can compute the complex reflection coefficient to a specifiable accuracy.

Program inputs include the density, sound speed, and attenuation in all materials, sound speed and density profiles in the sediment layers, and shear wave speed and attenuation in the substrate. The conventional output includes a tabulation of $|R|$ and arg(R) as well as a Calcomp and/or

a printer plot of $|R|$ on either a logarithmic (bottom loss) or linear (reflection coefficient) scale. In addition, a tabulation of $|\varphi|$ and $\arg(\varphi)$ at any given set of angles, throughout the entire subbottom, can be obtained. That no additional computation is necessary to obtain this information is a unique aspect of the numerical integration approach.

Future development of this model will include a Calcomp plot capability for the phase $\arg(R)$, as well as for $\varphi(z)$. A hybrid numerical-WKB technique, now under investigation, may significantly reduce the program execution time, as will the conversion of critical parts of the computer code to assembly language.

C. Sensitivity Assessment

In this section the results of several initial investigations are given. The questions addressed include the hidden depth question, as well as the effects and importance of a sound speed gradient, and the importance of shear waves in the underlying basement rock. Additionally, the effects of a density gradient are studied and the true linear gradient model for sound speed is compared with the pseudolinear model. All geoacoustic parameters used in the various bottom loss curves given in the remainder of this section are summarized in Table III-1.

1. Shear Waves and the Hidden Depths

It would be expected intuitively that if the sediment overburden were not too thick, the presence of shear waves in the substrate would provide an important loss mechanism, particularly at high grazing angles. To quantify this effect, we have studied the reflection coefficient for sediments of various types and thicknesses overlying the substrate. Figures III-1-4 display the effects of substrate shear waves for a 100 m thickness of either medium sand or medium clay. The sand (or clay) layer has a sound speed gradient of 1.2 sec^{-1}, but no density gradient.

TABLE III-1

Fig.	V-1	V-2	V-3	V-4	V-5	V-5	V-6	V-6	V-7	V-7	V-10	V-10	V-11	V-11	V-12	V-12
I_D	1059	1054	1074	1079	1550	1551	1552	1553	1554	1555	1536	1540	1537	1541	1538	1542
ρ_ω	1.053	1.053	1.053	1.053	1.053	1.053	1.053	1.053	1.053	1.053	1.053	1.053	1.053	1.053	1.053	1.053
c_ω	1540	1540	1540	1540	1540	1540	1540	1540	1540	1540	1540	1540	1540	1540	1540	1540
ρ_1	2.08	2.08	1.27	1.27	1.27	1.27	1.27	1.27	1.27	1.27	1.27	1.27	1.27	1.27	1.27	1.27
c_1	1723.8	1723.8	1526.6	1526.6	1526.6	1526.6	1526.6	1526.6	1526.6	1526.6	1526.6	1526.6	1526.6	1526.6	1526.6	1526.6
α_1	0.048	0.048	0.0057	0.0057	0.0014	0.0014	0.0029	0.0029	0.0057	0.0057	0.0057	0.0057	0.0057	0.0057	0.0057	0.0057
g_1	1.2	1.2	1.2	1.2	1.2	1.2	1.2	1.2	1.2	1.2	0	0	0.50	0.50	1.0	1.0
ρ_1'	0	0	0	0	0	0	0	0	0	0	0	0	0	0	0	0
D_1	100	100	100	100	100	100	100	100	100	100	150	150	150	150	150	150
ρ_B	2.6	2.6	2.6	2.6	2.6	2.6	2.6	2.6	2.6	2.6	2.6	2.6	2.6	2.6	2.6	2.6
c_B^c	5700	5700	5700	5700	5700	5700	5700	5700	5700	5700	5700	5700	5700	5700	5700	5700
c_B^s	3000	0	0	3000	0	2700	0	2700	0	2700	0	2200	0	2200	0	2200
α_B^c	0.003	0.003	0.003	0.003	0.00075	0.00075	0.0015	0.0015	0.003	0.003	0.003	0.003	0.003	0.003	0.003	0.003
α_B^s	0.01	-	-	0.01	-	0.005	-	0.01	-	0.02	-	0.010	-	0.01	-	0.01
F	100	100	100	100	25	25	50	50	100	100	100	100	100	100	100	100

ρ : density in g/cm^3
c : sound speed in m/sec
α : attenuation in dB/m
g : sound speed gradient in sec^{-1}
ρ': density gradient in $g/cm^3/m$

F : frequency in hertz
D : layer thickness in meters

TABLE III-1 (cont'd)

Fig.	V-13	V-13	V-14	V-15	V-16	V-17	V-18	V-18	V-19	V-19	V-20	V-20
I_D	1559	1543	1051	1052	73	74	1530	1533	1531	1539	1532	1535
ρ_ω	1.053	1.053	1.044	1.044	1.044	1.044	1.053	1.053	1.053	1.053	1.053	1.053
c_ω	1540	1540	1509.1	1509.1	1509.1	1509.1	1540	1540	1540	1540	1540	1540
ρ_1	1.27	1.27	1.29	1.29	1.29	1.29	1.27	1.27	1.27	1.27	1.27	1.27
c_1	1526.6	1526.6	1493	1493	1493	1493	1526.6	1526.6	1526.6	1526.6	1526.6	1526.6
α_1'	0.0057	0.0057	0.15	0.15	0.15	0.15	0.0057	0.0057	0.0057	0.0057	0.0057	0.0057
g_1	1.5	1.5	1.5	1.5	1.5	1.5	1.2	1.2	1.2	1.2	1.2	1.2
ρ_1'	0	0	0	0	0	0	0	0.002	0	0.002	0	0.002
D_1	150	150	4.5	4.5	4.5	4.5	50	50	100	100	200	200
ρ_2	-	-	1.57	1.57	1.57	1.57	-	-	-	-	-	-
c_2	-	-	1562	1562	1562	1562	-	-	-	-	-	-
α_2	-	-	0.006	0.006	0.006	0.006	-	-	-	-	-	-
g_2	-	-	1.5	1.5	1.5	1.5	-	-	-	-	-	-
ρ_2'	-	-	0	0	0	0	-	-	-	-	-	-
D_2	-	-	500	600	500	600	-	-	-	-	-	-
ρ_B	2.6	2.6	2.6	2.6	2.6	2.6	2.6	2.6	2.6	2.6	2.6	2.6
c_B^c	5700	5700	5700	5700	5700	5700	5700	5700	5700	5700	5700	5700
c_B^s	0	2200	0	0	0	0	3000	3000	3000	3000	3000	3000
α_B^c	0.003	0.003	0.003	0.003	0.003	0.003	0.003	0.003	0.003	0.003	0.003	0.003
α_B^s	-	0.01	-	-	-	-	0.01	0.01	0.01	0.01	0.01	0.01
F	100	100	100	100	100	100	100	100	100	100	100	100

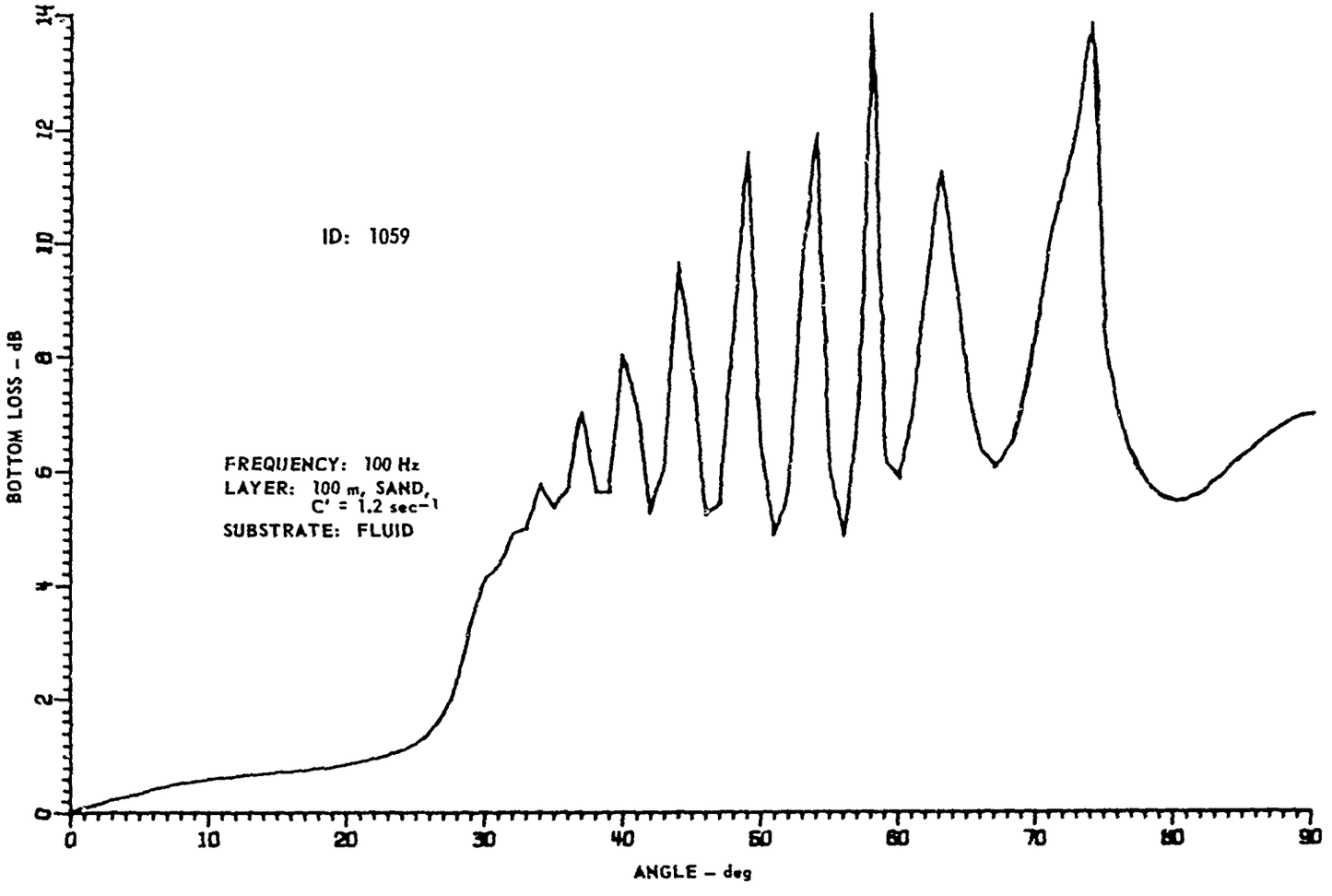

ARL - UT
AS-76-143
KEH - DR
2 - 18 - 76

FIGURE III-1
BOTTOM LOSS VERSUS GRAZING ANGLE FOR A
100 m SAND LAYER OVER A FLUID SUBSTRATE

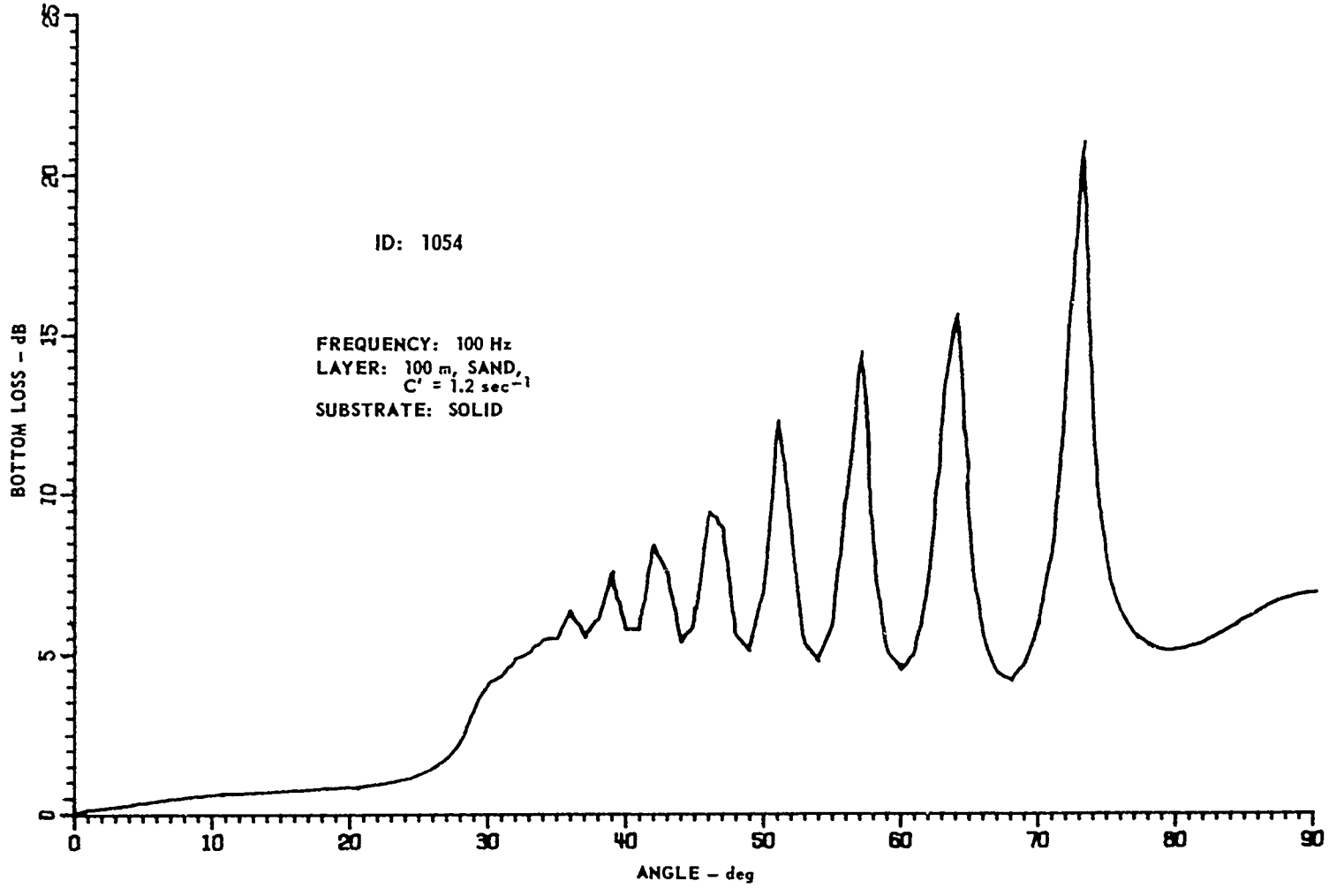

ARL - UT
AS-76-144
KEH - DR
2-18-76

FIGURE III-2
BOTTOM LOSS VERSUS GRAZING ANGLE FOR A
100 m SAND LAYER OVER A SOLID SUBSTRATE

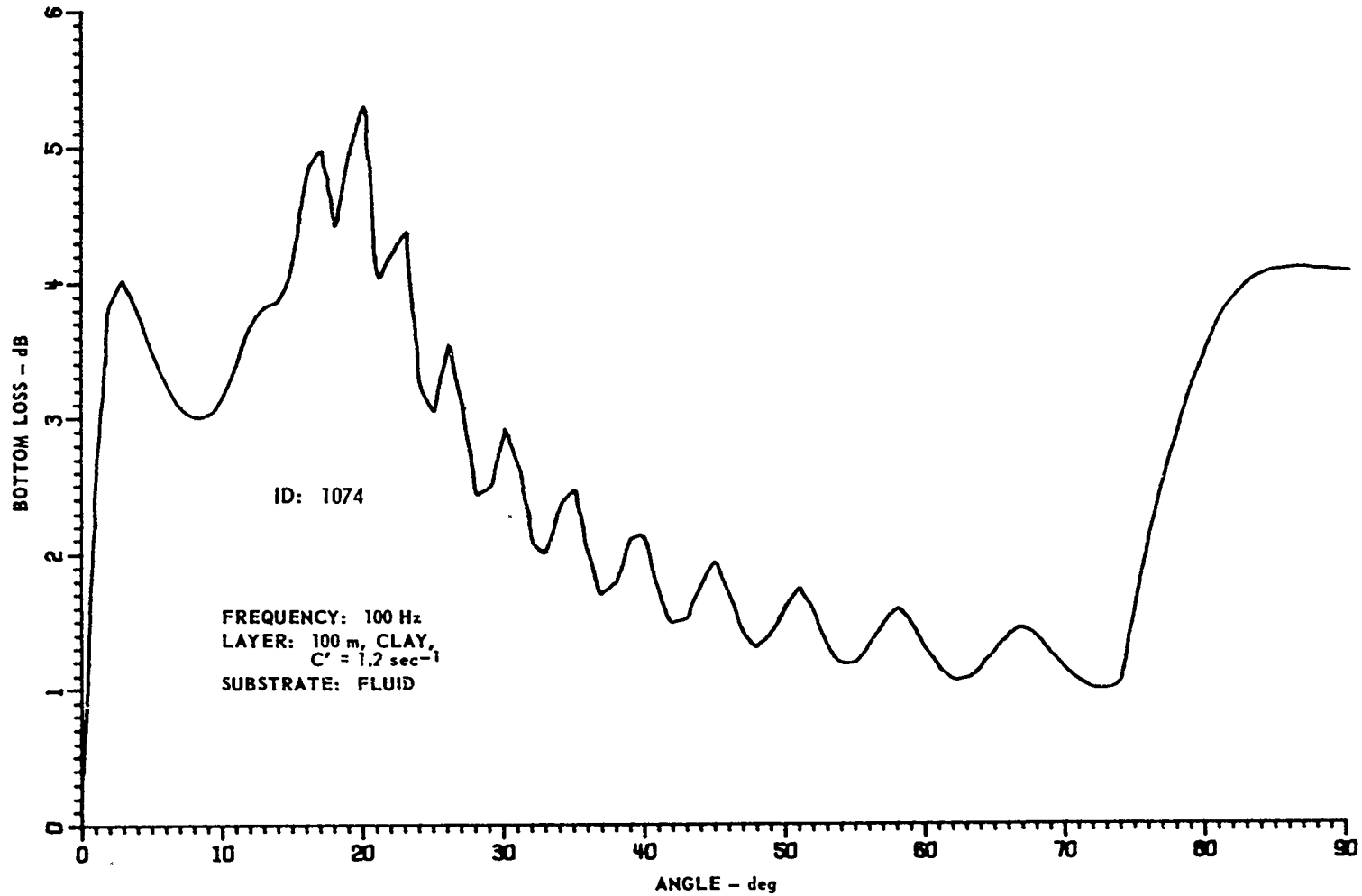

ARL - UT
AS-76-145
KEH - DR
2-18-76

FIGURE III-3
BOTTOM LOSS VERSUS GRAZING ANGLE FOR A
100 m CLAY LAYER OVER A FLUID SUBSTRATE

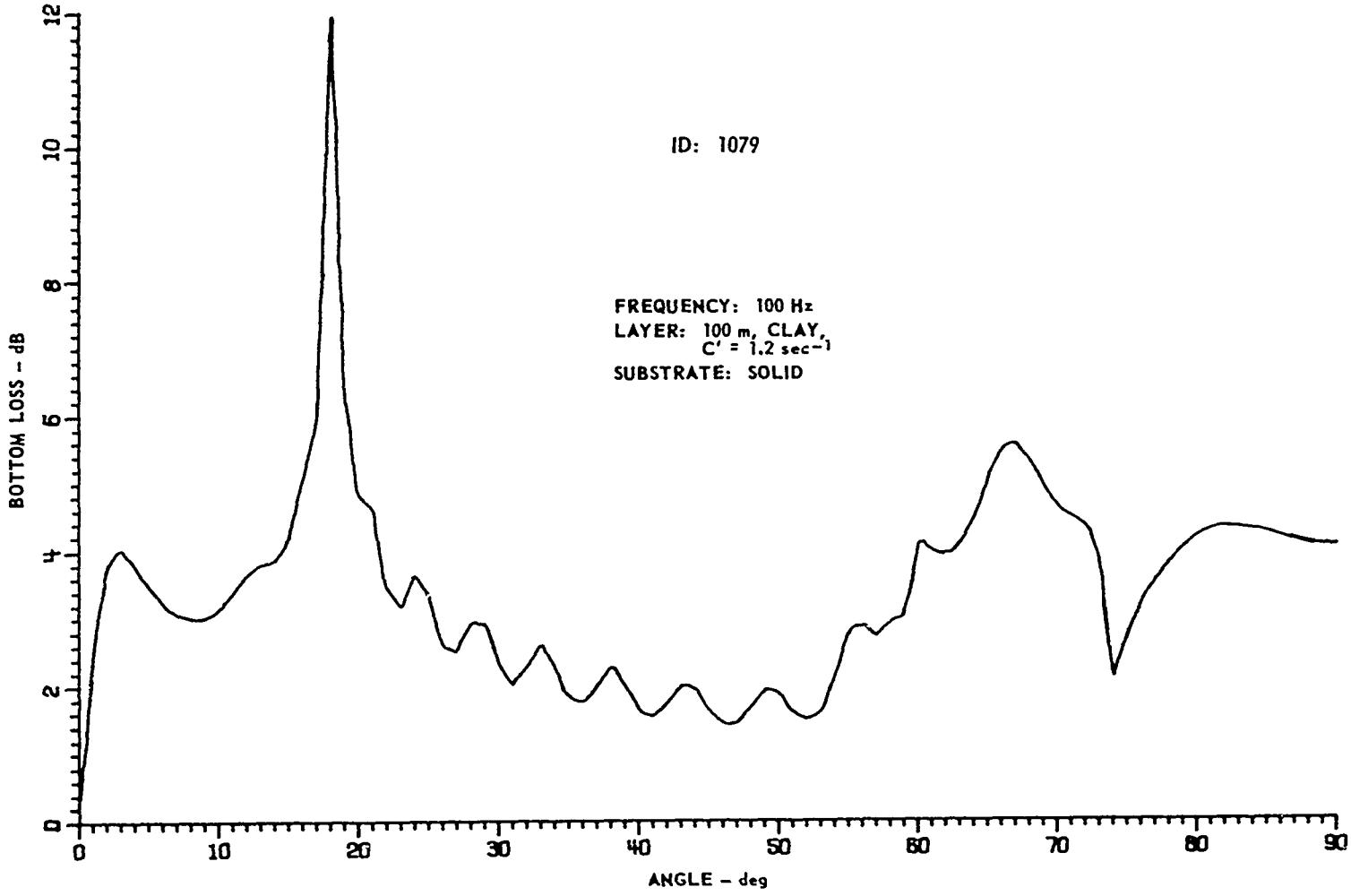

ARL - UT
AS-76-146
KEH - DR
2 - 18 - 76

FIGURE III-4
BOTTOM LOSS VERSUS GRAZING ANGLE FOR A
100 m CLAY LAYER OVER A SOLID SUBSTRATE

The most obvious effect of shear waves displayed in these results is the large peak in bottom loss in the neighborhood of 18°, for the clay layer. This effect is not a numerical artifact but is a real aspect of the mathematical model having this particular set of geoacoustic parameters. A similar peak has been observed, for a different set of parameters, in the case of the psuedolinear model discussed earlier. In this case, as well as all others, the "analytical" and numerical approaches yield identical predictions.

Further examples of this anomalous low angle loss and other effects of shear waves are given in Figs. III-5 through 7, which show the bottom loss for a 100 m clay layer at 25, 50, and 100 Hz. The large peak at approximately 17° is quite evident in all three cases although it is much broader, and somewhat lower, at 25 Hz than at 100 Hz. Since the angle at which a ray first encounters the substrate (ray turning depth equal to the layer thickness) is approximately 20.7°, the behavior shown here is a clear manifestation of the wave aspects of sound. Since the phenomenon is due to energy which is diffracted through the sound speed profile "barrier", it is not surprising that the peak in bottom loss is broader at lower frequencies. Other investigations show that the magnitude and the location of this effect is dependent upon layer thickness, sound speed gradient, sediment material, frequency, and shear wave attenuation. Further investigation is underway to determine the precise physical cause of this behavior. The near frequency independence of the angle of the maximum loss, as well as other factors, suggest that this effect may be due to a boundary (Stoneley) wave.

One way to attack the hidden depth question is to begin with a sediment layer of given type and thickness and to examine the effect on bottom loss of increasing the sediment thickness. A slightly more sensitive and informative test involves altering some property of the substrate for each layer thickness and observing the effect on bottom loss. In

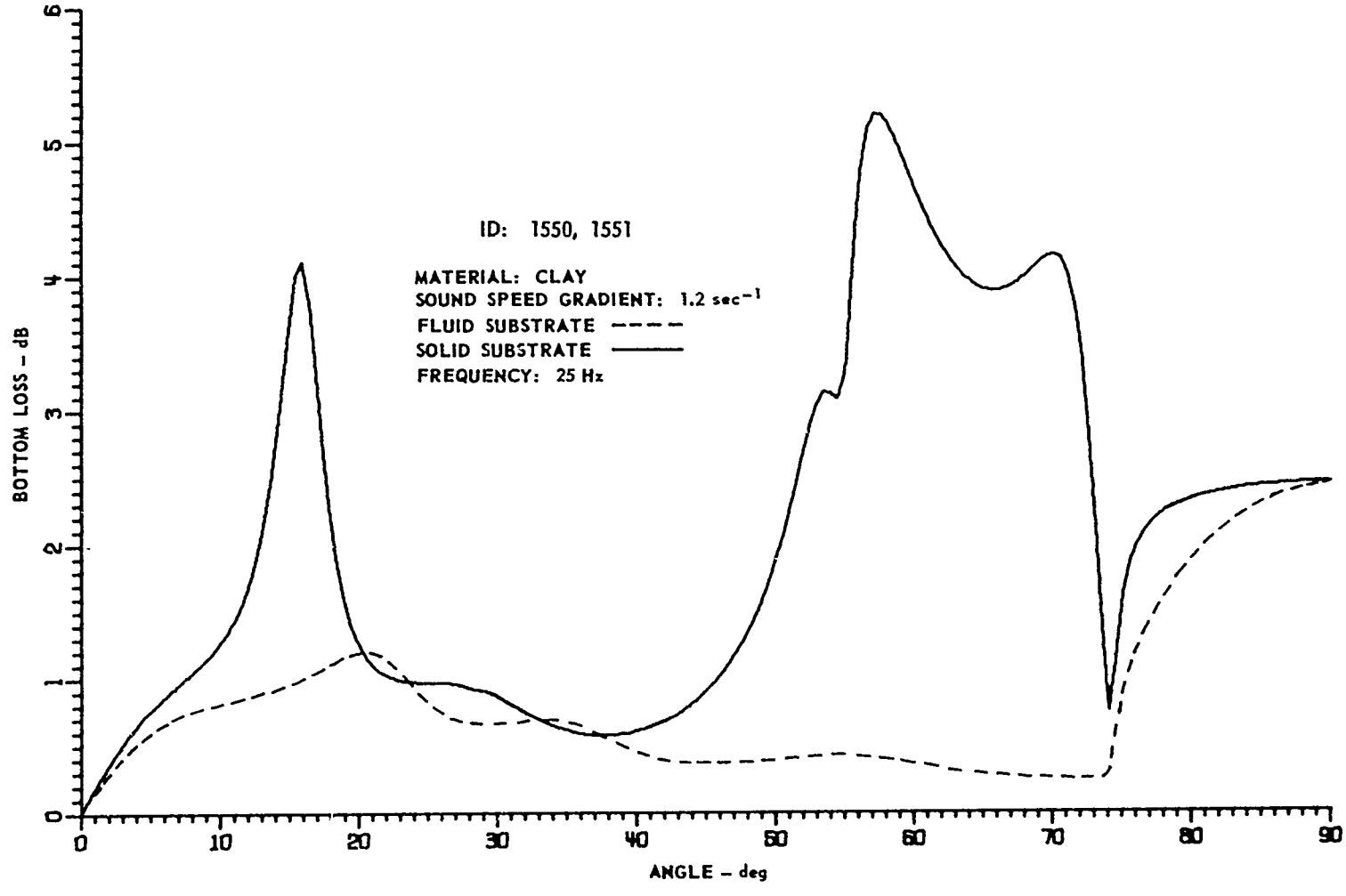

FIGURE III-5
BOTTOM LOSS VERSUS GRAZING ANGLE
FOR A 100 m CLAY LAYER AT 25 Hz

ARL-UT
AS-76-205
KEH-DR
2-27-76

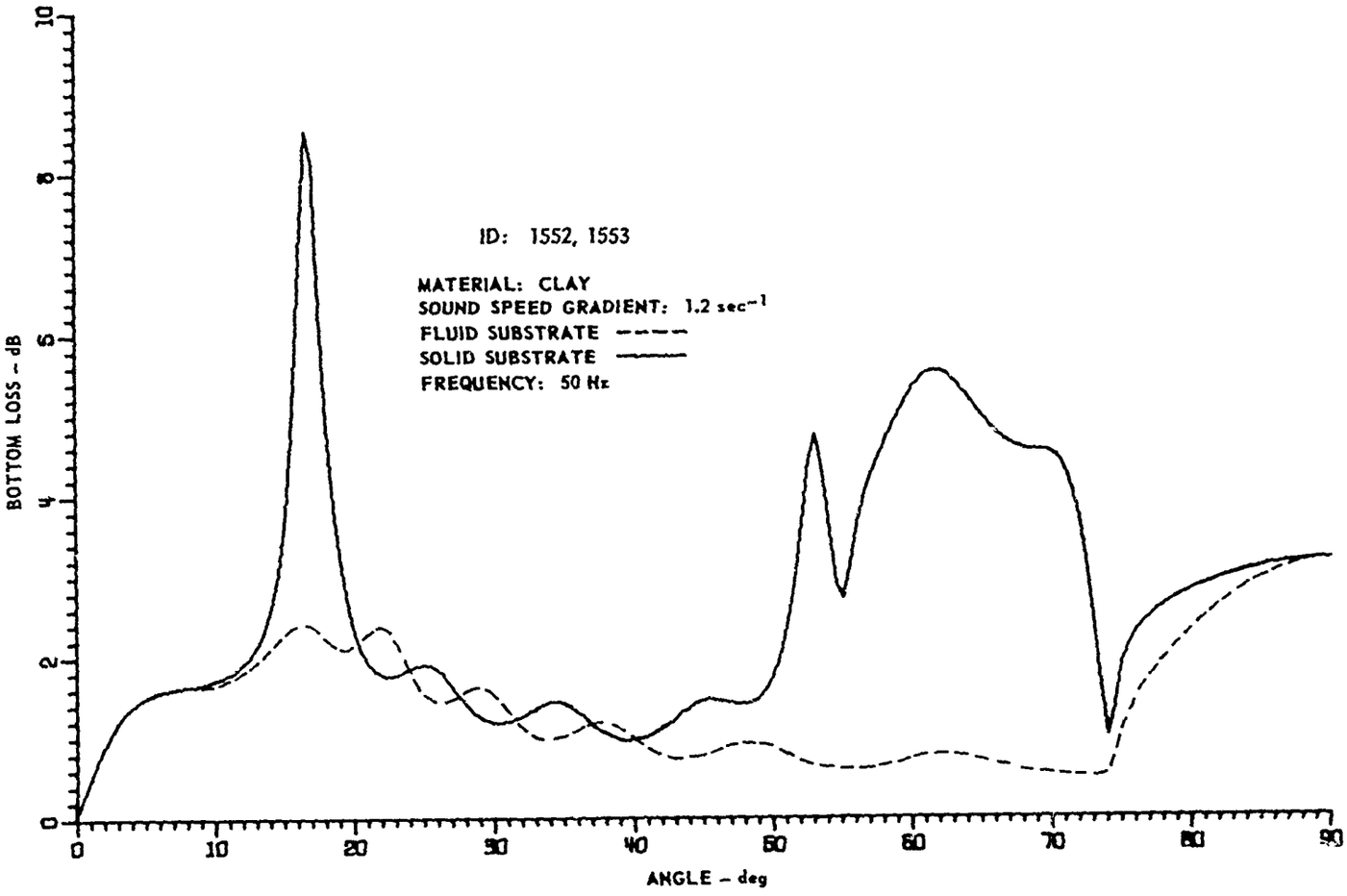

FIGURE III-6
BOTTOM LOSS VERSUS GRAZING ANGLE
FOR A 100 m CLAY LAYER AT 50 Hz

ARL, UT
AS-76-206
KEH - DR
2-27-76

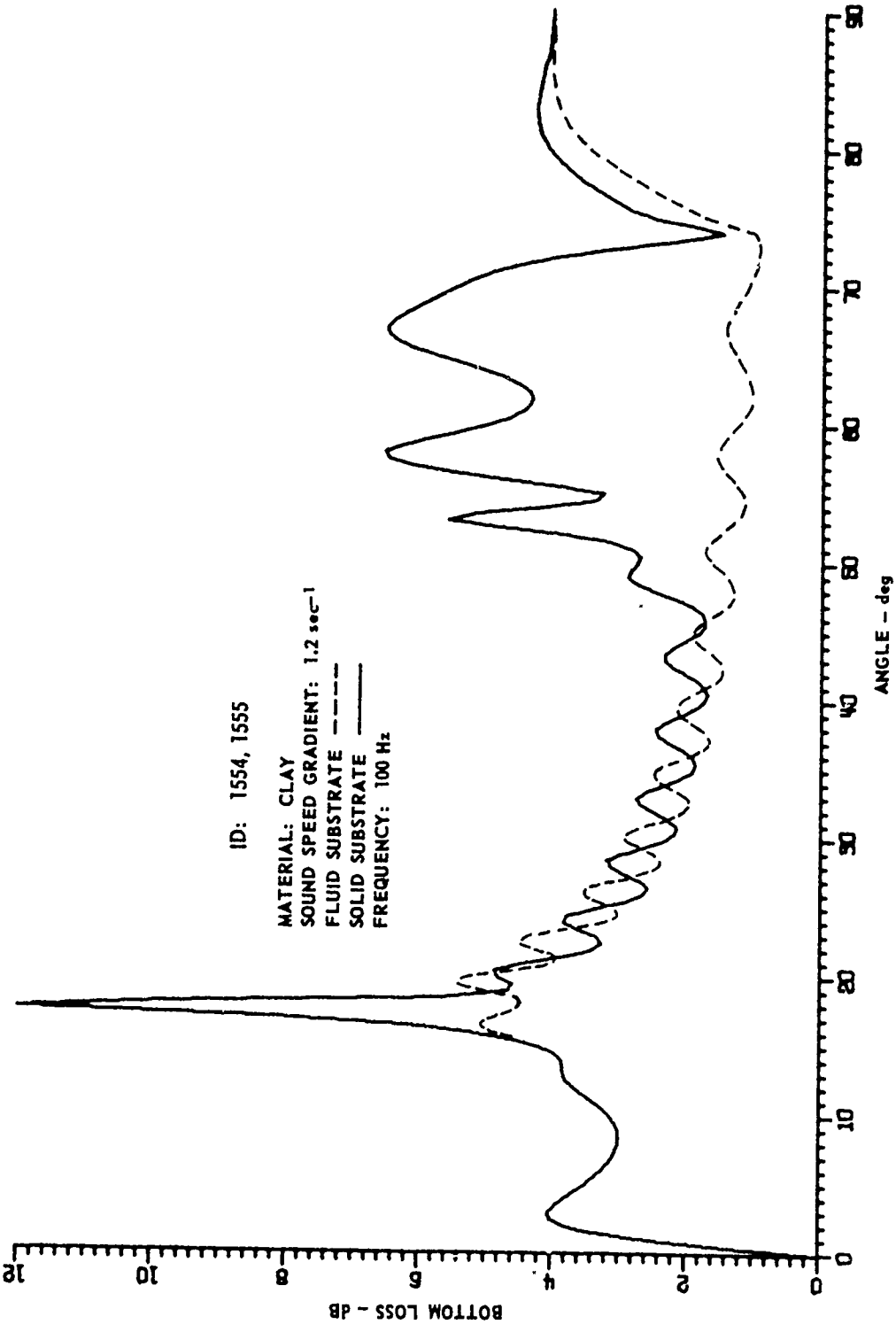

FIGURE III-7
BOTTOM LOSS VERSUS GRAZING ANGLE
FOR A 100 m CLAY LAYER AT 100 Hz

ARL - UT
AS-76-207
KEH - DR
2 - 27 - 76

addition to their intrinsic effects, shear waves provide a convenient mechanism to switch on and off in an investigation of the hidden depth question.

Figures (III-8-9) show the effect of shear waves at three specific angles (20°, 30°, 40°) for clay and silt of various thicknesses. It will be observed that in each case there is a thickness beyond which the bottom loss is insensitive to the presence of shear waves or to any further increase in layer thickness. For these situations, this depth would in fact constitute the hidden depth. The coincidence of the curves for fluid and solid substrates and the flattening of the curves holds to within 5×10^{-5} dB, which is on the order of the numerical error to be expected.

The depths marked $z_T(\theta)$ on these two figures are the thickness at which the turning point (ray turning depth) becomes coincident with the lower boundary for a given angle. It will be observed that the hidden depth is reasonably well correlated with the turning depth. It should be expected then that the turning depth would provide a crude first estimate of the hidden depth with an error on the order of a few sound wavelengths. The turning depth (ray penetration depth), together with other parameters for the sediment penetrating ray, were calculated as described in Appendix E. There are few systematic differences between the clay and silt cases, and in particular the hidden depth is essentially the same. In the case of silt the curve corresponding to 40° has been suppressed for clarity.

Finally, an alternate approach to the general hidden depth question has been taken by Williams, whose results are similar to those presented here. Williams' work is given in Appendix C.

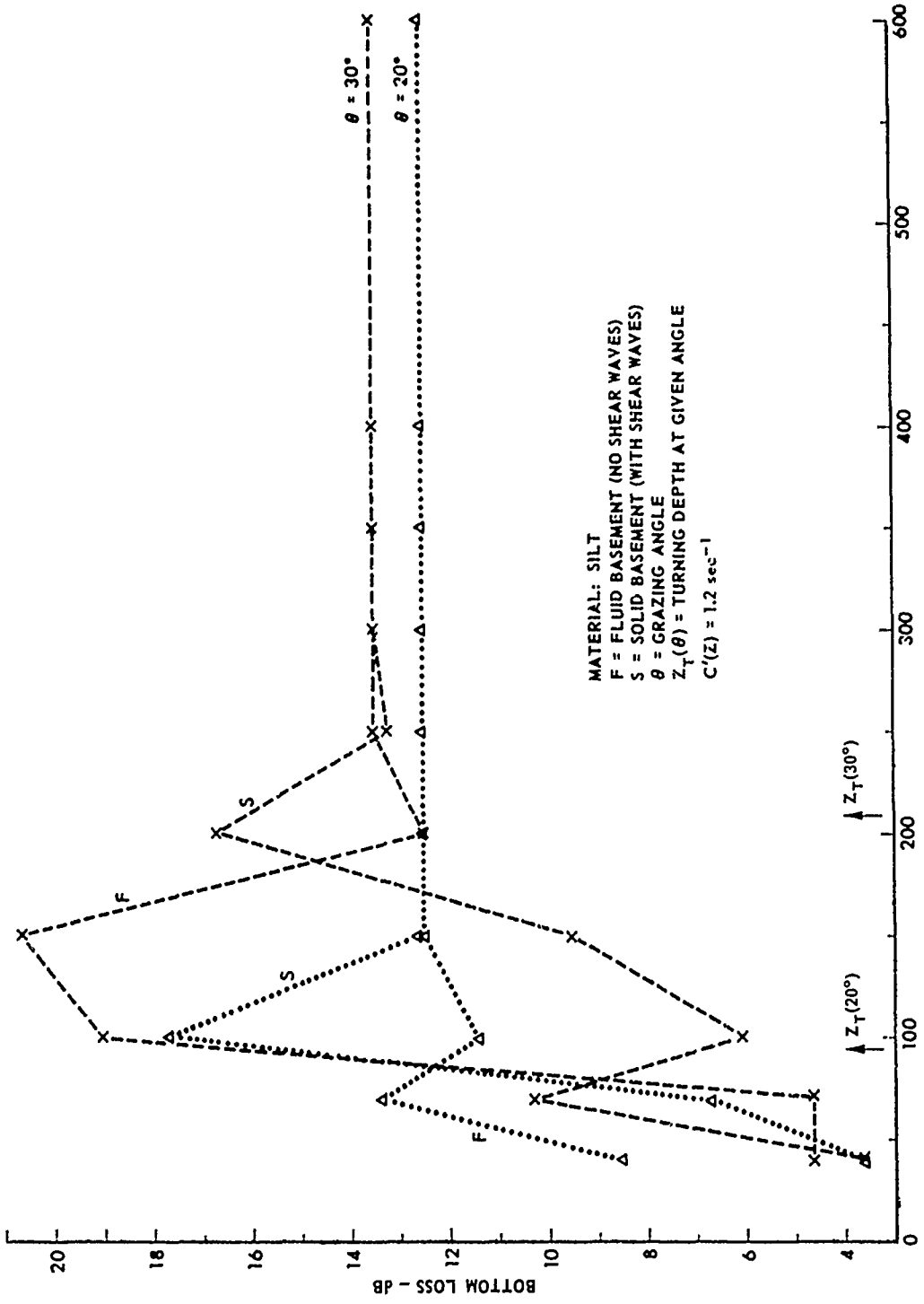

FIGURE III-8
BOTTOM LOSS VERSUS LAYER THICKNESS
FOR SEVERAL GRAZING ANGLES

ARL - UT
AS-76-45
KEH - DR
1 - 19 - 76

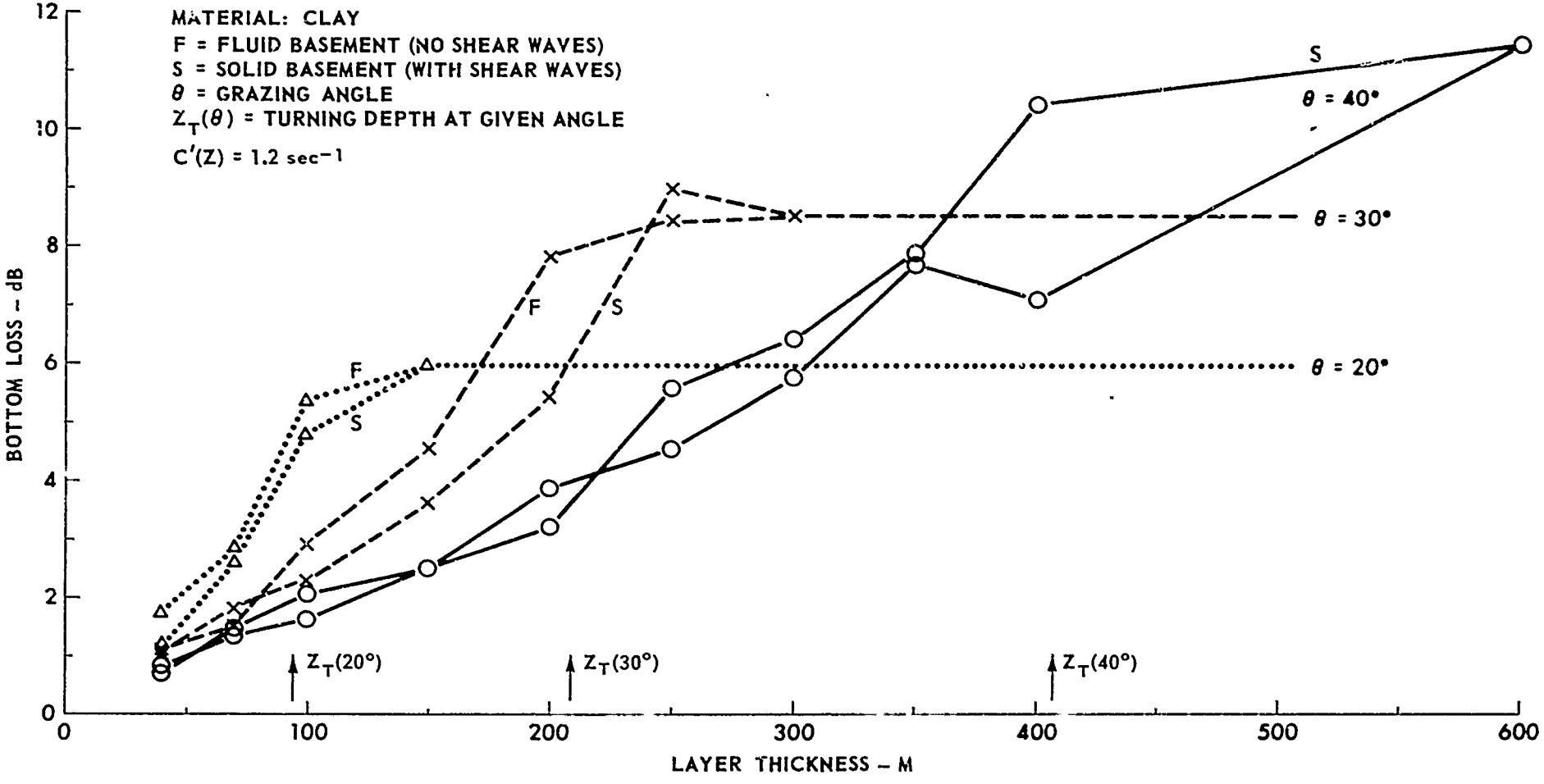

FIGURE III-9
BOTTOM LOSS VERSUS LAYER THICKNESS FOR SEVERAL GRAZING ANGLES

ARL - UT
AS-76-44
KEH - DR
1 - 19 - 76

2. Effects of a Sound Speed Gradient

It is already clear that the sensitivity of bottom loss to changes in any subbottom parameter can be strongly related to the sound speed gradient, especially if the question pertains to changes of a parameter deep in the sediment. As a beginning to the systematic study of the sensitivity of bottom loss to this gradient, the effects of increasing the sound speed gradient from 0 to 1.5, for a linear sound speed $c(z)=c(1+\beta z)$, were studied for the case of 150 m of clay overlying a substrate (both fluid and solid substrates were studied).

Some of the results of this study are presented in Figs. (III-10 through 13). In each case except for $c'=0$ it will be observed that there is an angle below which the bottom loss is insensitive to the presence or absence of shear waves. Furthermore, this angle increases as the sound speed gradient increases. This behavior is easily understood in terms of the increasing amount of upward refraction caused by the sound speed profile.

The most striking effect observed on these curves is the large change in bottom loss which occurs at low grazing angles when the sound speed gradient is changed. Since low angles are more important than high angles for long range propagation, this effect is quite important, and further study in this direction is indicated.

3. Comparison of Linear and Pseudolinear Models

Previously published calculations of bottom loss involving a nonzero sound speed gradient are based on the pseudolinear model $c(z)=c(1+\beta z)^{-1/2}$, whereas the bulk of the studies reported here are based on the linear model $c(z)=c(1+\beta z)$. Therefore, it is appropriate to illustrate the differences between these models for several situations.

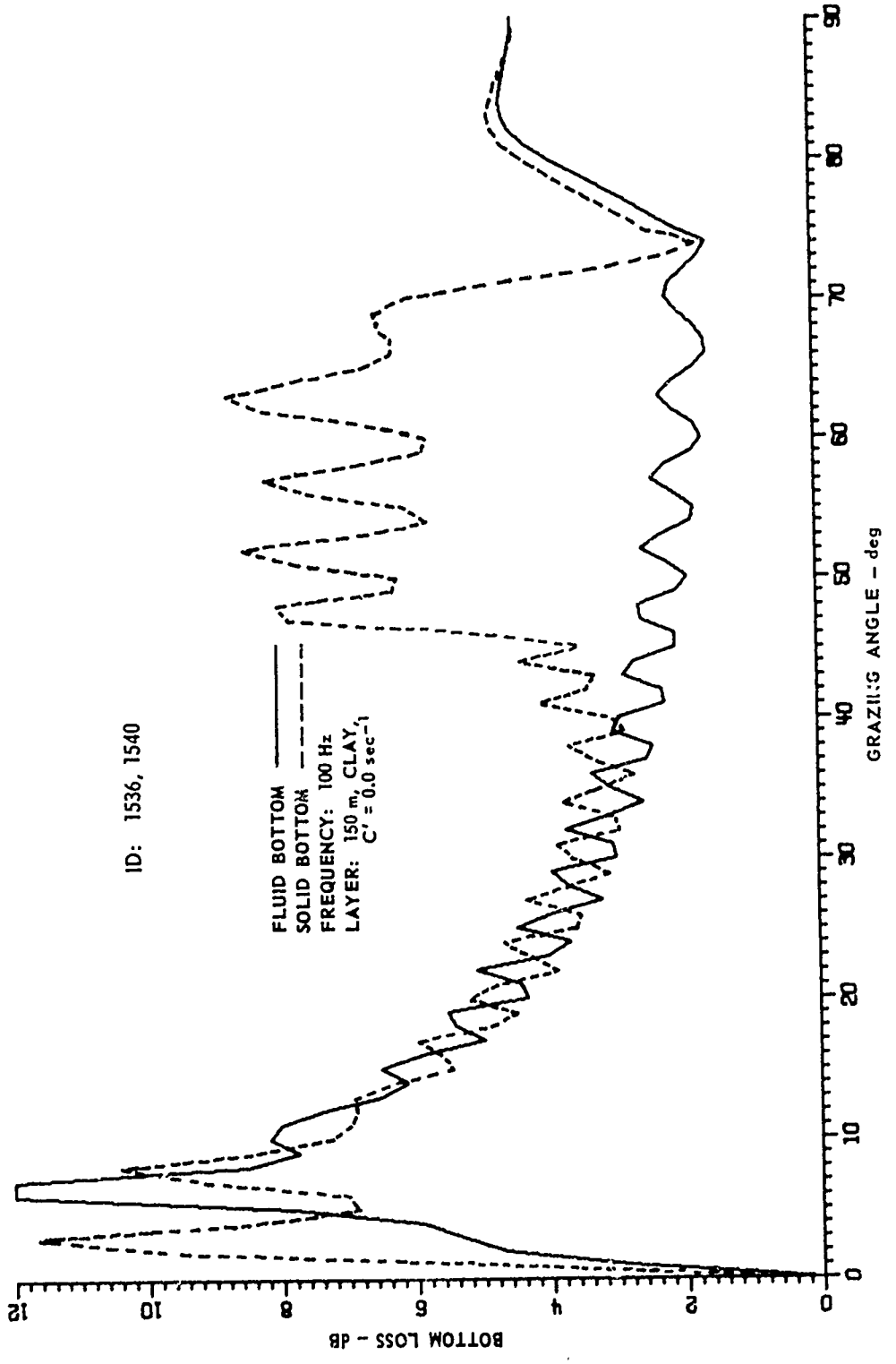

FIGURE III-10
BOTTOM LOSS versus GRAZING ANGLE FOR A 150 m CLAY LAYER HAVING A ZERO SOUND SPEED GRADIENT

ARL-UT
AS-76-150
KEH-DR
2-18-76

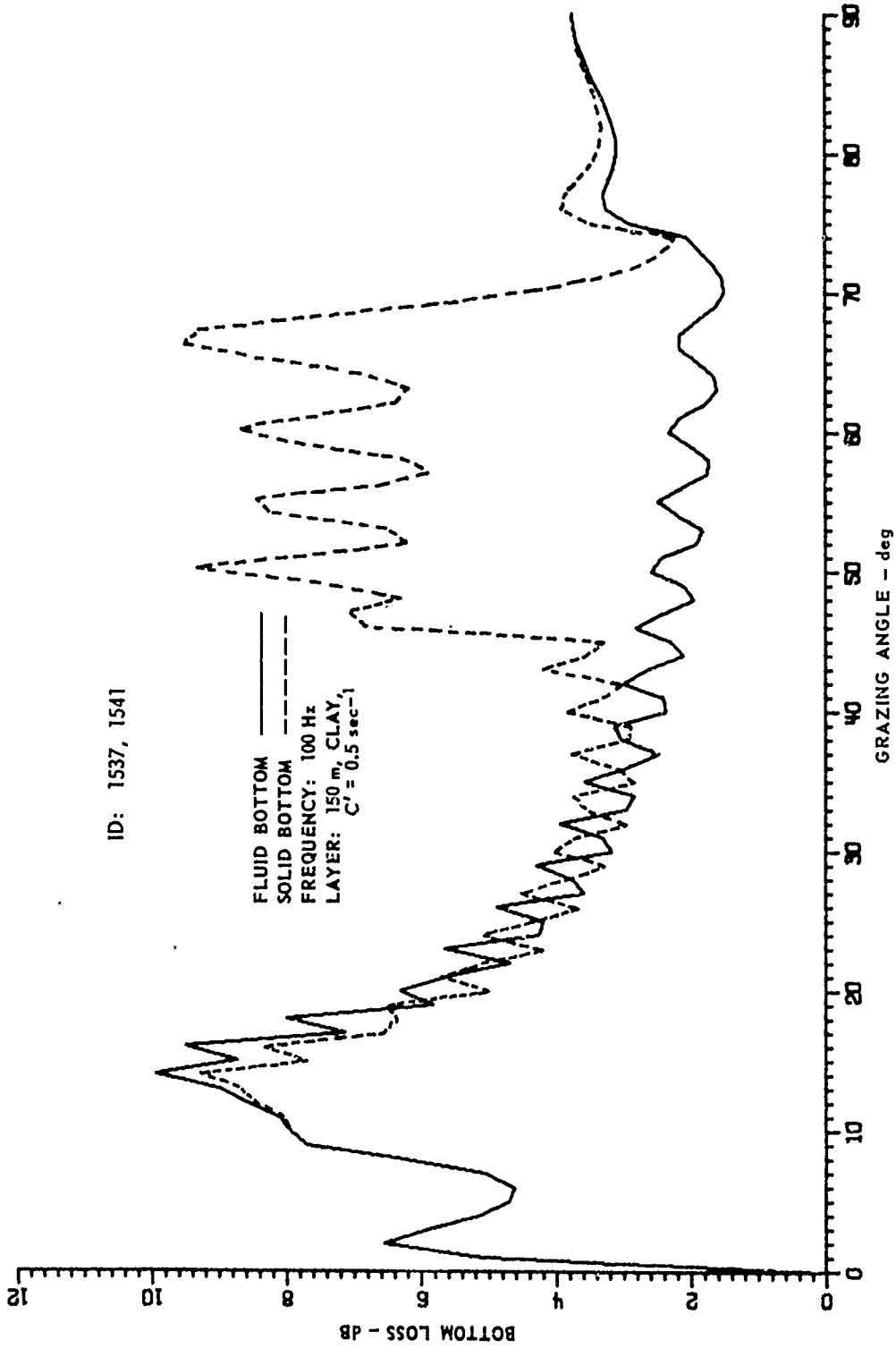

FIGURE III-11
BOTTOM LOSS versus GRAZING ANGLE FOR A 150 m CLAY LAYER HAVING A SOUND SPEED GRADIENT OF 0.5 sec^{-1}

ARL - UT
AS-76-151
KEH - DR
2 - 18 - 76

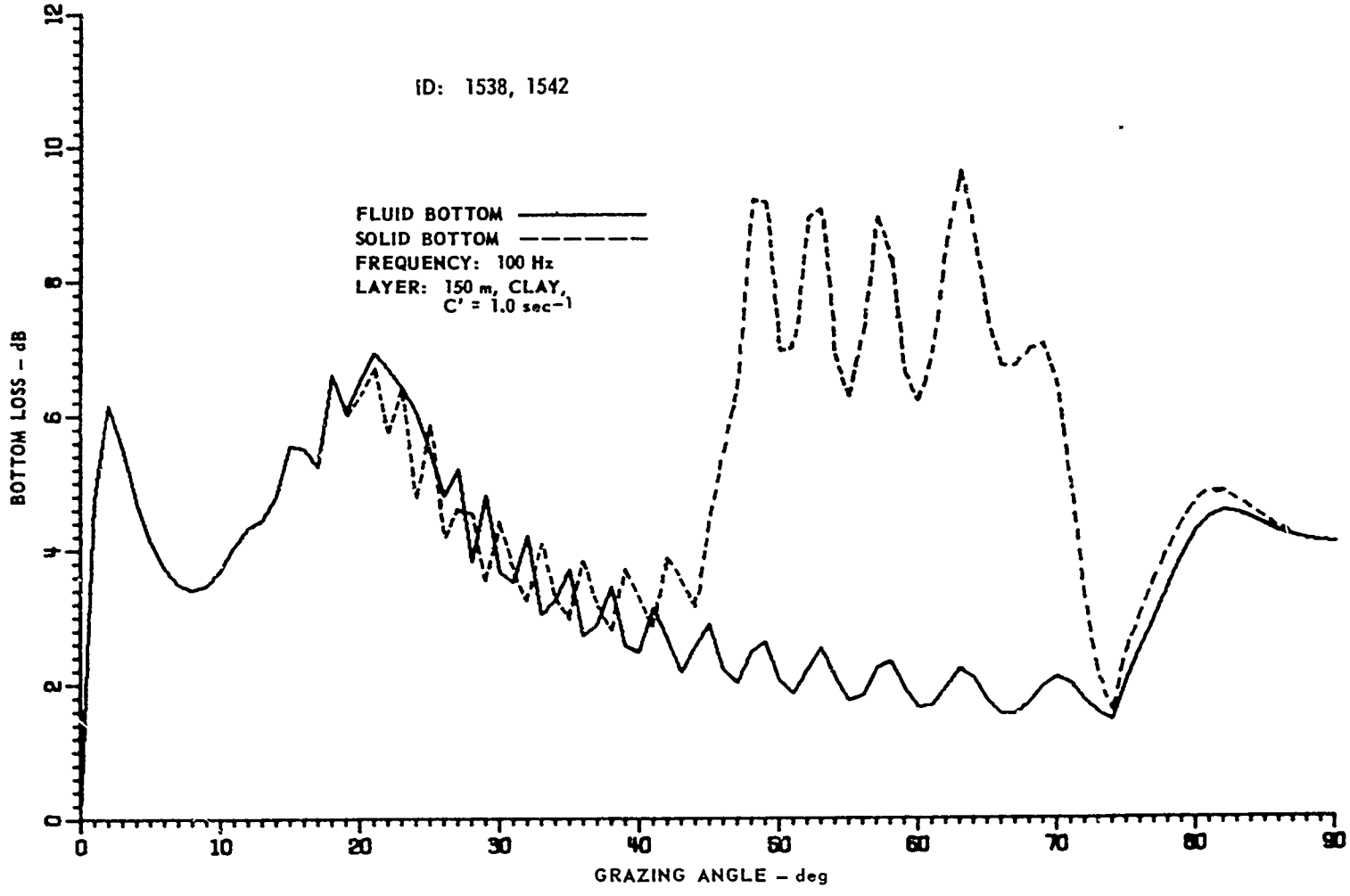

ARL-UT
AS-76-152
KEH-DR
2-18-76

FIGURE III-12
BOTTOM LOSS versus GRAZING ANGLE FOR A 150 m CLAY LAYER HAVING A SOUND SPEED GRADIENT OF 1.0 sec^{-1}

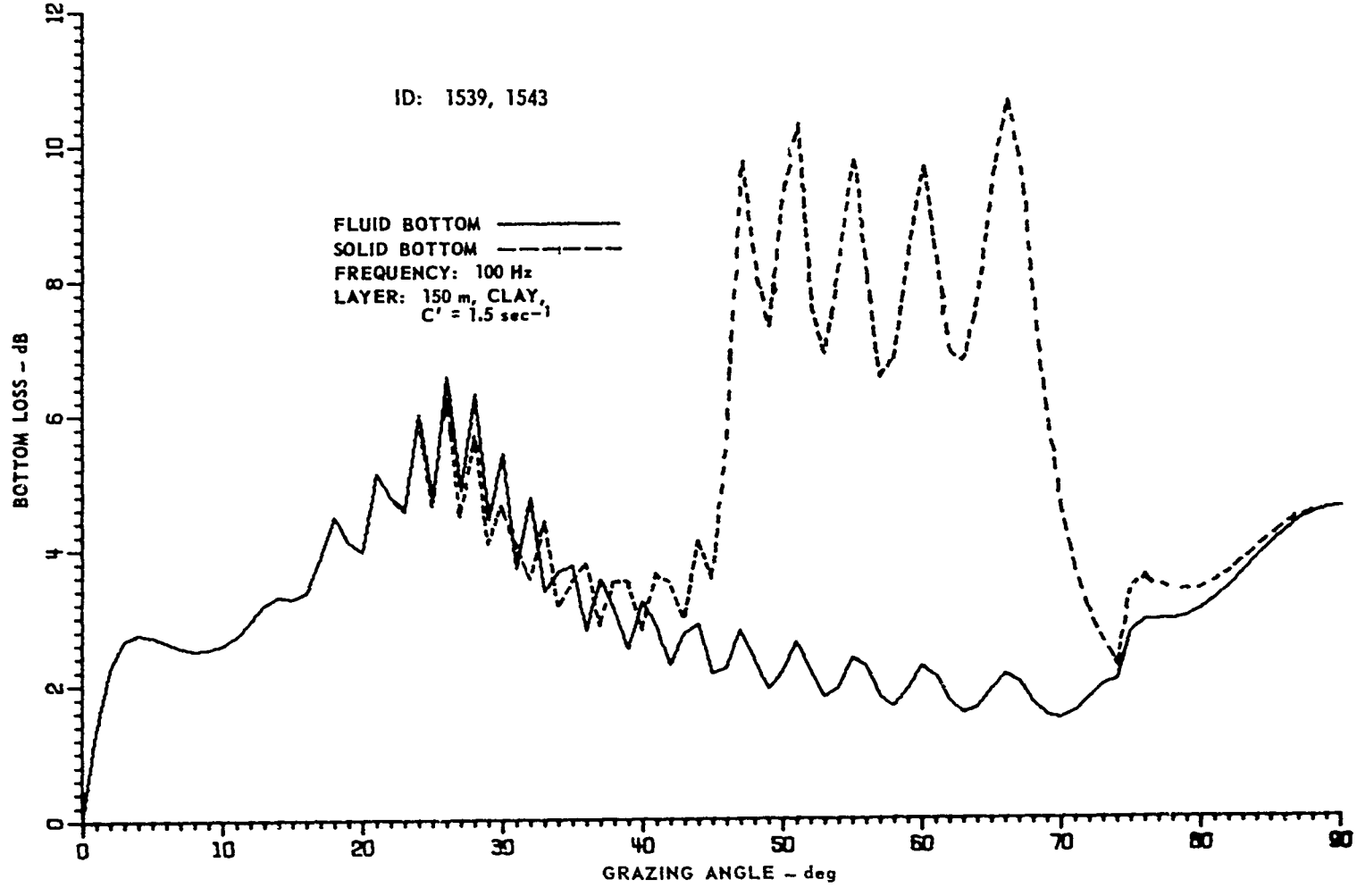

ARL-UT
AS-76-153
KEH-DR
2-18-76

FIGURE III-13
BOTTOM LOSS versus GRAZING ANGLE FOR A 150 m CLAY LAYER HAVING A SOUND SPEED GRADIENT OF 1.5 sec^{-1}

Figures (III-14 through 17) show, for a 500 m and 600 m thickness of clay, the bottom loss based on the linear and pseudolinear models. The sound speed gradient is specified at the top of the layer in the pseudolinear case, and the singularity in the pseudolinear model occurs at 521 m. It will be observed that the curves in the linear case are very nearly identical, whereas significant changes occur in the pseudolinear case. In fact, in the linear case the curves are identical up to a grazing angle of approximately 48°.

The general character of the curves can again be understood on the basis of the turning depth. In the linear case the angles at which the turning depth becomes coincident with the layer thicknesses are 49.3° and 52° for 500 m and 600 m respectively. In the pseudolinear case for 500 m the angle is 79° and is nonexistent for depths greater than 520 m. The general increase in bottom loss in the linear case from 20° to 48°-49° is then simply due to absorption over the longer refracted paths (i.e., the deeper turning points). Beyond 49° some energy is lost into the subbottom, but the pathlengths are shorter and the combination conspires to cause a decrease in loss. The initial peak at 11° is caused by a 4.5 m layer overlying the 500/600 m layer (see Williams[4]).

In the pseudolinear case the curves are found to be coincident up to 74° beyond which there are large differences. The large loss above this angle in the 500 m case is due to energy loss into the substrate. There is no increase in bottom loss at the midangles in the pseudolinear case.

Calculations carried out for thinner layers show that the pseudolinear model is a good approximation to the linear model for layer thicknesses much greater than one might expect. However, since a true linear model can be handled by numerical integration as easily as any other model, no further effort has been made to determine the regime of validity of the pseudolinear model.

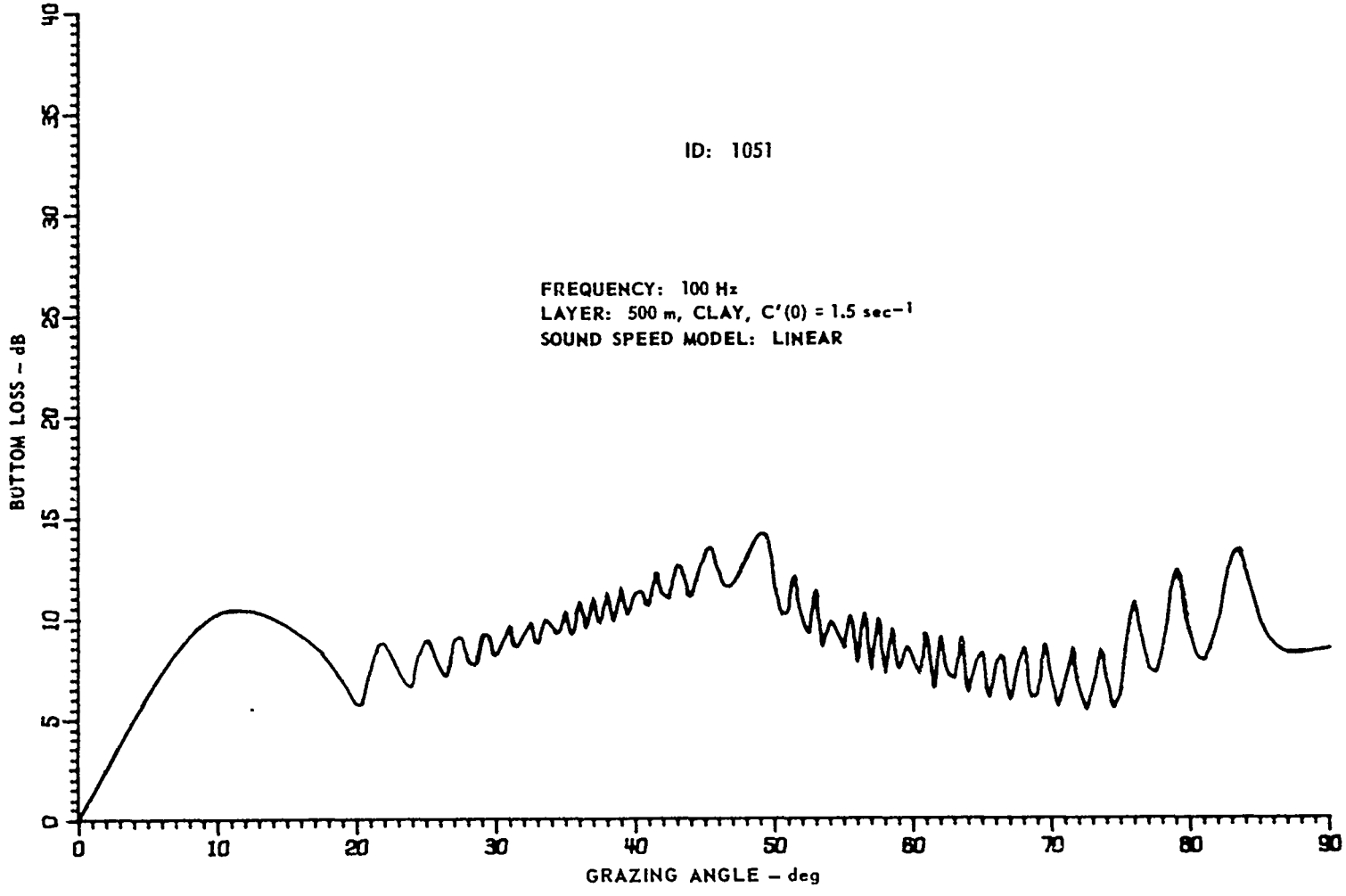

ARL-UT
AS-76-154
KEH-DR
2-18-76

FIGURE III-14
BOTTOM LOSS versus GRAZING ANGLE FOR A 500 m CLAY
LAYER HAVING A CONSTANT SOUND SPEED GRADIENT

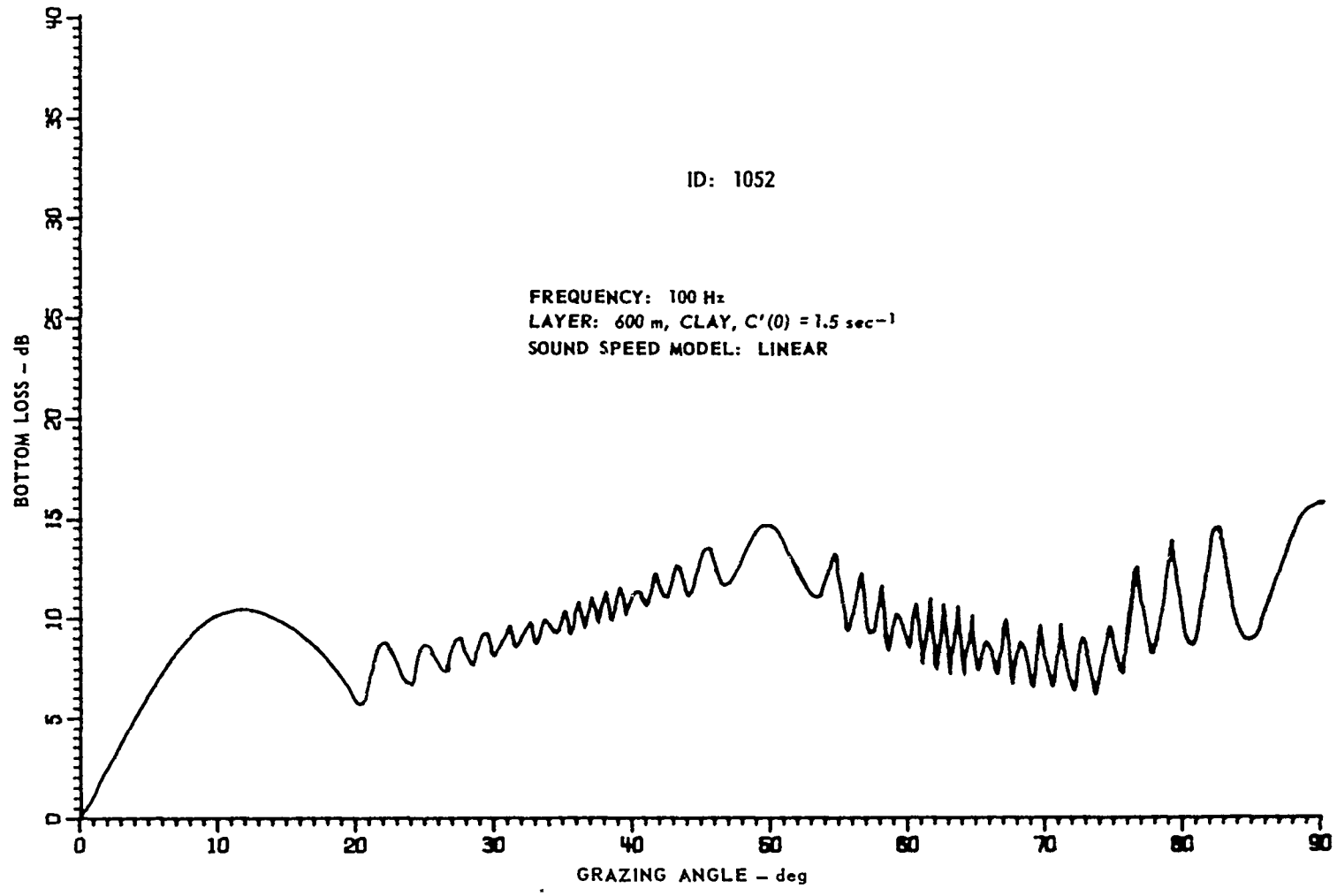

ARL - UT
AS-76-155
KEH - DR
2 - 18 - 76

FIGURE III - 15
BOTTOM LOSS versus GRAZING ANGLE FOR A 600 m CLAY
LAYER HAVING A CONSTANT SOUND SPEED GRADIENT

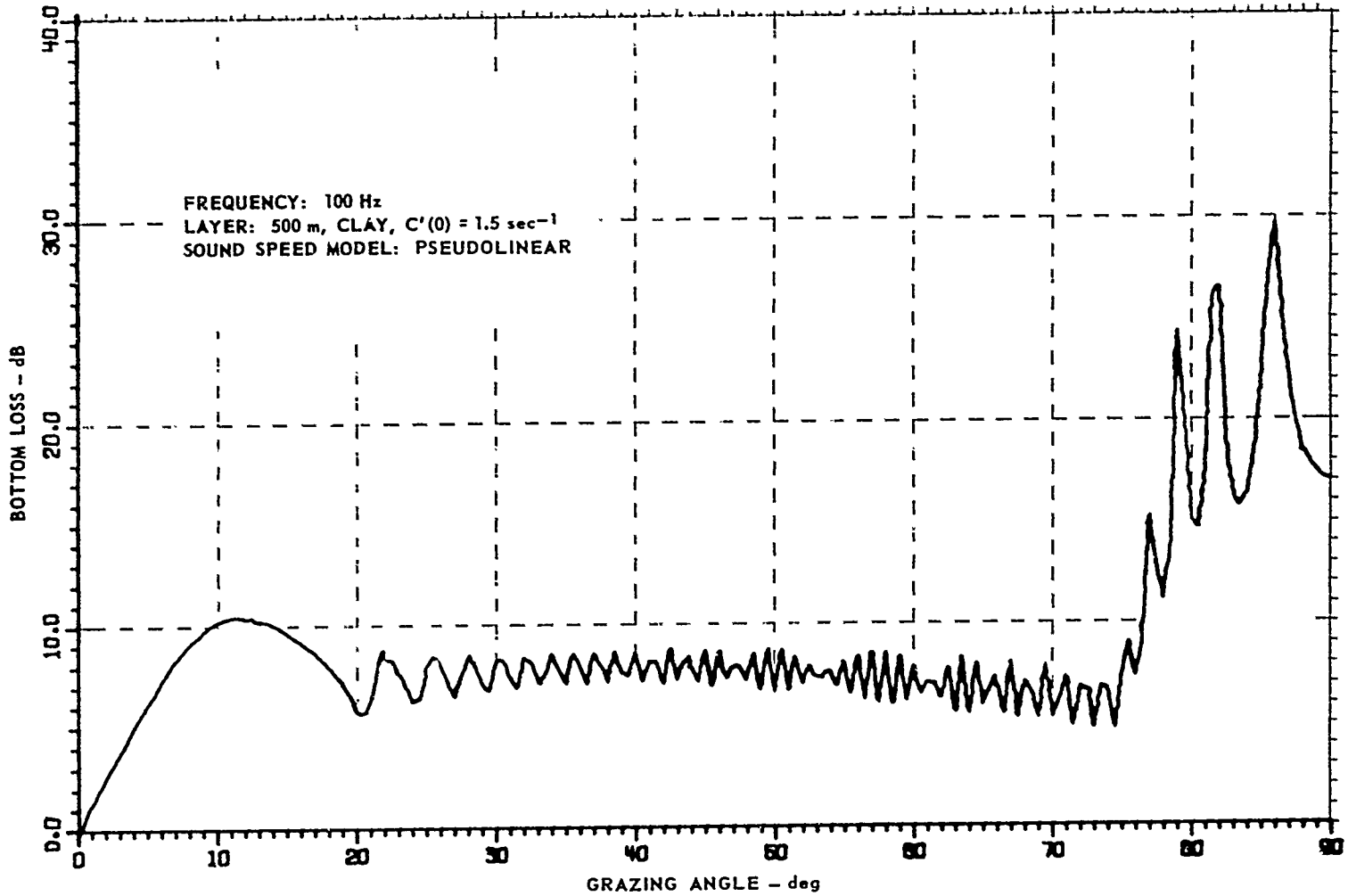

ARL - UT
AS-76-156
KEH - DR
2 - 18 - 76

FIGURE IV.3
BOTTOM LOSS versus GRAZING ANGLE FOR A 500 m CLAY LAYER HAVING A PSEUDOLINEAR SOUND SPEED PROFILE

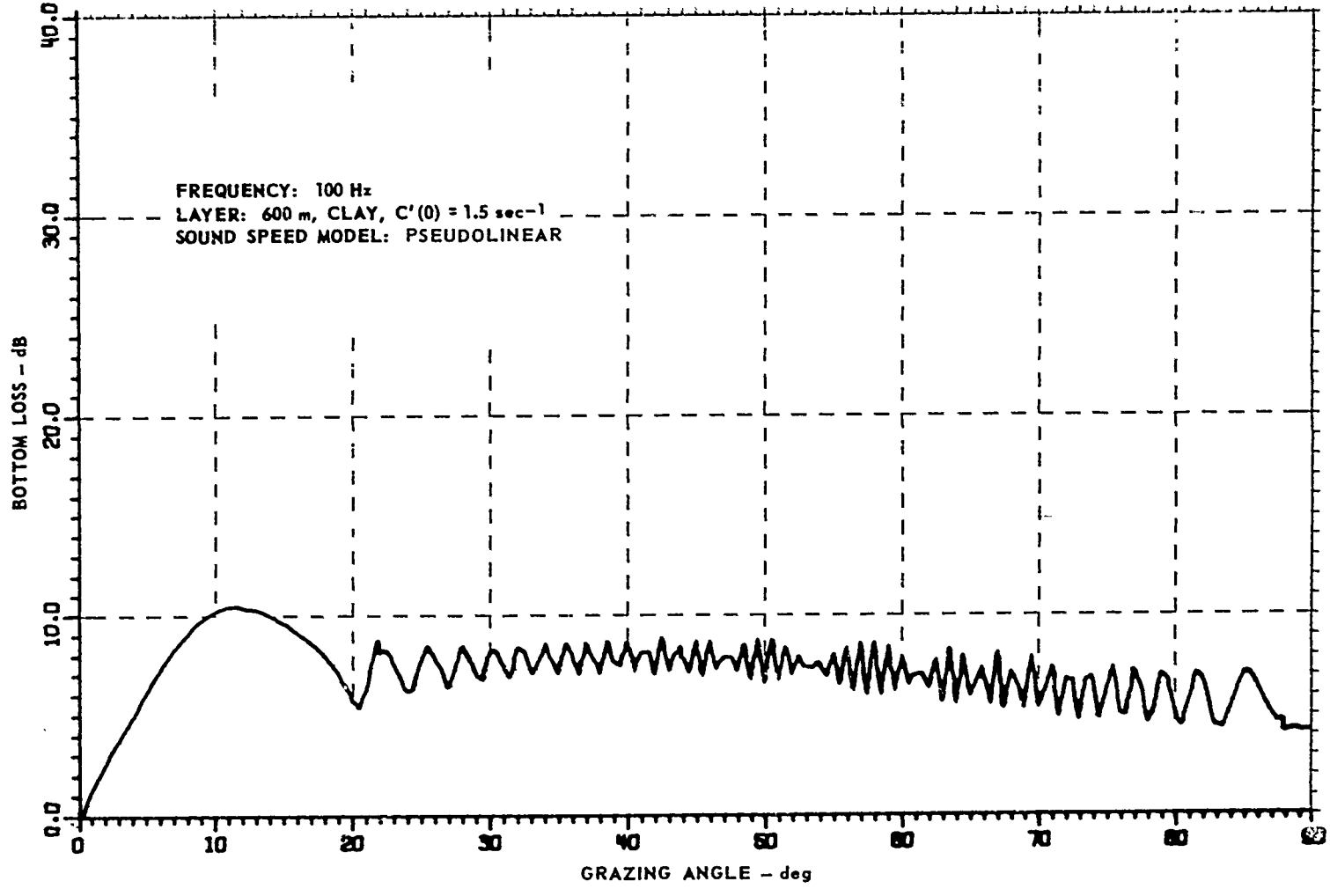

ARL - UT
AS-76-157
KEH - DJR
2 - 18 - 76

FIGURE IV.4
BOTTOM LOSS versus GRAZING ANGLE FOR A 600 m CLAY
LAYER HAVING A PSEUDOLINEAR SOUND SPEED PROFILE

4. Effects of a Density Gradient

As mentioned previously, the presence of a continuously variable density, $\rho(z)$, adds an additional term $(-\rho'/\rho)p/dz$ to the depth separated wave equation for the pressure. Although this has been known for a long time, no systematic effort has been made to determine the effects of a density gradient on bottom loss. Some discussion of the effects of a density gradient has been given by Tolstoy[10,11] and by Gupta[12], although no conclusions are reached which are immediately relevant to this project.

Although only a small amount of experimental data are available, enough is known about density gradients to warrant a theoretical study of the importance of the effect. Studies reported by Nafe and Drake[13] and by Hamilton[14] show an approximately linear increase of density with depth for several sediment types. The maximum gradient reported by Hamilton is 0.002 $g/cm^3/m$ with typical values in the range 0.0005 to 0.0015 $g/cm^3/m$. Although a linear model, $\rho(z)=\rho_o(1+\alpha z)$, is at best only a good approximation, the general importance of a density gradient can certainly be determined using such a model.

The effects of a density gradient on bottom loss have been examined for several cases. Figures (III-18 through 20) display curves for 50, 100, and 200 m of clay overlying a rock (basalt) substrate. The density gradient has the values $\rho'=0$ (solid line) and $\rho'=0.002$ dotted line. From these curves one can conclude:

1. the effects of a density gradient are small for most angles,
2. the effects of a density gradient increase with increasing layer thickness, and
3. at low angles the only appreciable effect will be on the low angle shear wave anomaly, if it is present. This effect can be large.

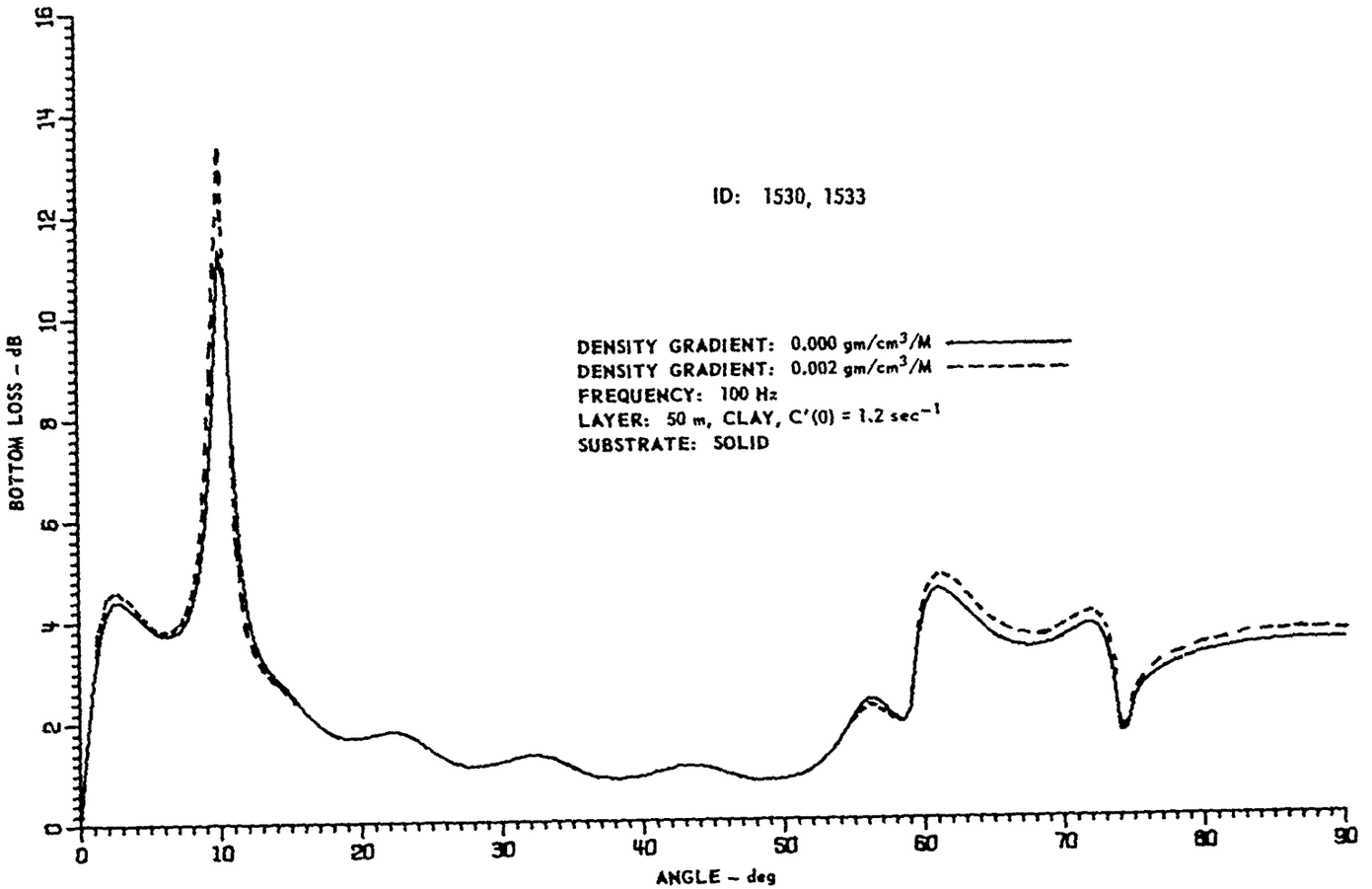

ARL-UT AS-76-158 KEH-DR 2-18-76

FIGURE III-18
BOTTOM LOSS VERSUS GRAZING ANGLE FOR A 50 m CLAY LAYER WITH AND WITHOUT A DENSITY GRADIENT

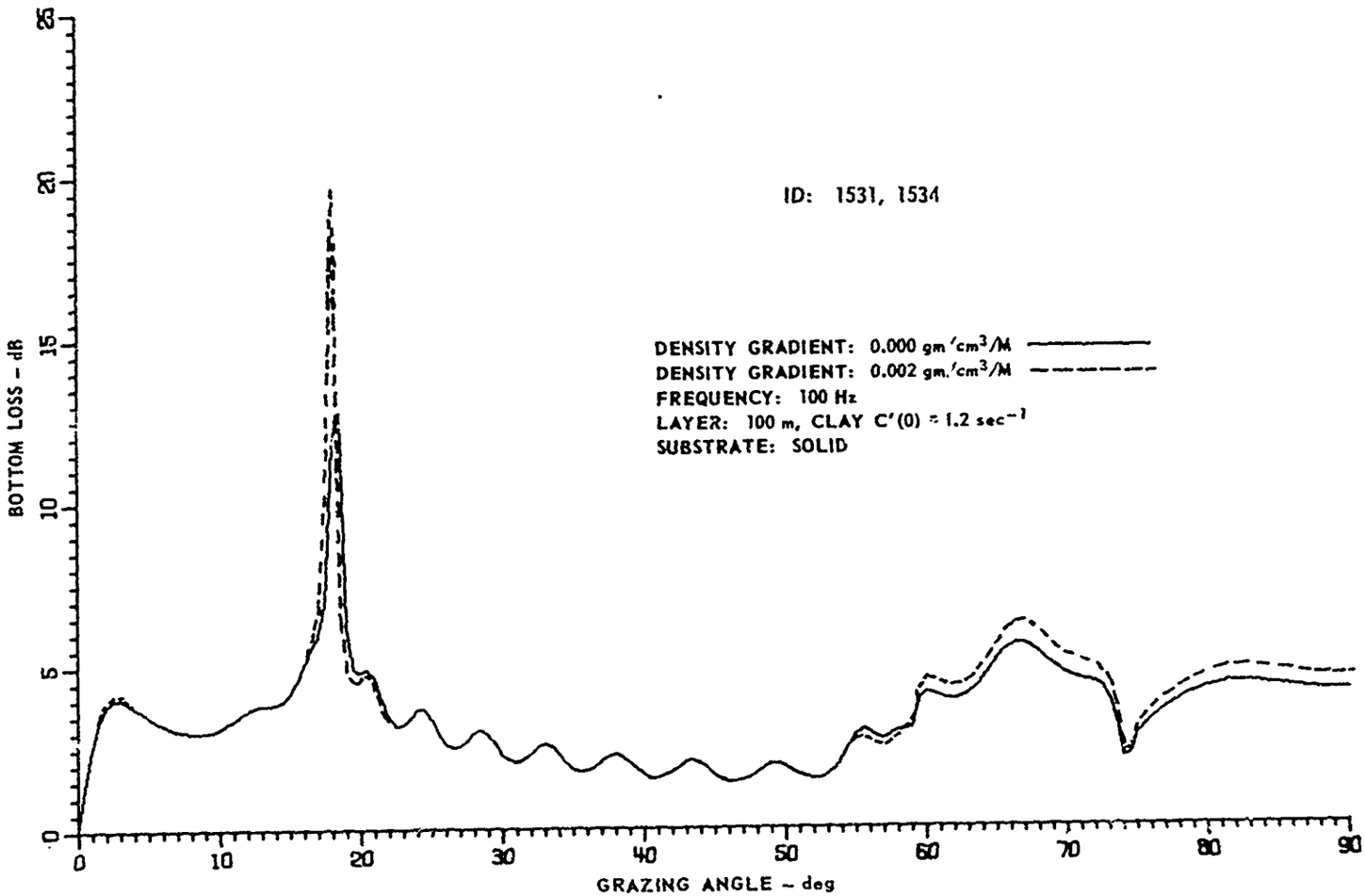

ARL - UT
AS-76-167
KEH - DR
2 - 18 - 76

FIGURE III - 19
BOTTOM LOSS versus GRAZING ANGLE FOR A 100 m CLAY LAYER WITH AND WITHOUT A DENSITY GRADIENT

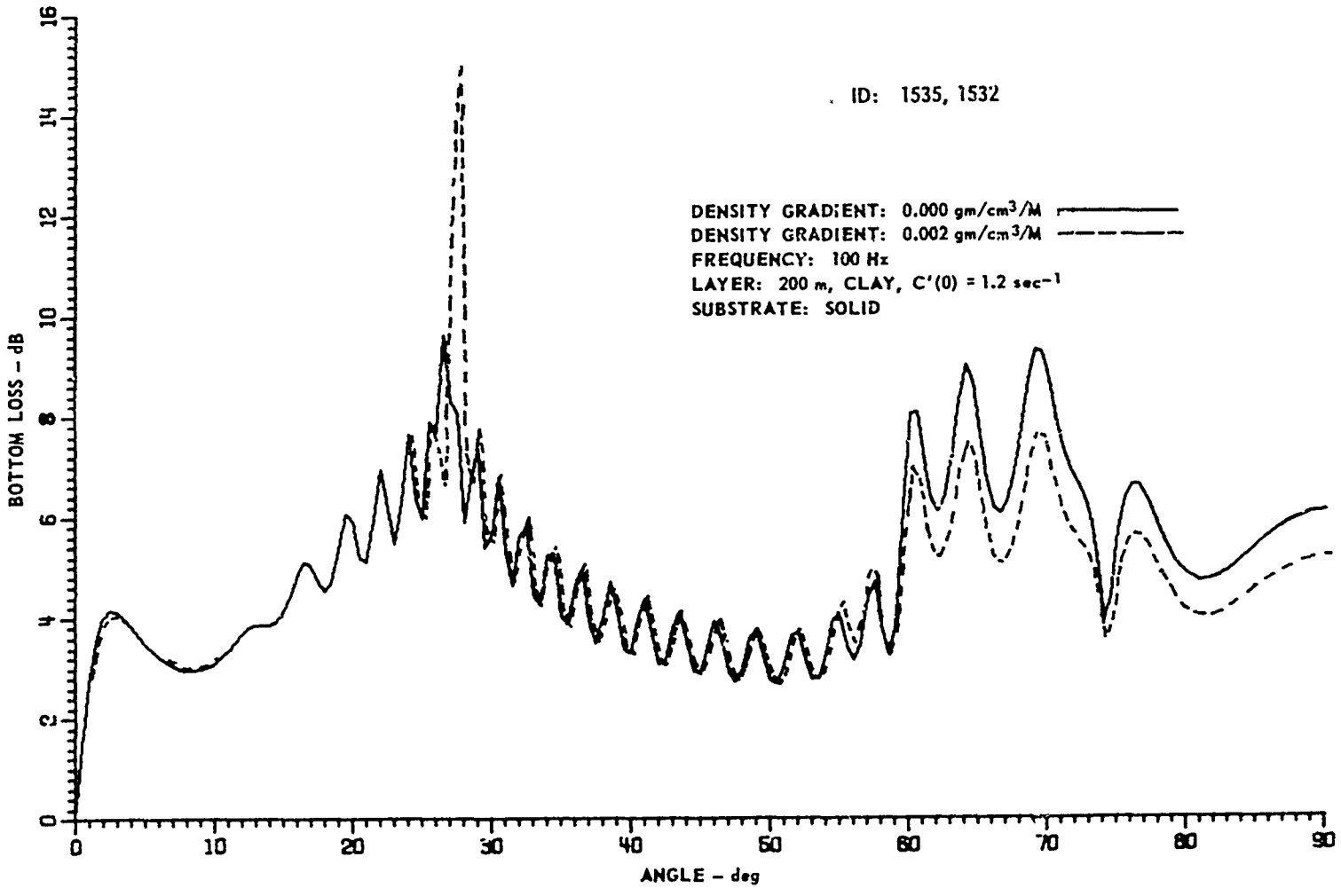

ARL - UT
AS-76-168
KEH - GR
2 - 18 - 76

FIGURE III-20
BOTTOM LOSS VERSUS GRAZING ANGLE FOR A 200 m CLAY
LAYER WITH AND WITHOUT A DENSITY GRADIENT

Figure (III-21) shows the results of smoothing several bottom loss curves for a 200 m clay layer overlying a rock substrate. Again, it is apparent that the effect of a density gradient of a physically plausible size is small, especially at low angles. At higher angles the dominant effect occurs between the shear wave critical angle, 45°, and the compressional wave critical angle, 74°, of the substrate.

From these studies we can conclude that the maximum modification of the bottom loss by a density gradient of presently known magnitude is on the order of 1 dB at low grazing angles. A possible exception to this is the low angle shear wave anomaly where a larger effect could occur.

D. Prognosis

Both model development work and sensitivity studies have been carried out this year. The state of this problem is summarized below and future directions are indicated.

1. Model Development

(1) The presently existing model works well and can incorporate essentially arbitrary profiles of sound speed and density. Shear waves are included in the substrate, but not in the sediment layers. A wide variety of input-output options make the program versatile and useful.

(2) Numerical error is controlled, but a running estimate of overall (global) error is as yet unavailable.

(3) Improvements in the computer code designed to shorten running time are nearly completed. An improvement of 50 to 100% is expected for thick layers or higher frequencies.

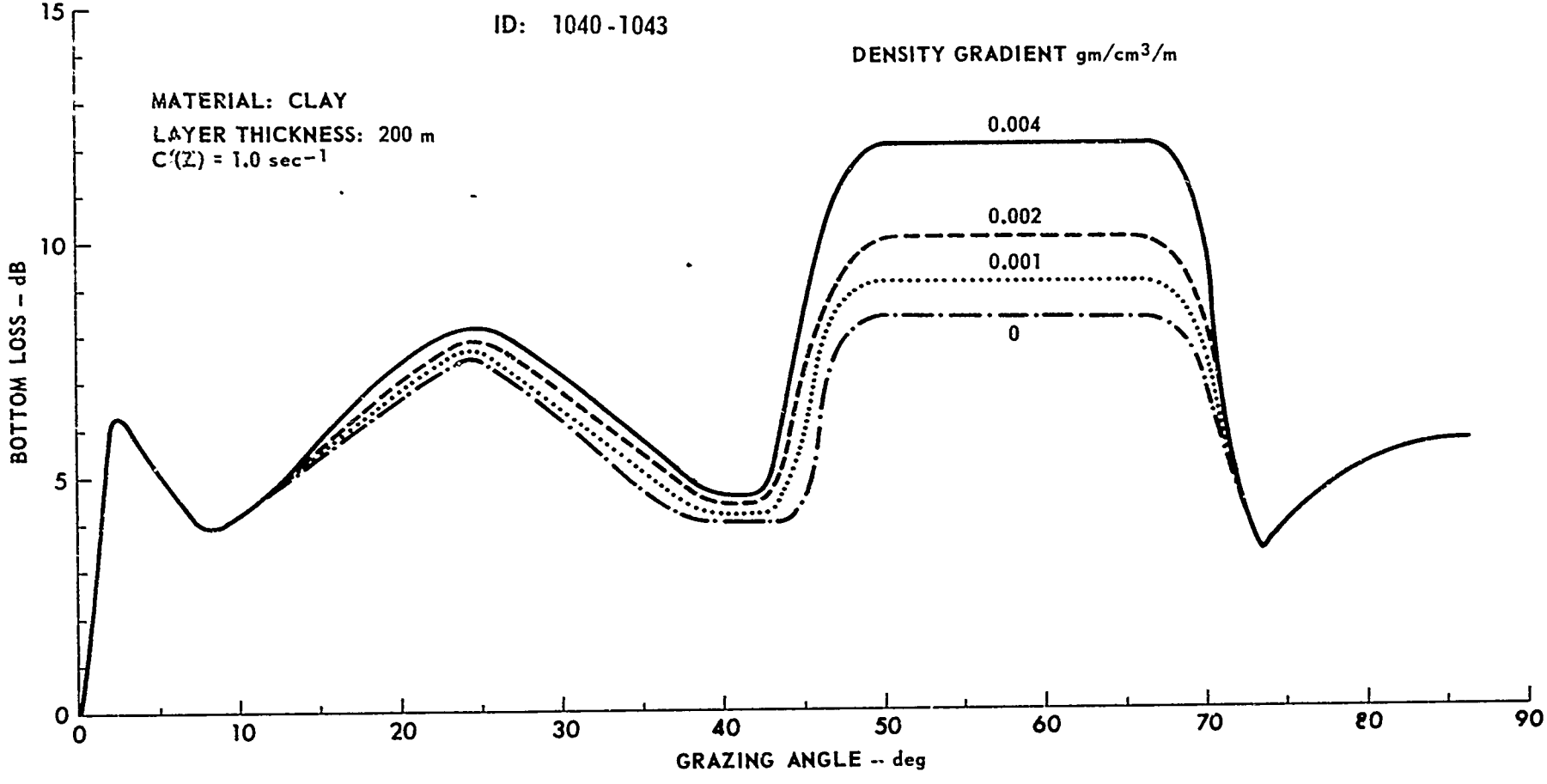

FIGURE III-21
BOTTOM LOSS VERSUS GRAZING ANGLE
FOR VARIOUS DENSITY GRADIENTS

ARL - UT
AS-76-43
KEH - DR
1 - 19 - 76

(4) An effort will be made to further decrease running time through a hybrid numerical-analytical method. This will make possible practical application beyond the present 50 to 100 λ limitation.

(5) An effort will be made to incorporate shear waves in the sediment layers as well as in the basement.

(6) An input option will be provided so that density and sound speed can be input as a sequence of discrete points with no assumption concerning functional dependence on depth.

2. Application to Sensitivity Assessment

(1) The hidden depth question has been investigated and, at 100 Hz, was found to lie within several wavelengths of the ray turning depth.

(2) Additional work in this direction must include an accurate characterization of the hidden depth for a variety of types of layering.

(3) The effects of shear waves in the substrate have been investigated and it was found that the dominant effects occurred between the shear wave critical angle ($\cong 50°$) and the compressional wave critical angle ($\cong 70°$).

(4) At low angles, in the case of clay and possibly silt, but not sand, there can occur a very large bottom loss over a narrow angular range. The cause of this is still being studied.

(5) The effects of a density gradient have been investigated and found to be small. At high angles--above the shear critical angle--the effects amount to 1 to 2 dB change in the bottom loss. At low angles very little effect is observed except in the vicinity of the low angle shear anomaly where it can amount to 2 to 8 dB.

(6) The direct effects of a sound speed gradient were investigated and found to be very large at low angles, indicating that refraction and absorption are quite important. Further work is being devoted to quantify the effects.

(7) The linear and psuedolinear models were compared and although the psuedolinear model was found to be a good approximation over a wide range of input parameters, its limitations on layer thickness preclude its use in the present studies.

(8) Future work involving sensitivity to changes in other physical parameters will require a well thought-out method of organization and parameterization of the data to avoid a large catalog of curves as the only result. In particular, following the work of Hamilton[14,15] and Akal,[16] most geoacoustic sediment properties can be empirically related to porosity. One approach would then be to parameterize bottom loss versus grazing angle as a function of porosity.

REFERENCES

1. Morris, H. E., "Bottom-Reflection Loss Model with a Velocity Gradient," J. Acoust. Soc. Am. 48, 1198 (1970).

2. Morris, H. E., "Comparison of Calculated and Experimental Bottom-Reflection Losses in the North Pacific," Naval Undersea Center Report, NUC TP 327 (1972).

3. Morris, H. E., "Bottom Reflection Model Validation with Measured Data from FASOR III Stations in the Pacific and Indian Oceans," Naval Undersea Center Report, NUC TP 460 (1975).

4. Williams, A. O., Jr., "Acoustic Reflection from a Structured Sea Bottom," J. Acoust. Soc. Am. 59, 62 (1976).

5. Abramowitz, M., and A. Stegun (eds.), Handbook of Mathematical Functions (National Bureau of Standards, Washington, 1964).

6. Olver, F. W. J., "The Asymptotic Expansion of Bessel Functions of Large Order," Phil. Trans. Roy. Soc. (London) A247 328 (1954).

7. Bergmann, P. G., "The Wave Equation in a Medium with a Variable Index of Refraction," J. Acoust. Soc. Am. 17, 329 (1946).

8. Brekhovskikh, L. M., Waves in Layered Media (Academic Press, New York, 1960).

9. Shampine, L. F., and R. C. Allen, Numerical Computing: An Introduction (W. B. Saunders Company, Philadelphia, 1973).

10. Tolstoy, I., "The Theory of Waves in Stratified Fluids Including the Effects of Gravity and Rotation," Rev. Mod. Phys. 35, 207 (1963).

11. Tolstoy, I., "Effects of density stratification on sound waves," J. Geophy. Res. vol. 70, p. 6009 (1965).

12. Gupta, R. N., "Reflection of plane elastic waves from transition layers with arbitrary variation of velocity and density," Bull. Seis. Soc. Am. 56, 633 (1966).

13. Nafe, J. E., and C. L. Drake, "Variation with depth in shallow and deep water marine sediments of porosity, density, and the velocity of compressional and shear waves," Geophysics vol. 22, p. 523 (1957).

REFERENCES (Cont'd)

14. Hamilton, E. L., "Acoustic and Related Properties of the Sea Floor: Density and Porosity Profiles and Gradients," Naval Undersea Center Report, NUC TP 459 (1975).

15. Hamilton, E. L., "Prediction of Deep-Sea Sediment Properties: State-of-the-Art," Deep-Sea Sediments: Physical and Mechanical Properties, A. L. Inderbitzen (ed.) (Plenum Press, New York, 1974).

16. Akal, T., "The Relationship between the Physical Properties of Underwater Sediments that Affect Bottom Propagation," Marine Geology 13, 251 (1972).

IV. THE EFFECTS OF BOTTOM ROUGHNESS ON PROPAGATION

A. Introduction

The purpose of this task is to assess the importance of bottom roughness in long range acoustic propagation in the ocean. Such an assessment necessarily requires consideration of the validity of various methods of accounting for roughness. Before discussing such methods, a brief comment will be made on the nature of the roughness itself and its expected effects discussed qualitatively.

For purposes of this study the entire spectrum of bathymetry variation is divided into two classes, sloping bottom (deterministic) and rough bottom (stochastic). The surface roughness component is the small scale roughness which does not show up on an ordinary bathymetric chart. The vertical relief of such roughness ranges upward to several tens of meters although more typical values are of the order of a few meters or less. A more detailed breakdown of roughness scales for a region of the eastern Atlantic has been given by Clay and Leong.[1] At typical echo sounder beamwidths, the horizontal resolution in the deep ocean basins is on the order of a few kilometers. Since the horizontal wavelength of roughness features of the type we are considering is expected to be on the order of a few hundred meters, this roughness will not be resolvable with such depth sounders. Larger scale bottom variations are considered together under the general heading of sloping bottoms and in this chapter we shall deal with a small (stochastic) component superimposed on these.

B. The Reflection Coefficient Approach

The reflection coefficient method is based upon two essentially simple observations: (1) scattering from an irregular surface is

described, relative to a plane surface, by a scattering (reflection) coefficient, and (2) it is possible to replace a direct calculation of the field in the bottom material with a reflection coefficient and deal with the field in the water only. This is possible within either a ray or wave theory approach. A consequence of these ideas is that scattering may be accounted for in a propagation problem by multiplying the ordinary reflection coefficient by the scattering coefficient and treating the product as a modified reflection coefficient.

This view, if correct, would indeed be useful because it allows separation of the scattering and propagating problems. The scattering problem, though still difficult, is much better understood than the combined scattering-propagation problem. Moreover, there is a body of empirical knowledge which suggests that this view is largely correct.

Initial work on this problem was to examine the range of validity of the underlying scattering theory, to use it for making estimates of scattering loss which could be used in propagation loss calculations. The remainder of this section will discuss the conventional view and what can be learned from it. The last section of this chapter will discuss alternate approaches.

A systematic and careful effort to derive the (coherent) scattering coefficient for penetrable rough interfaces was made by Boyd et al.[2] After writing integral expressions for the scattered and transmitted fields, using continuity of pressure and normal component of velocity, and making a single scattering assumption, these authors arrive at an expression for the scattered field which contains, in addition to conventional scattering terms, the ordinary reflection coefficient. However, in this case, it is referenced to the local surface slope, not the (zero) slope of the mean plane of the interface. Far from the interface the scattered pressure field in the specular direction, for a point source, is given by

$$p_s = \frac{ik}{2\pi} \iint \frac{e^{ik(R_o+R_1)}}{R_o R_1} e^{-ik\gamma\zeta} R(\theta,n)[\eta \cos\theta - \sin\theta]dx\,dy, \quad (1)$$

where the surface height is $\zeta(x,y)$ and $\eta=\partial\zeta/\partial y$, R_o and R_1 are distances from source and field points to the area element, and $R(\theta,n)$ is the usual reflection coefficient referred to the local slope η. The coherent field is then given by

$$\begin{aligned} \langle p_s\rangle &= \langle e^{-ih\gamma\zeta}\rangle \frac{ik}{2\pi} \iint dx\,dy \frac{e^{ik(R_o+R_1)}}{R_o R_1} \langle R(\theta,\eta)[\eta\cos\theta - \sin\theta]\rangle \\ &= \langle e^{-ik\gamma\zeta}\rangle \langle R[\eta\cos\theta - \sin\theta]\rangle P_o \quad , \end{aligned} \quad (2)$$

where $\gamma = 2\sin\theta$ and $\langle e^{-ik\gamma\zeta}\rangle$ is the characteristic function of surface relief, and p_o is the pressure reflected from a perfectly reflecting plane surface (image solution).

The important points to be noted are (1) that Boyd et al. do not obtain the "expected" result $\langle p_s\rangle=\langle e^{-ih\gamma\zeta}\rangle Rp_o$, with R the usual reflection coefficient, and (2) if $R(\theta,\eta)$ were not a function of η the usual result would be obtained since $\langle\eta\rangle=0$. This last conclusion does not hold away from the specular direction due to shadowing corrections which make $\langle\eta\rangle\neq 0$. Another oddity of this theory is that when it is specialized to a perfectly reflecting interface, $|R|=1$, there remains an anomalous factor of $1 - \langle\eta\rangle \cot\theta_r$ which, due to shadowing corrections, becomes unity only in the specular direction.

The presence of slope dependent terms both in R, and in the scattering slope corrections as well as the concomitant shadowing corrections, are the distinguishing aspects of this theory. Due to the difficulties of evaluating the average $\langle R(\theta,\eta)[\eta\cot\theta - 1]\rangle$, Boyd et al. were only able to examine $\langle p_s\rangle/p_o$ in a very rough approximation which broke down near a critical or intromission angle. In order to test

more fully the dependence of $\langle p_s \rangle / p_o$ on the distribution of slopes and other parameters, a computer program was written to carry out numerically the one-dimensional integral yielding the slope averaged term $\langle R(\theta,\eta)[\eta \cot \theta - 1] \rangle$. Apart from a factor of $\langle e^{-ik\gamma\zeta} \rangle$, this is the roughness dependent reflection coefficient. In Figs. (IV-1-2) appear several examples of bottom loss where this roughness dependent reflection coefficient term has been neglected, not because it is unimportant, but for the purpose of displaying the effects of the slope dependent terms. The sediment-to-water sound speed ratio is denoted by N_o and the sediment-to-water density ratios are given by ρ_2/ρ_1. In all cases the rms slope, s, is 14° for the rough interfaces (and 0° for the flat), which corresponds to what would be commonly thought of as a very rough surface. The ratio α/β is the ratio of the imaginary to the real part of the wave number $k=\beta+i\alpha$. It is clear that the effects of surface slope on bottom loss are appreciable and moreover that this effect is more pronounced for larger values of absorption (larger α/β). At high angles the curves for flat and rough surfaces converge rapidly.

Of course, the true bottom loss, according to this theory, is obtained by multiplying the factor plotted in Figs. IV-1, IV-2 by the additional term $\langle e^{-ih\gamma\zeta} \rangle$. For a normally distributed surface this equals $e^{-g/2}$, where $g=(k\gamma\sigma)^2$ and σ is the rms surface height. For example, at 100 Hz and 10° for an rms height of 1 m this factor is approximately 0.1 dB and therefore produces only a small additional modification of the plotted bottom loss.

The large effect of roughness shown in Figs. IV-1 and IV-2 is, of course, reduced considerably when the rms slope is taken to be a more realistic figure of a few degrees. Nevertheless, the fact that surface slopes can cause such large changes in the reflection coefficient is disturbing and at variance with intuition. Moreover, the effects of shadowing are not necessarily small since, without such corrections, the scattering coefficient is unbounded near 0°. The shadowing "corrections" are therefore seen to be necessary to make the theory well defined and are not necessarily small.

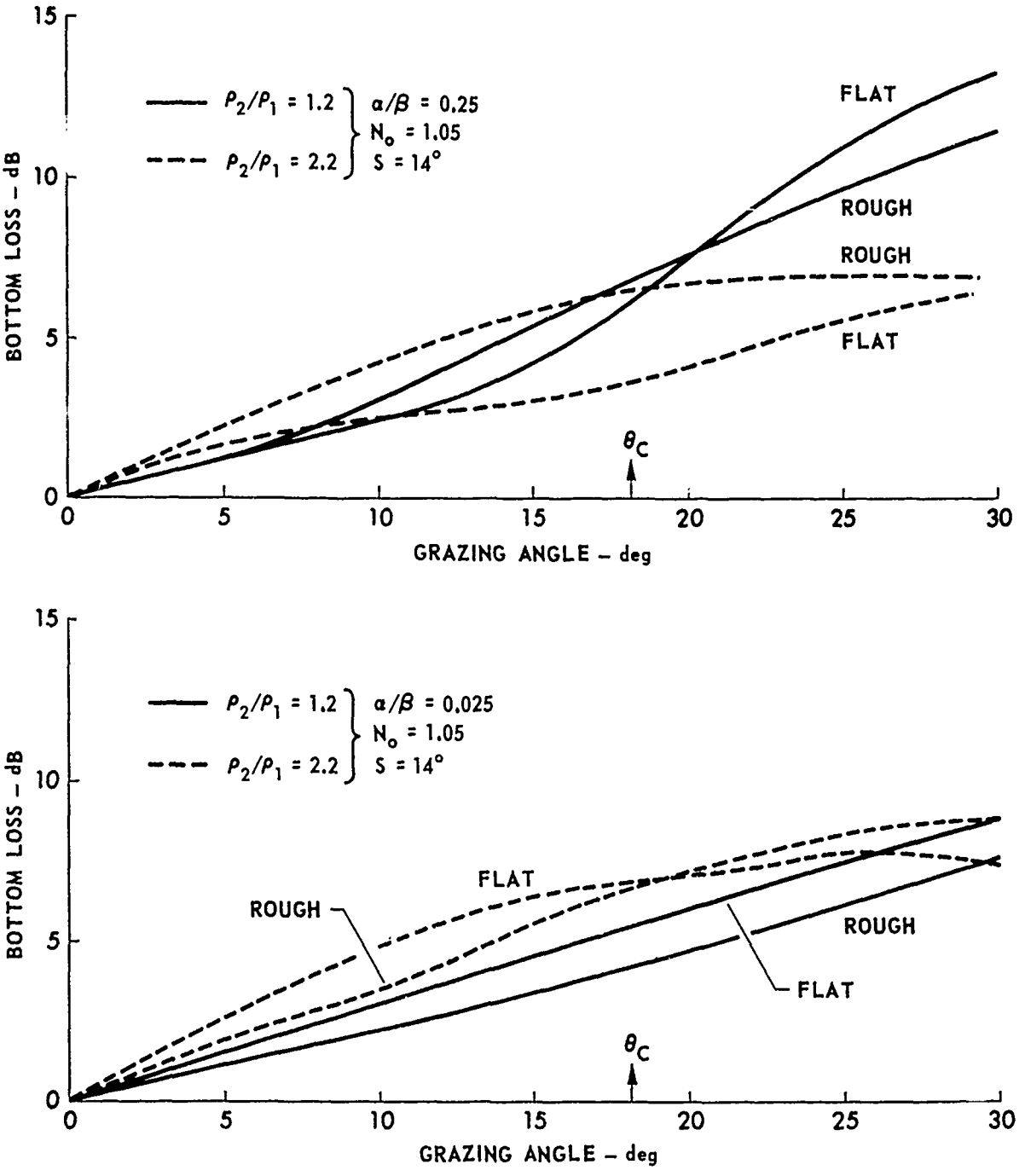

FIGURE IV-1
BOTTOM LOSS VERSUS GRAZING ANGLE
FOR THE CASE OF A FAST BOTTOM

ARL - UT
AS-76-90
KEH - DR
2 - 4 - 76

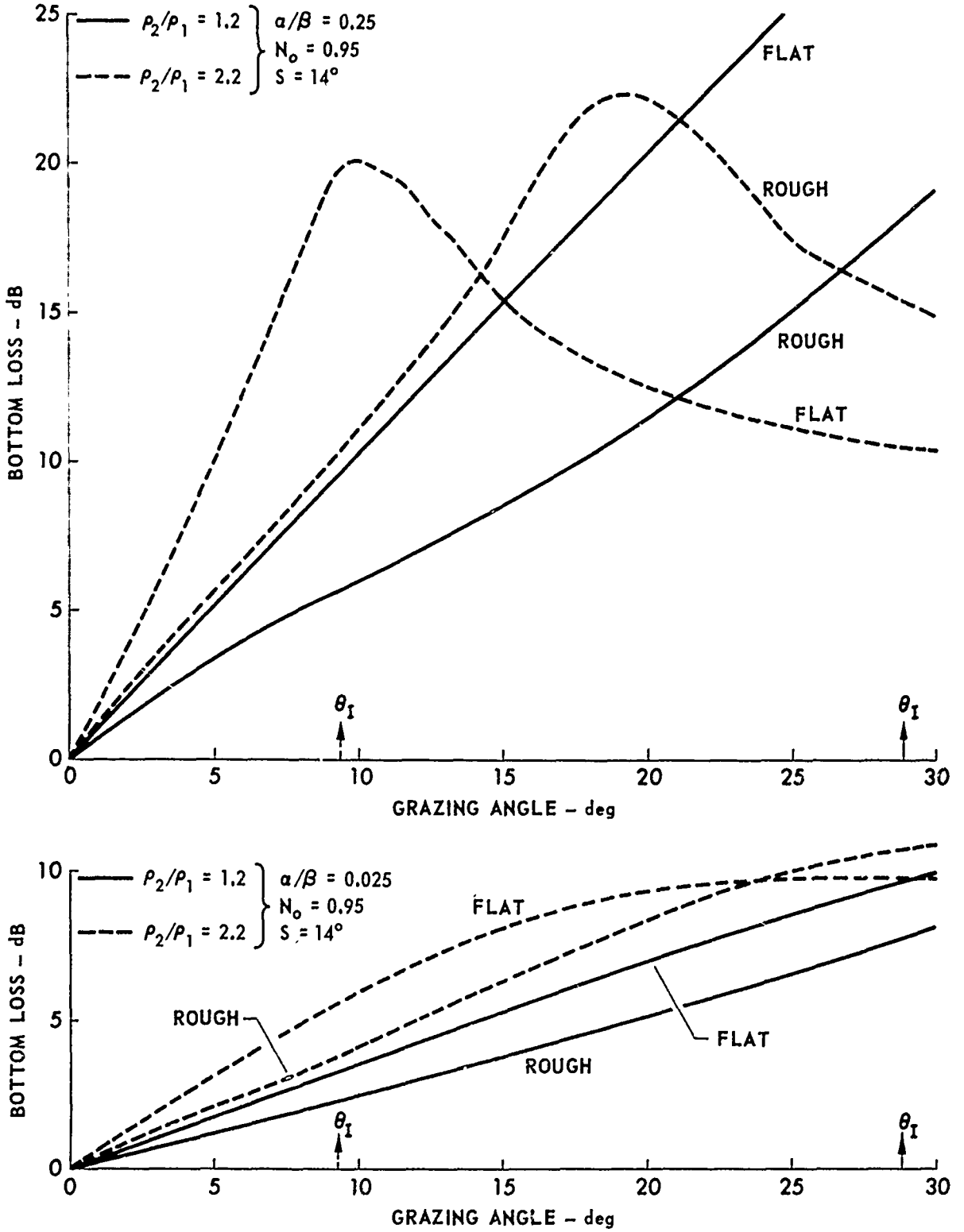

FIGURE IV-2
BOTTOM LOSS VERSUS GRAZING ANGLE
FOR THE CASE OF A SLOW BOTTOM

ARL - UT
AS-76-91
KEH - DR
2 - 4 - 76

It is characteristic of physical theory that a small correction in the development which leads to a large change in the prediction may be indicative of an error. The problem in this theory may be the single scattering assumption which strictly requires zero surface slopes. It is quite plausible that, to remain consistent with the original single scattering assumption, the surface slopes must be taken to be zero thereafter. If this is done the result for the coherent field is simply $\langle p_s \rangle = \langle e^{-ih\gamma\zeta} \rangle p_o$, the classical result.

From the point of view of simplicity and predictability, it would be desirable for the classical result to be correct and useful in propagation modeling. The classical coherent scattering coefficient can be made to agree quite well with scattering data. For example, Boyd and Deavenport[3] show such a curve for scattering from pressure release surfaces, and the agreement is excellent. The impact of such close agreement is lessened by the realization that the results are quite sensitive to the choice of the distribution of heights. Nevertheless, the simple coherent scattering coefficient is the best founded result of scattering theory and it is important to know just what its limitations are and how far its usefulness extends.

C. Further Considerations

To understand what is entailed in such a reflection coefficient description, it is helpful to discuss qualitatively the expected physical effects of boundary roughness on propagation. From scattering theory we know that the scattered field above the interface is composed of a mean field $\langle \varphi \rangle$ and a stochastic field ψ such that the mean (coherent) field is highly concentrated in the specular direction. Moreover, the stochastic (incoherent) field, although contributing in the specular direction, is more diffuse and becomes increasingly so with increasing roughness.

In a propagation problem these simple facts imply that acoustic energy encountering the bottom is partitioned in two ways: the first is the division into mean and stochastic fields, whatever the angle; the second is between specular and nonspecular components. For a slightly rough surface (Rayleigh parameter of the order of unity or less) the coherent field may be regarded as being identical with the specular component, whereas the nonspecular component is entirely stochastic.

If this assumption is valid, it therefore follows that the stochastic field enters the propagation theory through mode-mode coupling or, in ray theory terms, multipath conversion. This relatively simple picture is complicated by multiple scattering in the vicinity of the rough surface, which causes the fields to be coupled.

This brief discussion brings out two significant features of the problem which are often lost in an eagerness to apply some simple reflection coefficient formula. Within scattering theory itself, it is clear that the distinction between mean and stochastic fields is of paramount importance, as is the fact that energy leaving the rough interface will do so in all directions, not only in the specular one. The most serious step in applying scattering theory results is the restriction to the specular direction. If this is valid, then for slightly rough surfaces the coherent field will dominate in a scattering situation.

The only remaining problem then is to argue that these results can be applied in a propagation situation. The extension is not necessarily possible (much less simple) since scattering is mathematically an exterior problem, whereas propagation is an interior one. The approximate solution to the field in the exterior case is being asked to provide an appropriate boundary condition in the interior case.

These questions have not yet been satisfactorily resolved, although it appears that there are tools available which can be used to at least

provide partial answers. A potentially useful approach to the problem of obtaining a correct boundary condition for the coherent field was the work by Lysanov[4] on pressure release surfaces. This work was extended to the two-fluid case by Kuperman.[5] Related work in this direction has also been reported by Wenzel.[6] This approach is not based upon scattering theory, but rather seeks to replace the exact boundary conditions on a surface $z=H+\zeta(x,y)$ with approximate boundary conditions on the mean plane $z=H$. The results are to be found only to lowest order in ζ, the stochastic function describing surface relief. The power of this method is that it indisputably sets out to obtain a boundary condition on the mean plane rather than extending an expression for the field at a distant point back to the surface. Also, there is no difficulty, in principle, in treating nonisovelocity water, and indeed Lysanov considers a pseudolinear sound speed model as an example. The results obtained by Lysanov and Kuperman were applied to a propagation problem by Kuperman and Ingenito,[7] who considered a shallow water case with a rough sea surface and a flat sea bottom. The results of these authors agree with those of Lysanov in suggesting that the effects of roughness are heavily influenced by the sound speed profile as well as by the power spectrum (or correlation function) of surface relief.

It is a characteristic feature of this perturbative approach that the boundary condition (reflection coefficient) for the coherent field does in fact contain the correlation function of surface relief. This is in marked contrast to the scattering theory approach which requires knowledge of only the distribution of surface heights. The details of the relationships between these two approaches have not been explored nor have the limitations of the perturbative method been well defined. Nevertheless, it is clear that this later method offers potential for considerable progress in this problem. A systematic effort to exploit the method is underway.

REFERENCES

1. Clay, C. S., and W. K. Leong, "Acoustic Estimates of the Topography and Roughness Spectrum of the Sea Floor Southwest of the Iberian Peninsula," in Physics of Sound in Marine Sediments, Loyd Hampton (ed.), (Plenum Press, New York, 1974).

2. Boyd, M. L., R. L. Deavenport, and P. J. Welton, "Scattering and Propagation of Acoustic Waves in the Presence of Rough Penetrable Boundaries," Applied Research Laboratories Technical Report No. 71-16 (ARL-TR-71-16), Applied Research Laboratories, The University of Texas at Austin, 1971.

3. Boyd, M. L., and R. L. Deavenport, "Forward and Specular Scattering from a Rough Surface: Theory and Experiment," J. Acoust. Soc. Am. 53, 791 (1973).

4. Lysanov, Yu. Y., "Mean Coefficient of Reflection from an Uneven Surface Bounding an Inhomogeneous Medium," Sov. Phys. Acoust. 15, 340 (1970).

5. Kuperman, W. A., "Coherent Component of Specular Reflection and Transmission at a Randomly Rough Two-Fluid Interface," J. Acoust. Soc. Am. 58, 365 (1975).

6. Wenzel, A. R., "Smoothed Boundary Conditions for Randomly Rough Surfaces," J. Math. Phys. 15, 317 (1974).

7. Kuperman, W. A., and F. Ingenito, "Relative Contribution of Surface Roughness and Bottom Attenuation to Propagation Loss in Shallow Water," presented at The 1975 SACLANT Conference on Ocean Acoustic Modeling.

V. PROPAGATION OVER A SLOPING BOTTOM

A. Introduction

Broadly speaking, the sloping bottom problem is one of determining the influence of range changing bathymetry on acoustic propagation in the ocean. As mentioned previously, the general problem of bottom topographic effects has been broken down into the sloping bottom problem and the rough interface problem. The sloping bottom problem then deals with bathymetry variations which would show up on ordinary echo sounding apparatus (midocean ridges, abyssal hills, seamounts, continental slopes and margins, etc.). Of these types of bathymetry variation, we have chosen at the beginning to concentrate on the influence of continental slopes and margins on propagation both over deep water (basin) and into shallow water area (continental shelves). The archetypal sloping bottom problem, for present purposes, is then described by a bathymetry which displays a smooth decrease in water depth from a large flat bottom region (basin) through a gently sloping region to a steeply sloping region (continental slope) into an extended shallow water region (continental shelf).

Having set out such a problem it is necessary to ask what tools are available to investigate sound propagation in such a region. Several of the computerized propagation models developed at various laboratories are sufficiently powerful to attack some aspects of such a problem. Ray theory models, TRIMAIN and GRASS, developed at NRL, can carry out ray tracing in a range changing environment, and can compute transmission loss versus range. Another is the recently developed parabolic equation model. At least two versions of this model have been developed: one at the Acoustic Environmental Support Detachment (AESD) of ONR and

another at SACLANT ASW Research Centre. There are other such models, some of which are to be used in future work on the sloping bottom problem. During the first year, TRIMAIN and the AESD parabolic equation model have been implemented at ARL. They are being used in an assessment of sensitivity (of propagation loss over a sloping bottom) to variations in the bottom description.

A second approach to these problems uses more analytical methods to extract information in the case of simplified geometries and sound speed profiles. These studies are useful for calibrating other methods such as computerized propagation models. Some effort is being made to use the mode-mode coupling approach of Pierce[1] and Milder.[2] Although this method is in principle rather general, in practice it may be restricted to the isovelocity case (when the bathymetry is range changing). Work in this direction is therefore to be regarded as a study of the purely geometric effects of the sloping bottom problem. The interaction between these geometric effects and refraction effects caused by a variable sound speed are being studied using the computer propagation models. The last section of this chapter deals with some aspects of the work on a coupled mode approach.

Before moving on to the specific details of the work, it will be worthwhile to discuss qualitatively the effect of a sloping bottom on propagation. These effects can be divided into five categories, not all of which are independent or separable:

1. megaphone and inverse megaphone (funnel) effects,
2. mode-mode coupling (multipath conversion),
3. interaction of variable sound speed and bathymetry,
4. interaction of variable sound speed, bathymetry, and bottom reflection coefficient, and
5. partitioning of energy between water and bottom paths.

The megaphone and funnel effects are simply changes in acoustic energy density due to changes in water cross sectional area at any fixed range. This can occur - and indeed will be maximized - in the case of a perfectly reflecting bottom. These effects are two examples of a more general class of effects referred to as mode-mode coupling, or in ray theory terms multipath conversion. In this process, for example, a particular mode traveling up slope into shallower water is converted to various higher order modes. The ray aspects of such a process are depicted schematically in Fig. V-1, which shows the effect of a funnel geometry of changing slope along the funnel on three initially parallel rays in the case of a constant sound speed. The process depicted in this figure is an important component in the so-called slope enhancement effect, a specific example of which will be given in the next section.

The interplay between refraction due to a variable sound speed and reflection from a bottom slope can be quite complex, especially when the bottom is not perfectly reflecting but has a reflection coefficient that is variable with angle. One particularly simple example of the interaction between a variable sound speed and bathymetry is depicted in Fig. V-2. In this figure it is supposed that there is a sound channel and a single axial ray is shown reflecting from the bottom in the case of three different slopes. Because of the negative sound speed gradient in the near surface region, there will be for fixed axial ray and shallow water depths an optimum slope for the transmission of energy into the shallow water region. This situation is depicted in the middle illustration in which the ray has an upper turning point that is tangential to the sea surface. Due to the large number of bottom bounces in the first and third cases, the sound intensity in the shallow water region due to axially transmitted energy will be lower than in the "optimum" case. It is not difficult to see that the optimum bottom slope, θ_o, will be given by $\theta_o = 1/2 \cos^{-1}[C(A)/C(o)]$ where $C(o)$ is the sound speed at the surface and $C(A)$ the sound speed on the axis. This discussion is adapted from Urick.[3]

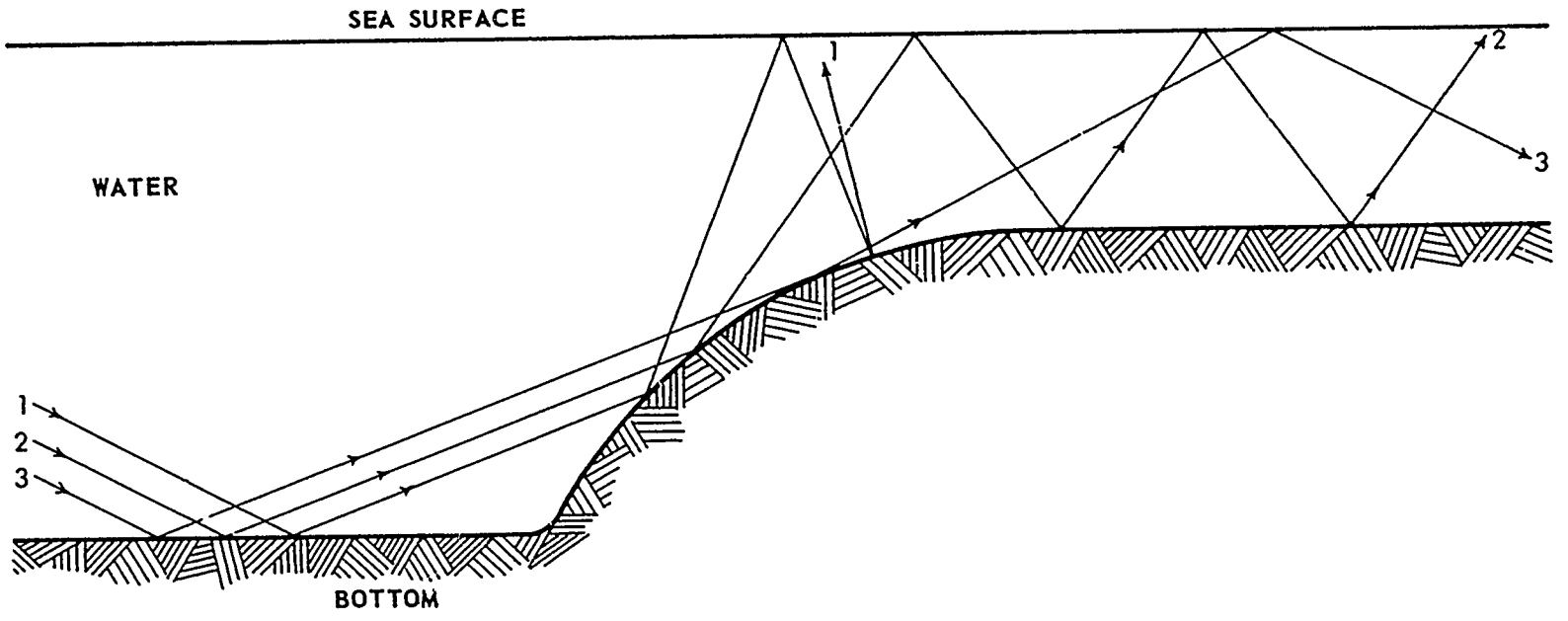

FIGURE V-1
SCHEMATIC ILLUSTRATION OF MULTIPATH CONVERSION

ARL - UT
AS-76-108
KEH - DR
2 - 5 - 76

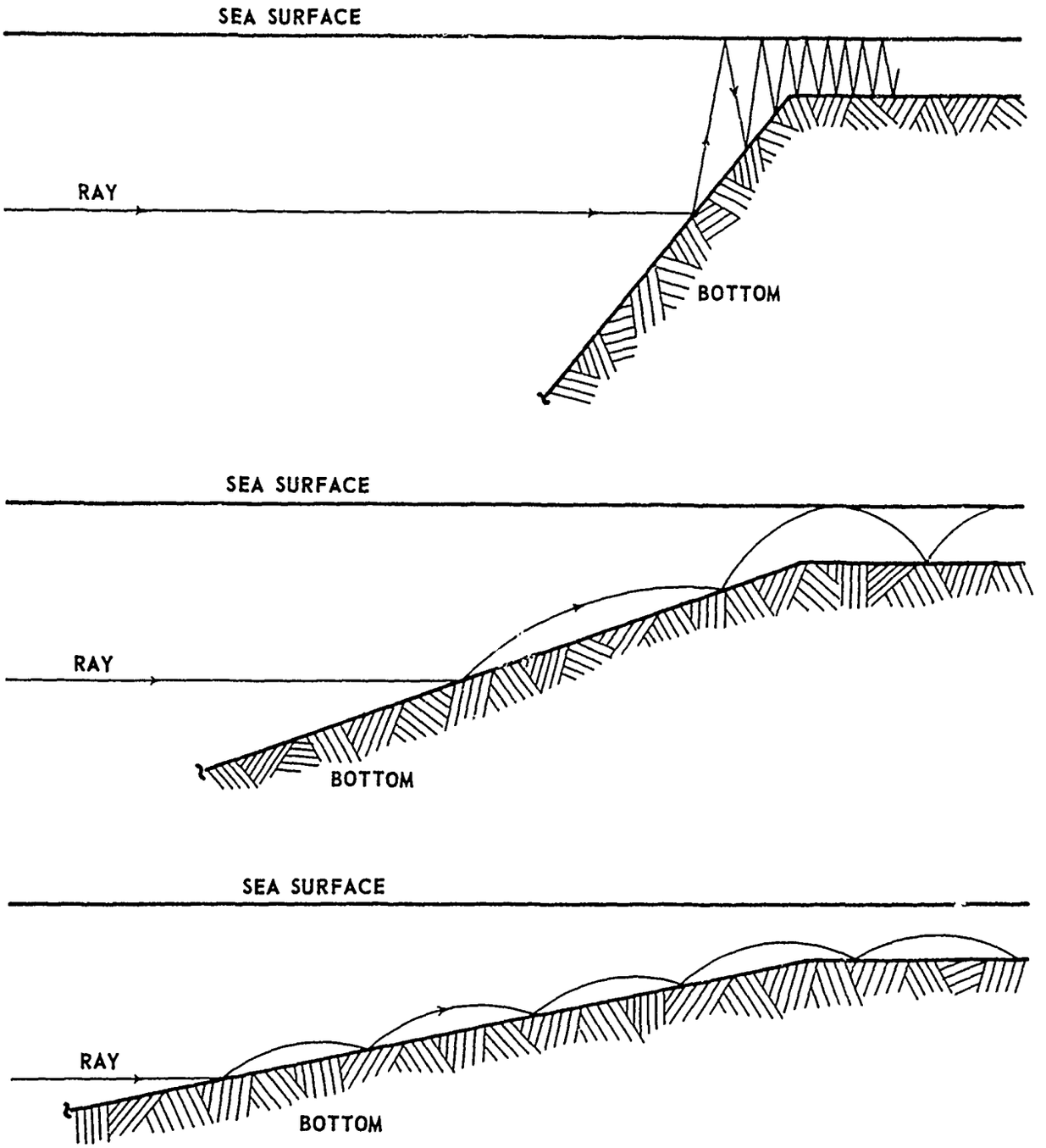

FIGURE V-2
SCHEMATIC RAY DIAGRAMS FOR A SINGLE RAY ON SOUND CHANNEL AXIS FOR THREE DIFFERENT BOTTOM SLOPES

ARL - UT
AS-76-107
KEH - DR
2 - 5 - 76

The more complex and realistic situation, where the reflection coefficient also is variable with angle, is more difficult to illustrate. It is clear, though, that a bottom loss critical angle on the slope will play a crucial role in determining the sound transmitted from deep to shallow water (or the reverse). One goal of the ongoing effort is to develop an understanding of the role played by such a critical angle in relation to the source depth, sound channel axis, and shallow water depth.

B. Investigation and Use of Existing Models

During the past year some effort was made to implement appropriate models for use in several tasks of this investigation. The case of a range constant environment could be adequately treated by the FACT model which had already been implemented at ARL in another study. Various specialized models were developed including RANGER (EIGENRAY) and BOTLOSS. (These are described in Appendices A and B.)

Study of the case of a range changing environment (sound speed profile or bathymetry changing with range) requires other types of models. Accordingly, the ray model TRIMAIN that was developed at NRL was adopted for use in this project, as was a current version of the parabolic equation model developed at AESD. The next subsection deals with the implementation of these models, and the final subsection with an example of their application to a particular problem.

1. Implementation of Models

The ray trace model TRIMAIN is discussed in detail by Roberts.[4] This model functions by tracking a large (specifiable) number of rays from the source through a range changing environment (sound speed and bathymetry). Various types of intensity (coherent, incoherent, range averaged, depth averaged) are obtained by an interpolation procedure between rays bracketing a receiver in depth.

The report by Roberts contains a complete listing of the program which was used directly to obtain a machine readable version. The original program was written for a CDC 3800 computer. Due to the large storage requirement, the program was adapted to run on the CDC 6600 located on the main campus of The University of Texas at Austin.

After exhaustive checks and examination of test cases, the program has been determined to be running correctly in nearly all its modes. In particular, the ray trace and depth averaged intensity modes are operational. Figures V-3 and V-4 allow a comparison between TRIMAIN and FACT for a particular horizontally stratified test case. For this case, the bottom loss is 3 dB at all angles and the sound speed profile has a sound channel axis at 801 m. The agreement is seen to be good, and the small discrepancies present are attributable to the different modes of intensity calculation used. The report by Roberts on TRIMAIN contains a rather complete set of test cases for the programs various modes. These have been checked in detail with the ARL version and for the operational modes found to be in complete agreement.

At the present time only printer plot outputs are available for the ray trace and intensity modes. Figure V-5 shows an example of a ray trace output from TRIMAIN (the sound speed profile is also shown). The bathymetry corresponds to a transition from the edge of a continental shelf to a deep ocean basin. It should be observed that the effects of the double sound channel of the sound speed profile show up clearly in the ray trace. The coupling to the lower channel occurs via multipath conversion on the slope. This same bathymetry was also used, with source and receiver locations interchanged, in the study reported in the next subsection. Work is in progress to add a Calcomp plot capability. The ray trace part of TRIMAIN is being adapted for use on ARL's CDC 3200 as a ray tracing program, without intensity calculation capability. This will prove a valuable diagnostic tool for the sloping

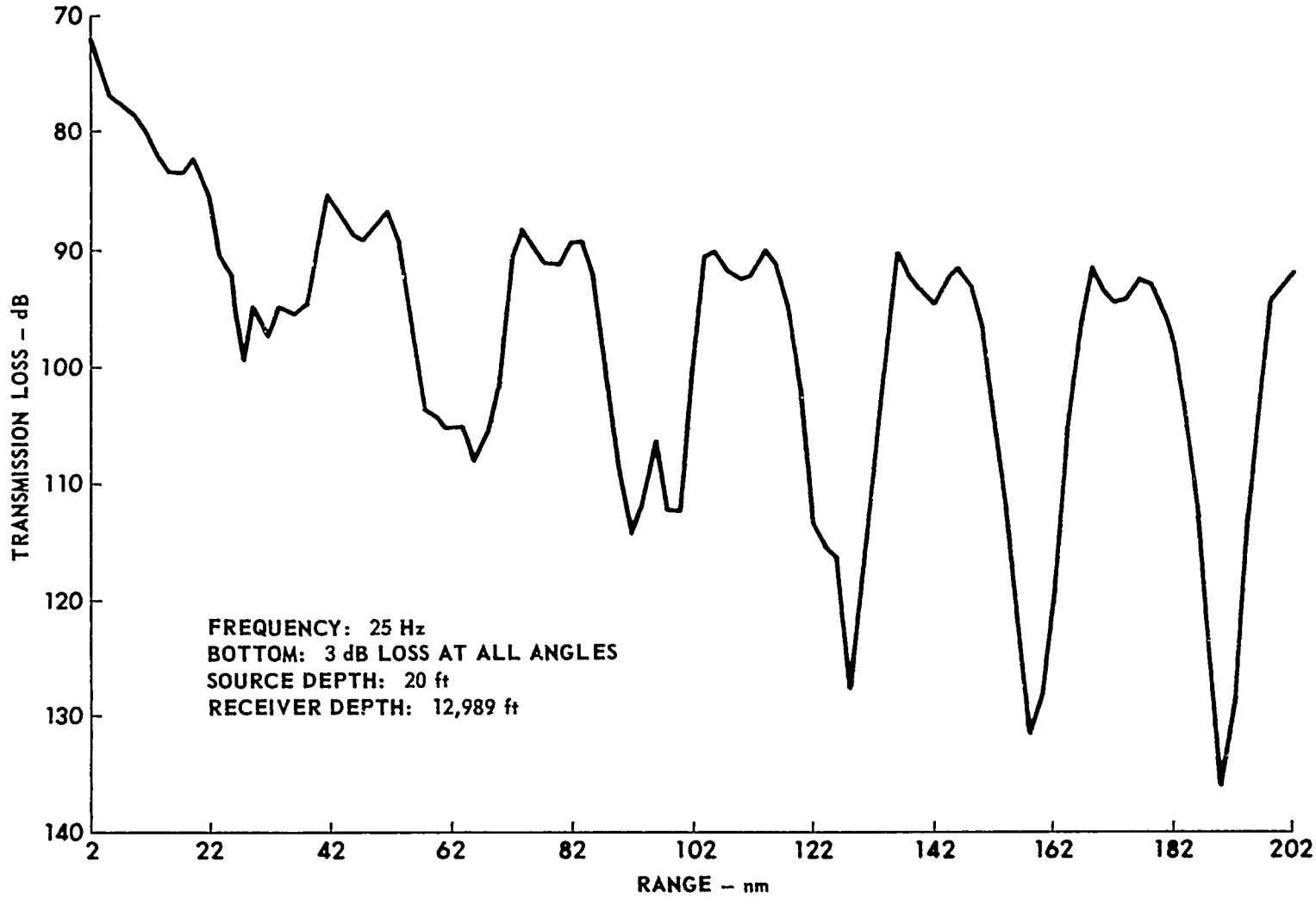

FIGURE V-3
TRANSMISSION LOSS VERSUS RANGE FOR TRIMAIN MODEL

ARL - UT
AS-76-98
KEH - DR
2 - 4 - 76

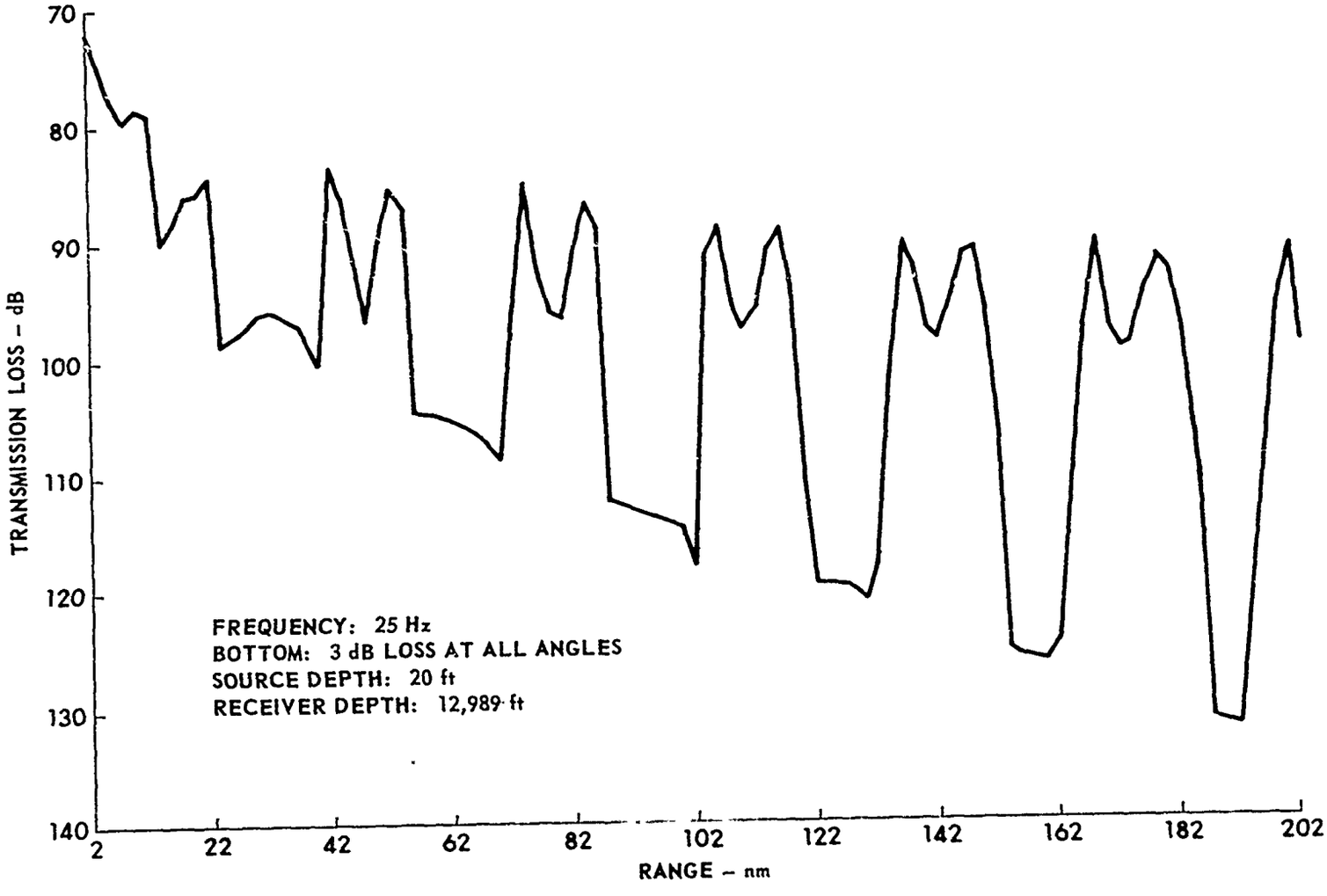

FIGURE V-4
TRANSMISSION LOSS VERSUS RANGE FOR FACT MODEL

ARL - UT
AS-76-99
KEH - DR
2 - 4 - 76

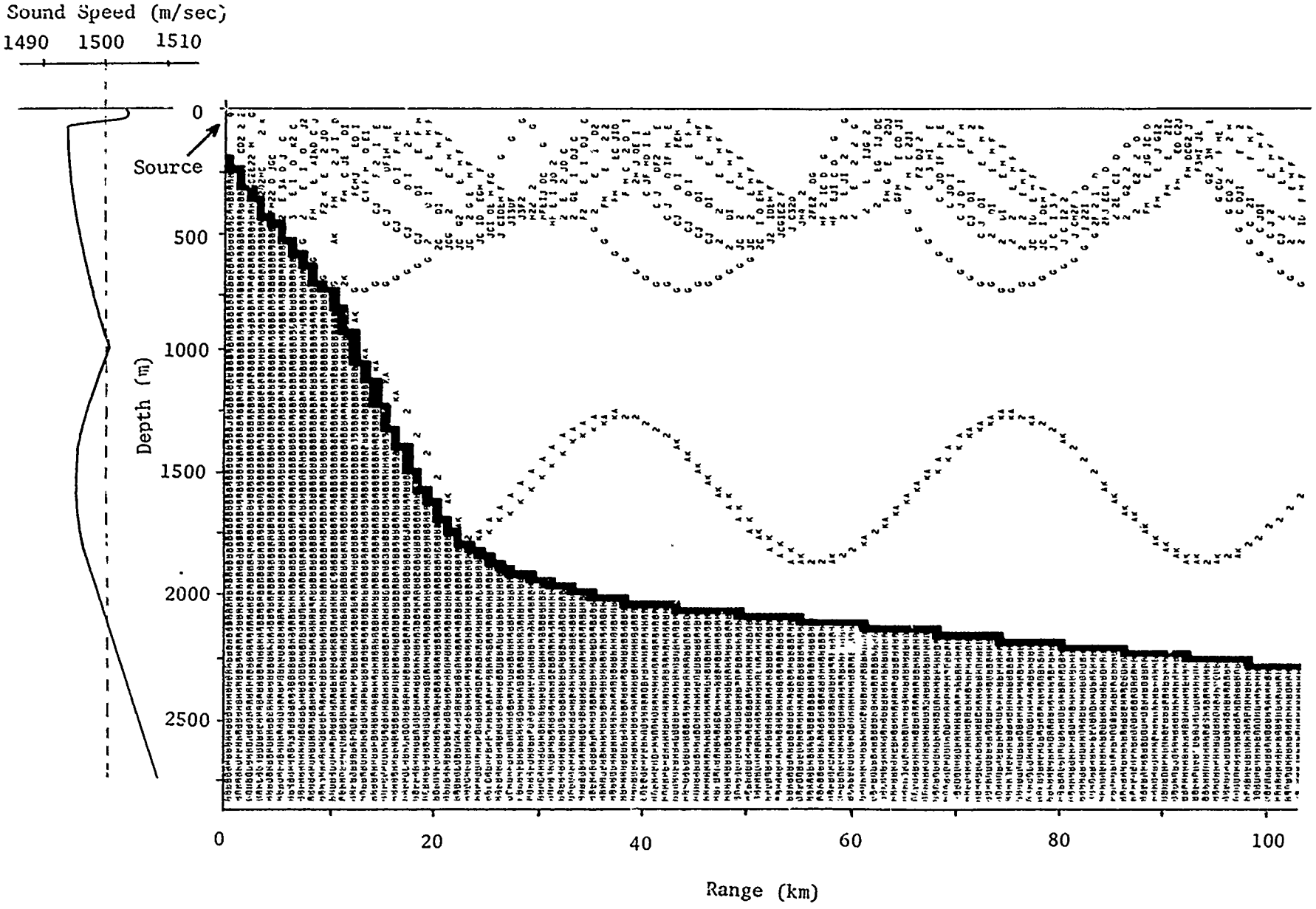

FIGURE V-5
SAMPLE TRIMAIN RAY TRACE OUTPUT
WITH SOUND SPEED PROFILE

bottom problem; the cost is low and the machine has a short turn around time.

In addition to TRIMAIN, the parabolic equation model has been implemented. This particular version of PE treats the cases of range changing sound speed profile and bathymetry and can also treat the case of bottom loss which is zero below a specified critical angle (and essentially infinite above it). Although this model is presently running on the ARL computer, the storage requirements are such that nearly all output manipulations must be handled by a separate program. Output features include a complete map (printer plot) of the sound field at all depths and ranges along with the bathymetry, printer plots of intensity versus range for selected receiver depths, Calcomp plots of intensity versus range, and a range filter which may be applied to either plot type.

Work is now in progress to convert the program to run on the UT CDC 6600 machine. This is being done for two reasons: (1) to use a larger FFT which will permit application at higher acoustic frequencies and/or larger water depths, and (2) to obtain additional accessible storage which will be used to add features such as depth average to the program.

Figure V-6 shows a typical output from the present implementation of the parabolic equation model. The bathymetry and sound speed profiles are the same as for the trace given in Fig. V-5. The receiver depth is 18 m and the source depth 715 m. The output shown here is unfiltered and the apparent multiple valuedness results from the compression of a number of points into one range interval by the printer plot routine. The convergence zone structure of the intensity is clearly evident as is the highly detailed fine structure characteristic of a wave theory.

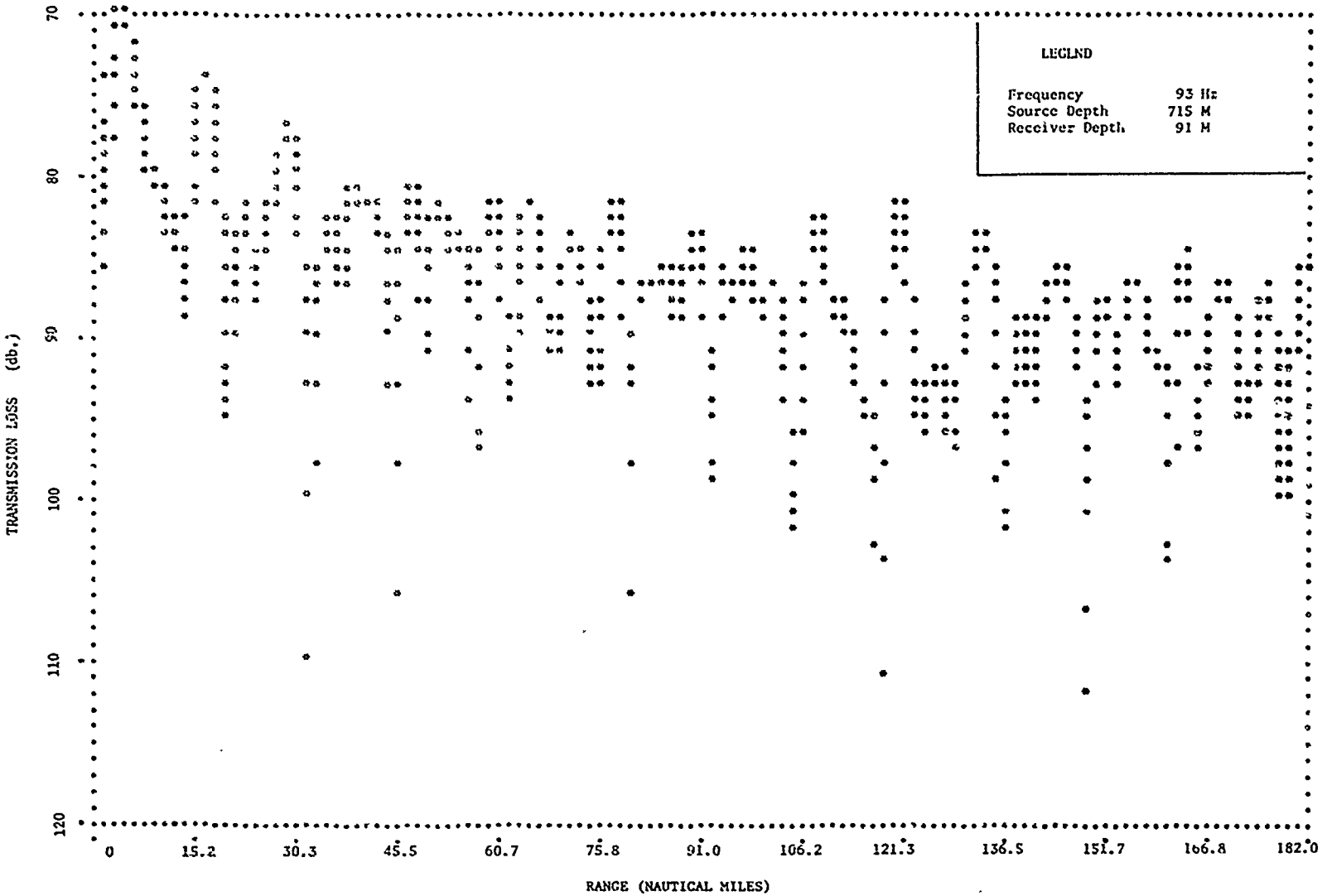

FIGURE V-6

PRINTER PLOT OF TRANSMISSION LOSS VERSUS RANGE FOR P.E. MODEL

2. Application to a Specific Problem: Slope Enhancement Theory and Experiment

Although much of the work on the sloping bottom problem is of a hypothetical nature, i.e., sensitivity assessments without reference to a specific experiment, the large amount of acoustic propagation data acquired in recent years allows meaningful comparison of the models and specific experimental results. Several sets of experimental data have been examined for slope effects. One such piece of data has shown a strong slope enhancement feature. These data are shown only to encourage the examination of model runs to determine the important parameters of the problem. Detailed comparison model runs and data will be made at a later stage in the study.

Figure V-7 shows some 93 Hz propagation data from a recent exercise in the Northeastern Atlantic. The receiver was located at zero range on this plot and at a depth of 715 m. The track of the continuous wave source, at a depth of 18 m, passes from deep water, over the continental slope, and into the continental shelf region. The bathymetry and sound speed profiles are shown in Fig. V-8 with the receiver located at the range point marked "B". The obvious peak in the data, centered at approximately 190 nm, corresponds to a source location at approximately the top of the continental slope.

For model calculations relevant to this situation, the bathymetry and sound speed profiles were modeled as shown in Fig. V-9. The same sound speed profile was used throughout the track since there appears to be little variation over the range interval of primary interest.

Figure V-10 shows the results of several TRIMAIN runs using this model bathymetry and profile. To determine the maximum possible slope enhancement that could occur in these circumstances, the slope

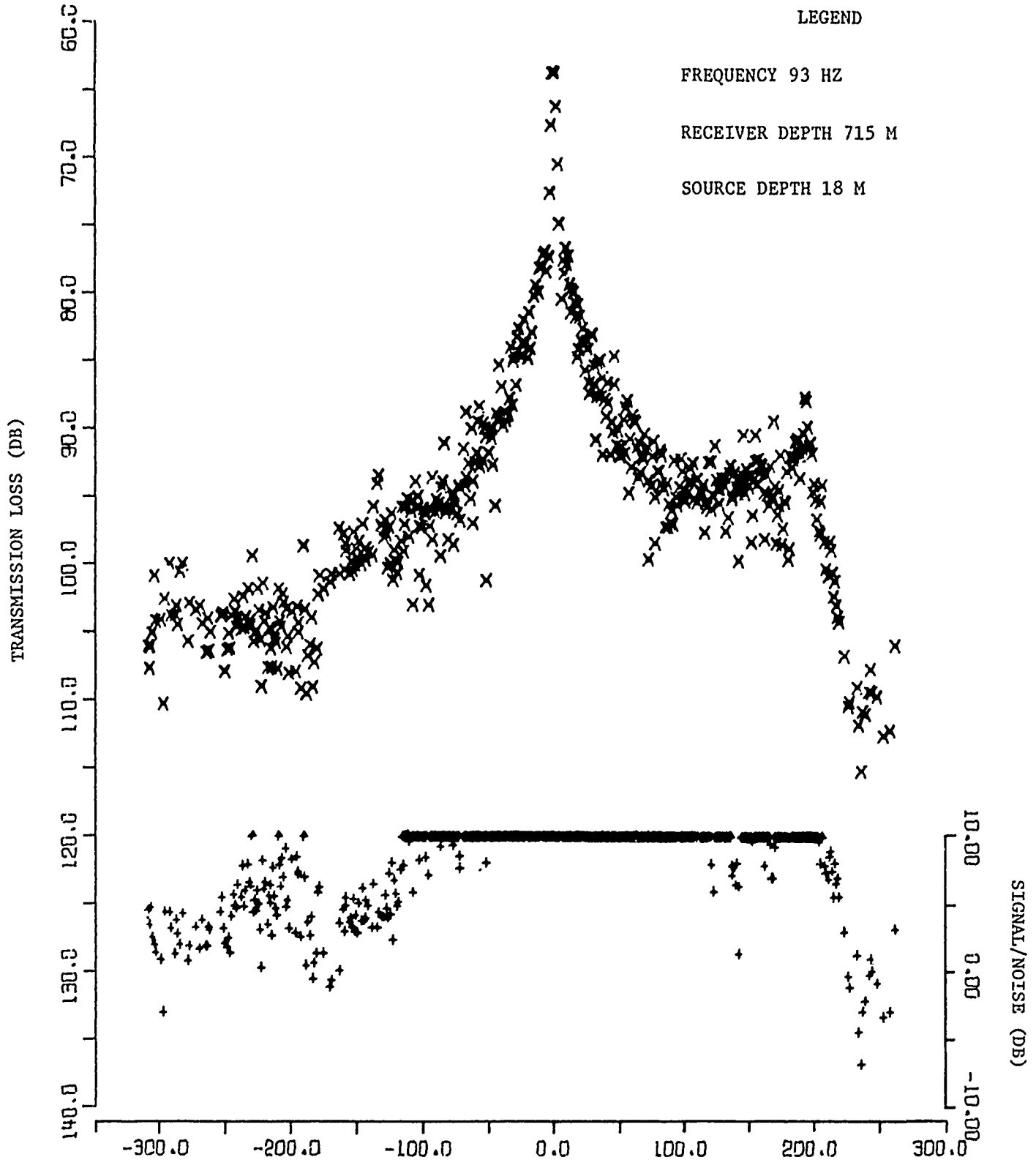

FIGURE V-7

TRANSMISSION LOSS AND SIGNAL-TO-NOISE VERSUS RANGE

AS-76-163

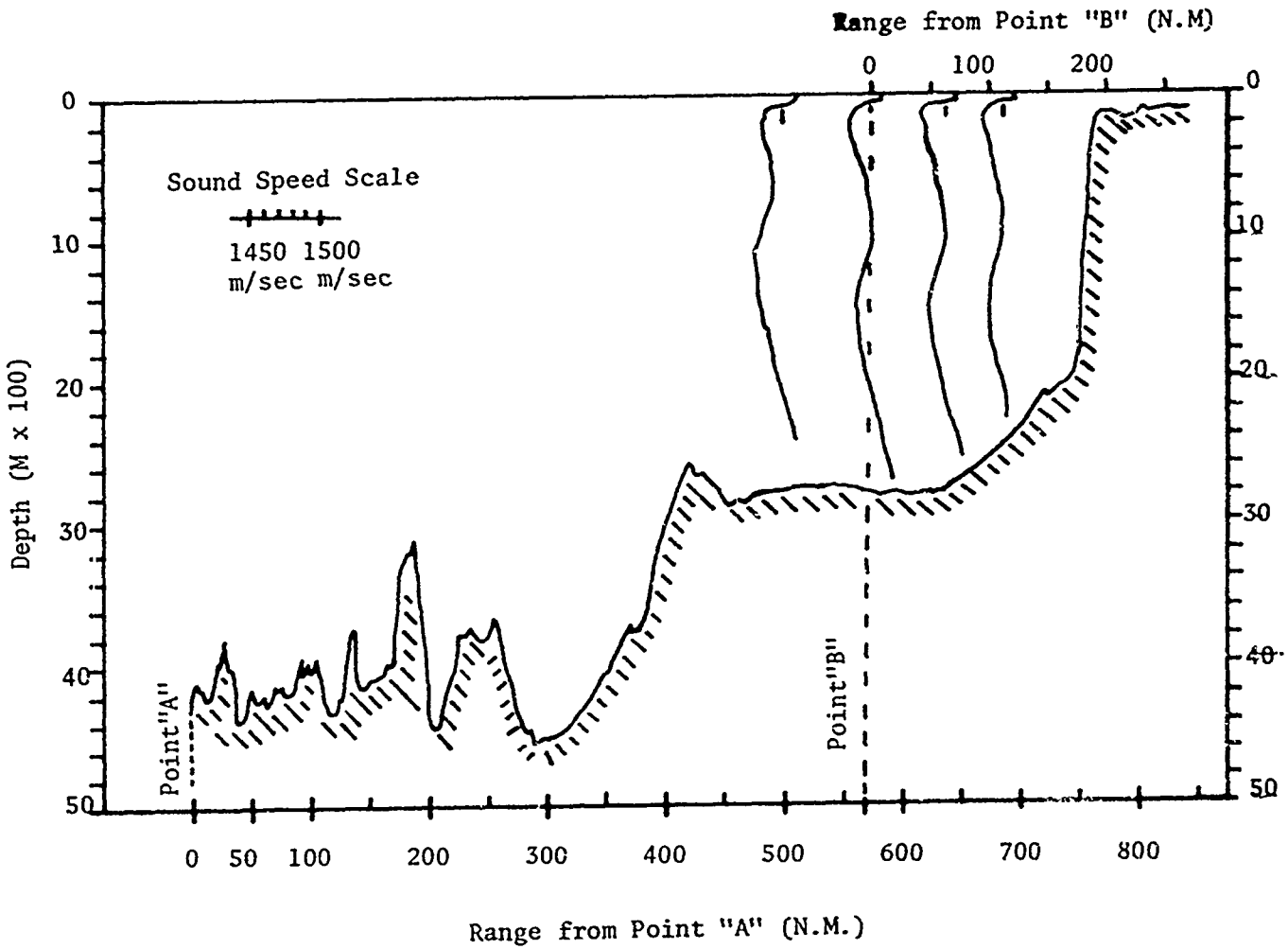

FIGURE V-8
Bathymetry and Sound Speed Profiles

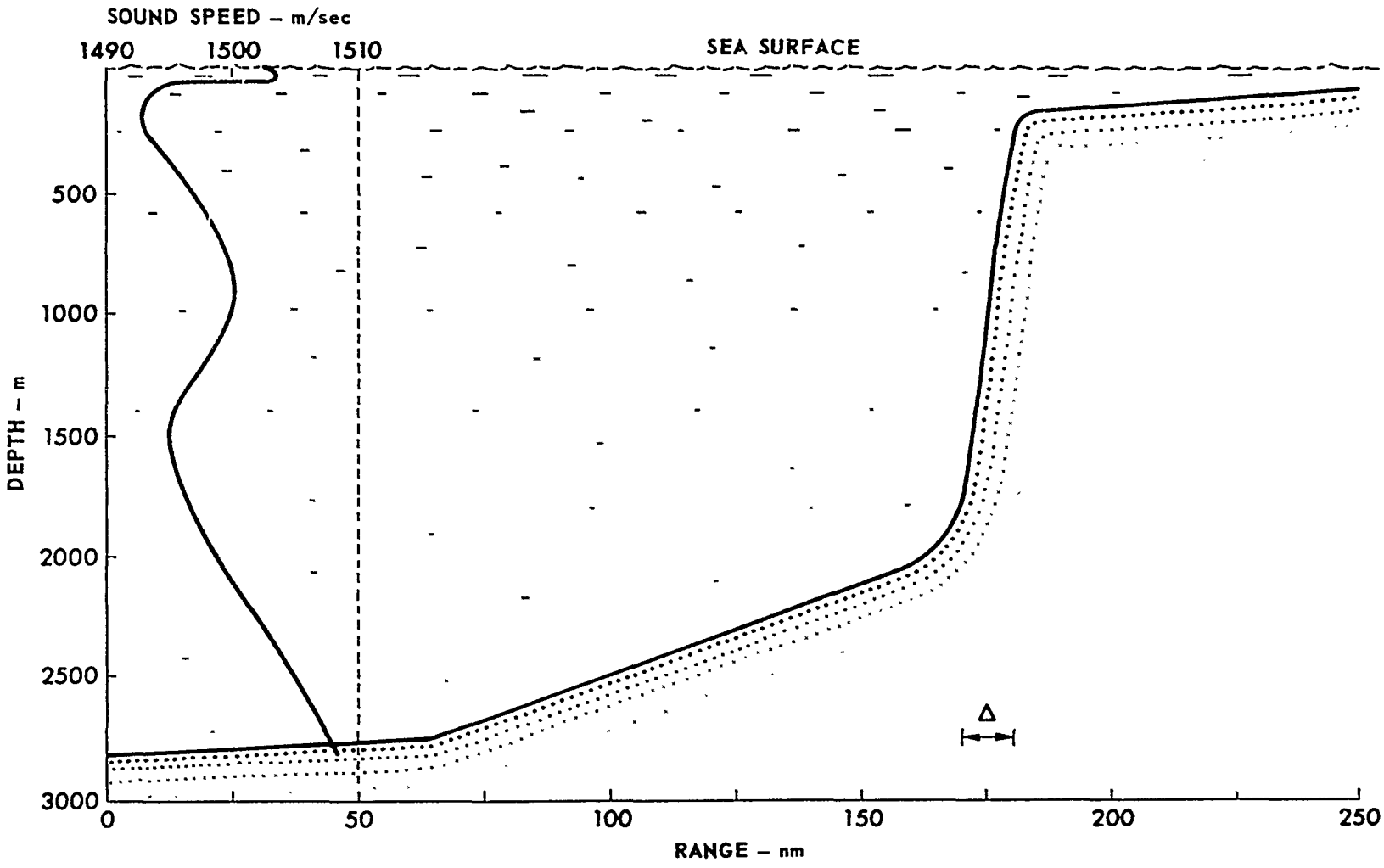

ARL - UT
AS-76-96
KEH - DR
2 - 4 - 76

FIGURE V-9
SOUND SPEED PROFILE AND BATHYMETRY

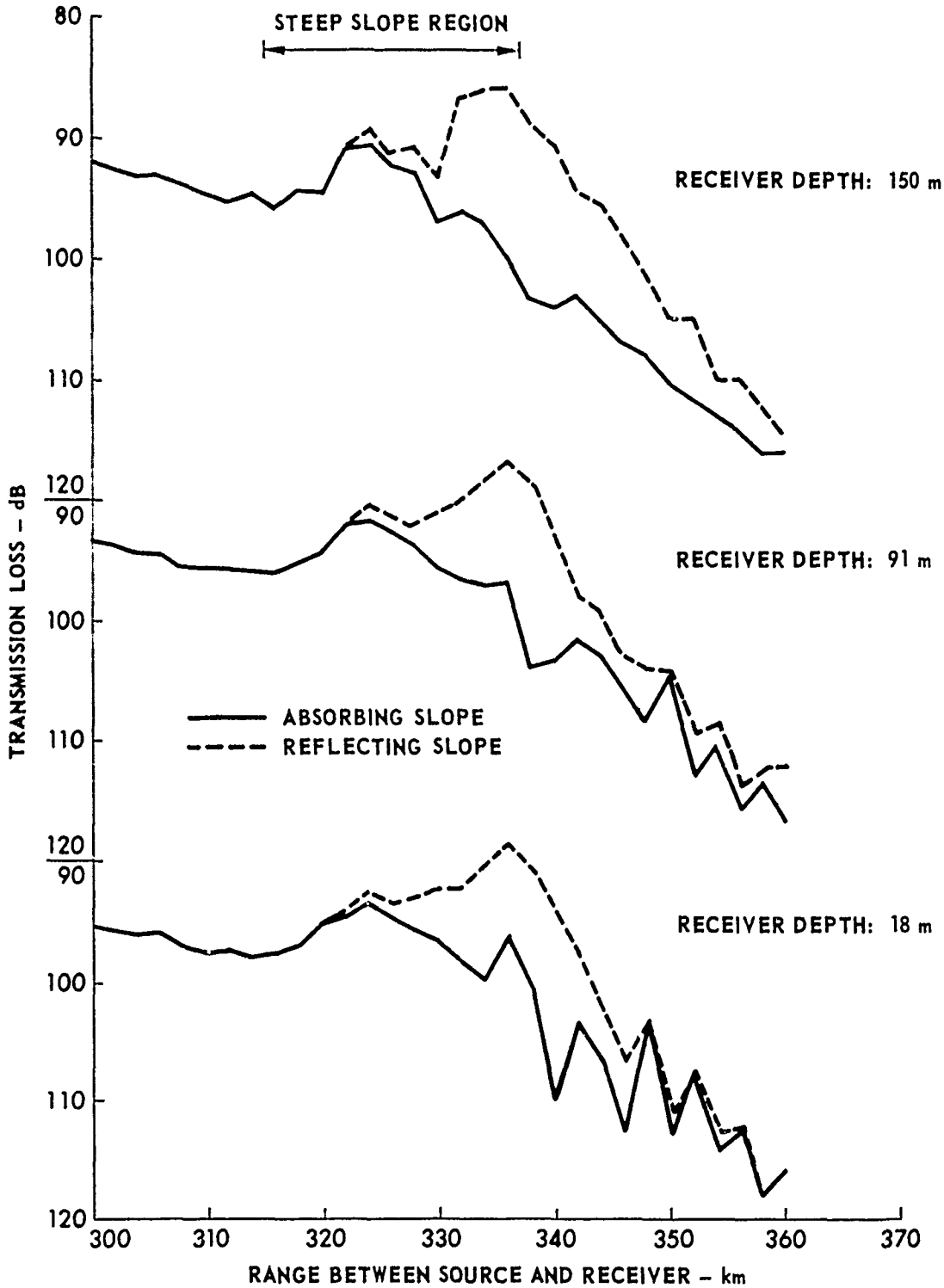

FIGURE V-10
TRANSMISSION LOSS VERSUS RANGE FOR REFLECTING AND ABSORBING SLOPES
(RAY MODEL)
SOURCE DEPTH: 715 m

ARL - UT
AS-76-97
KEH - DR
2 - 4 - 76

itself was made to be alternately a perfect reflector and a perfect absorber. All other regions of the bottom were modeled as possessing a reflection coefficient with a critical angle of 5° with zero loss below this angle and 3 dB loss above.

Several important features are shown in the curves of Fig. V-10, as follows.

(1) All receiver depths show a slope enhancement with the enhancement increasing with decreasing depth. The 18 m location is just inside the surface duct which ends at 20 m.

(2) The enhancement begins at a location corresponding to approximately 40% up the continental slope and peaks at the top of the slope.

(3) Although the "enhanced energy" decays with distance beyond the top of the slope, the decay rate is nearly the same in all cases. The apparent increase in this rate with increased receiver depth is actually due to differing slopes of the unenhanced curves. The decay of the enhanced energy is probably a manifestation of multipath conversion to steeper ray paths which suffer more loss when they reflect from the bottom. In the loss model used for these calculations, this amounts to conversion from below to above critical angle for the bottom encounters. This model is probably most useful for examining some features of the propagation in the deep water and over the slope. Accuracy of the results of this ray theory model in the shallow water portion of the path are still to be tested.

The same bathymetry and sound speed profile were used in a series of runs with the parabolic equation model. Figure V-11 is a plot of transmission loss versus range. The corresponding bathymetry is also shown. The bottom loss was modeled as having a 5° critical angle (with zero loss below this angle) everywhere except on the steep

FIGURE V-11

TRANSMISSION LOSS AND ASSOCIATED BATHYMETRY VERSUS RANGE

BS-76-165

slope (170 to 180 nm) on which it had a 20° critical angle. The slope enhancement is similar to that shown by the TRIMAIN model. The differences between the PE and corresponding TRIMAIN model runs are (1) with the PE model it is not possible to obtain a perfect reflector at all angles, and (2) above the critical angle the TRIMAIN runs were made using a 3 dB loss, whereas in the PE model the loss is 50 dB. The raw parabolic equation output has been range filtered using a 2 nm window (equal weighting) and a step size of 0.5 nm.

Figures V-12 through 14 show the results of several parabolic equation model runs for the cases of 0° (perfect absorber), 5°, 10°, and 20° critical angle on the continental slope with a 5° critical angle elsewhere. The three figures are for receiver depths of 18, 91, and 149 m, respectively, the same depths considered in the TRIMAIN model study. The propagation loss curves are displayed with 20 dB offset per curve for graphic clarity. It can be observed that the enhancement increases with decreasing receiver depth. Also, it is clear from any one of these figures that the energy encountering the slope and contributing to the field beyond the slope does so largely at angles below 10° or 15°. In other words, there are only small differences between 0° and 5° critical angles and between 15° and 20°, but between 5° and 15° the differences are large.

Figures V-15 and V-16 show a corresponding calculation of transmission loss versus range, for 18 m, 91 m, and 149 m receiver depths and 0° and 20° critical angles on the slope with source depths of 715 m and 2467 m, respectively. The receiver depth dependence of the enhanced energy is much less in the case of the deep source.

Unlike the TRIMAIN model runs, the 715 m source case does not display a decay of the enhanced energy to the level of the unenhanced case. A single TRIMAIN run, using the same bottom loss model as used in the PE runs (50 dB loss above 5° in the shallow water regime) shows

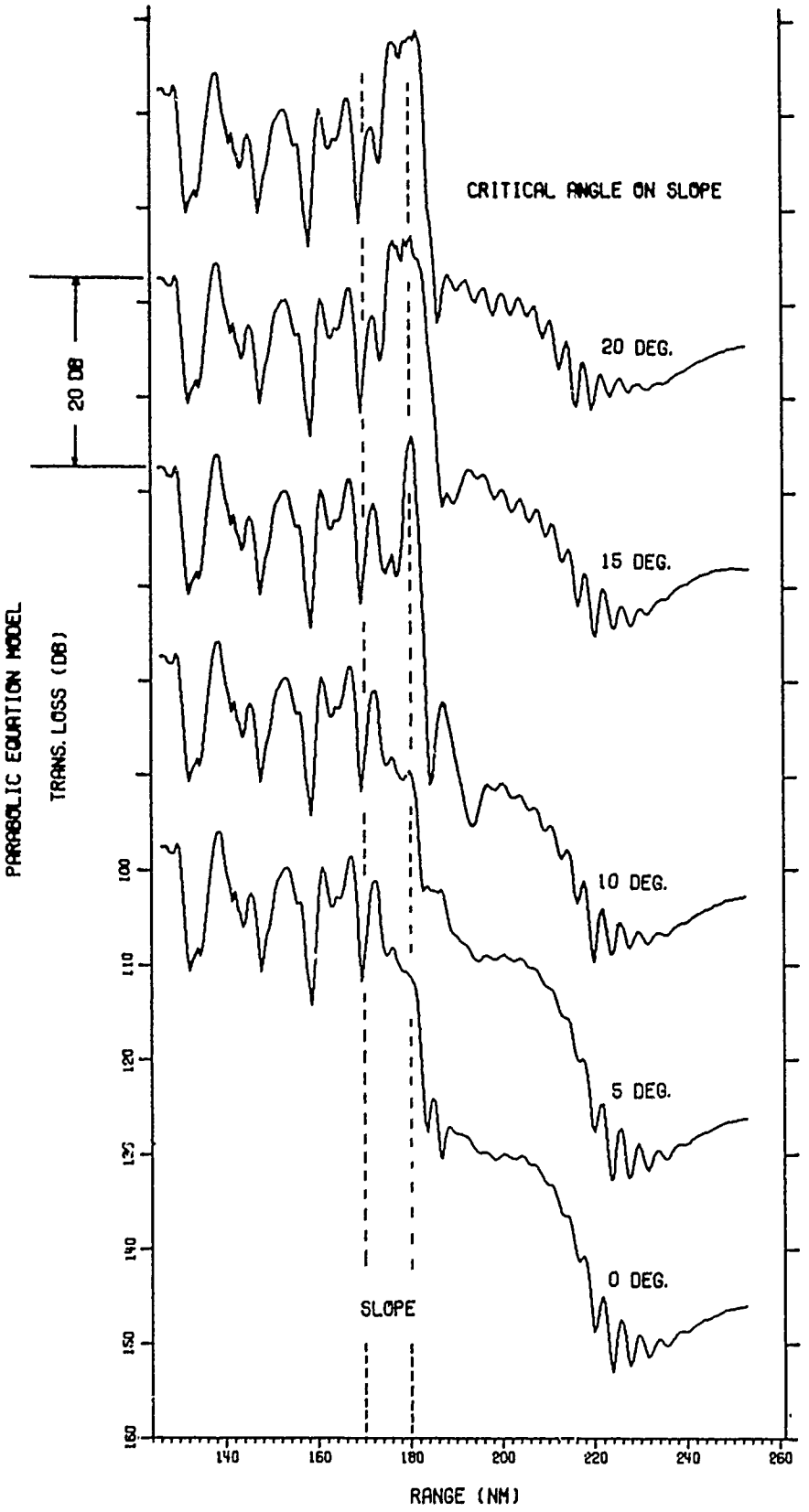

FIGURE V-12

TRANSMISSION LOSS VERSUS RANGE FOR AN 18m RECEIVER FOR VARIOUS SLOPE CRITICAL ANGLES

BS-76-121

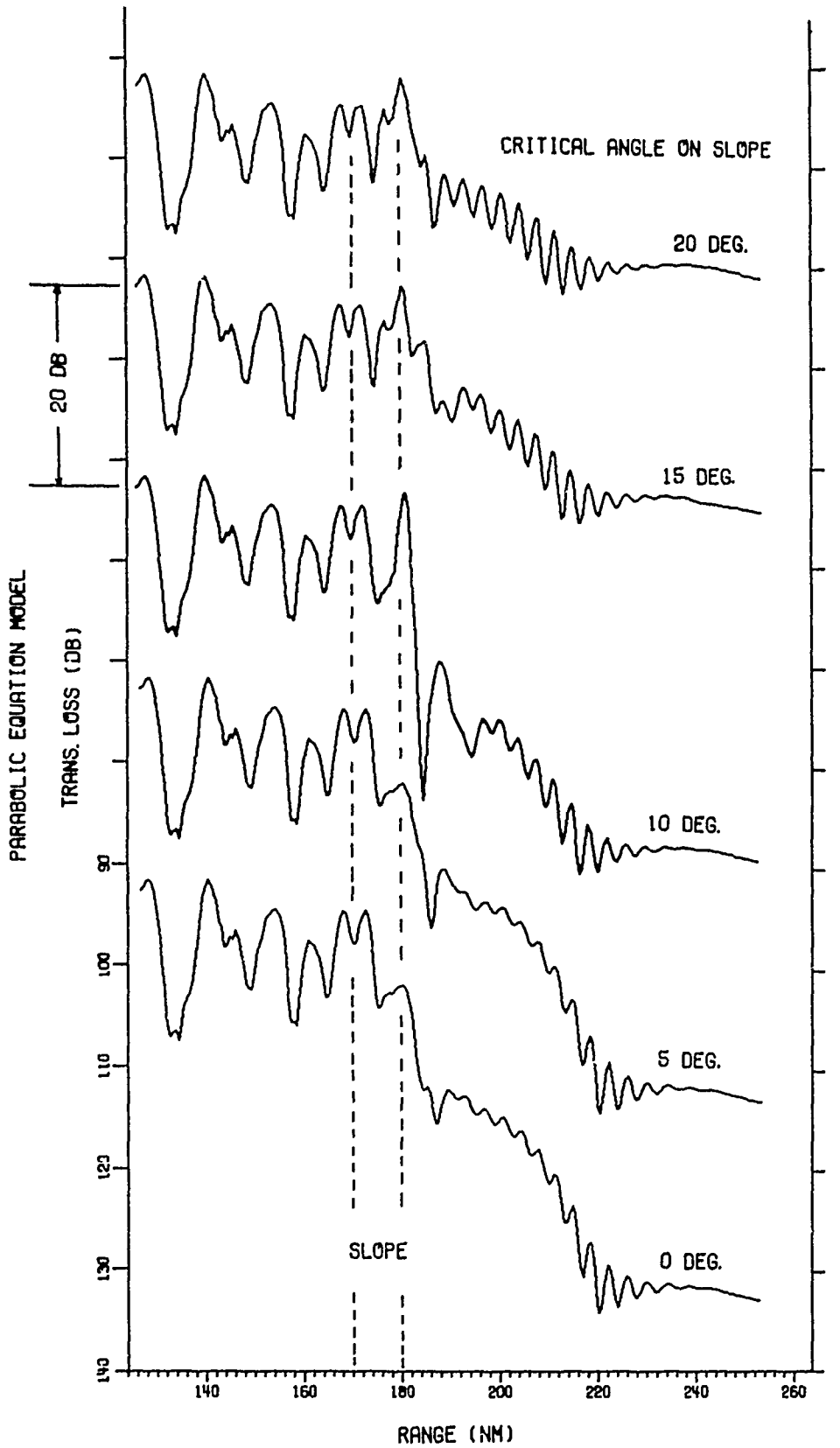

FIGURE V-13

TRANSMISSION LOSS VERSUS RANGE FOR A 91m RECEIVER DEPTH FOR VARIOUS CRITICAL ANGLES ON THE SLOPE

BS-76-136

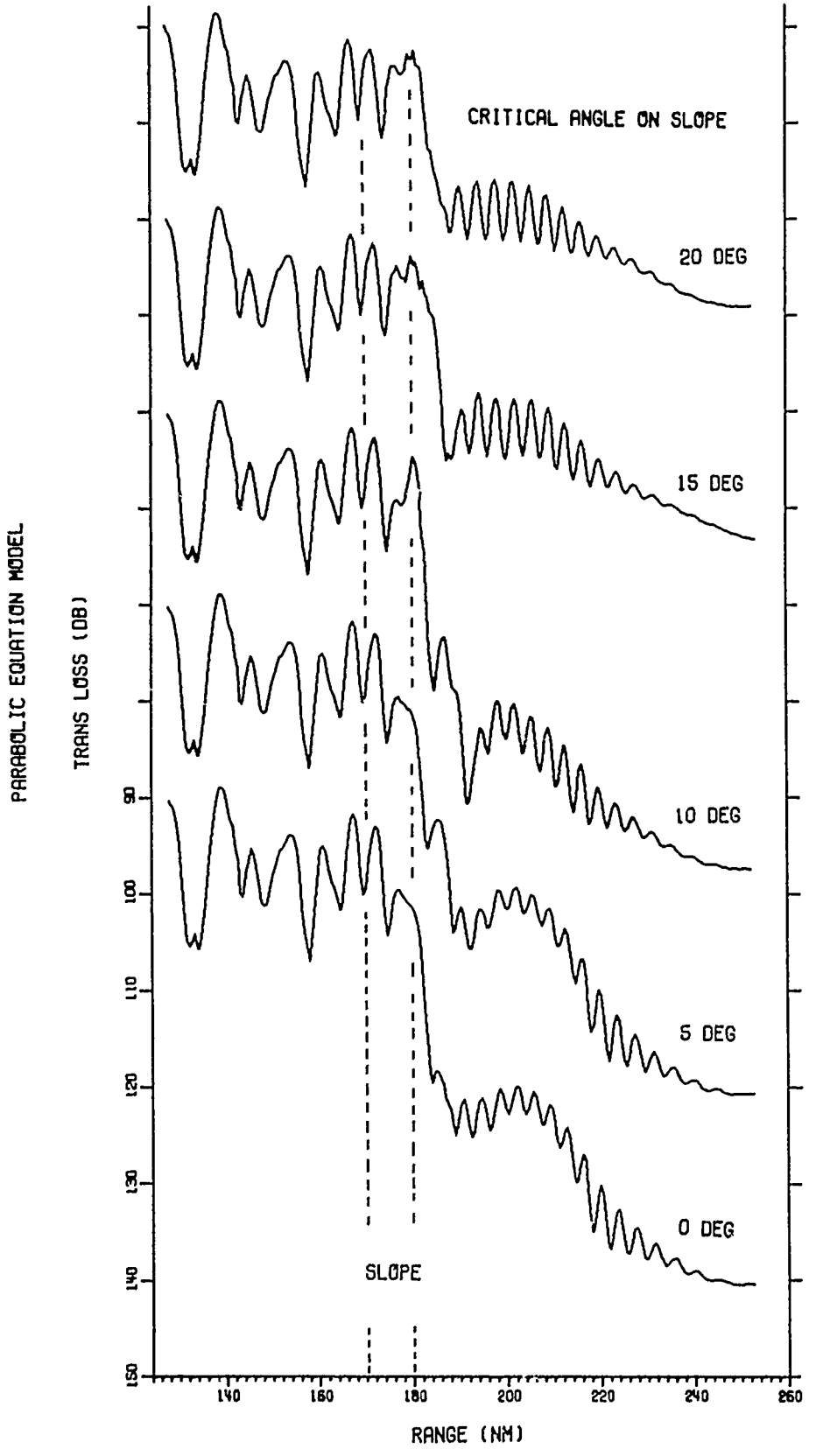

FIGURE V-14

TRANSMISSION LOSS VERSUS RANGE FOR A 150m RECEIVER DEPTH FOR VARIOUS CRITICAL ANGLES ON THE SLOPE

BS-76-137

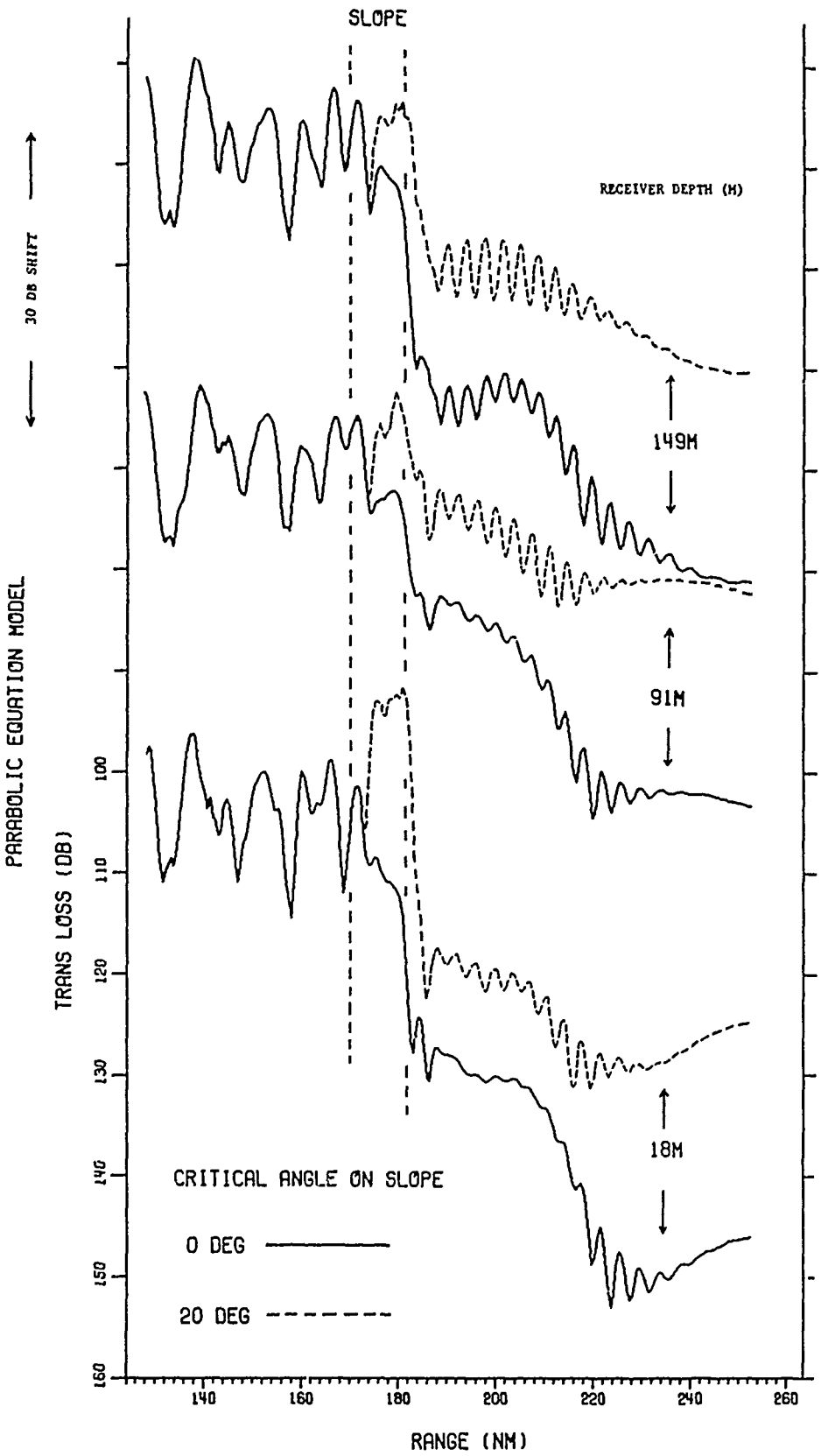

FIGURE V-15

TRANSMISSION LOSS VERSUS RANGE FOR 3-RECEIVER DEPTHS WITH A 715m SOURCE DEPTH

BS-76-162

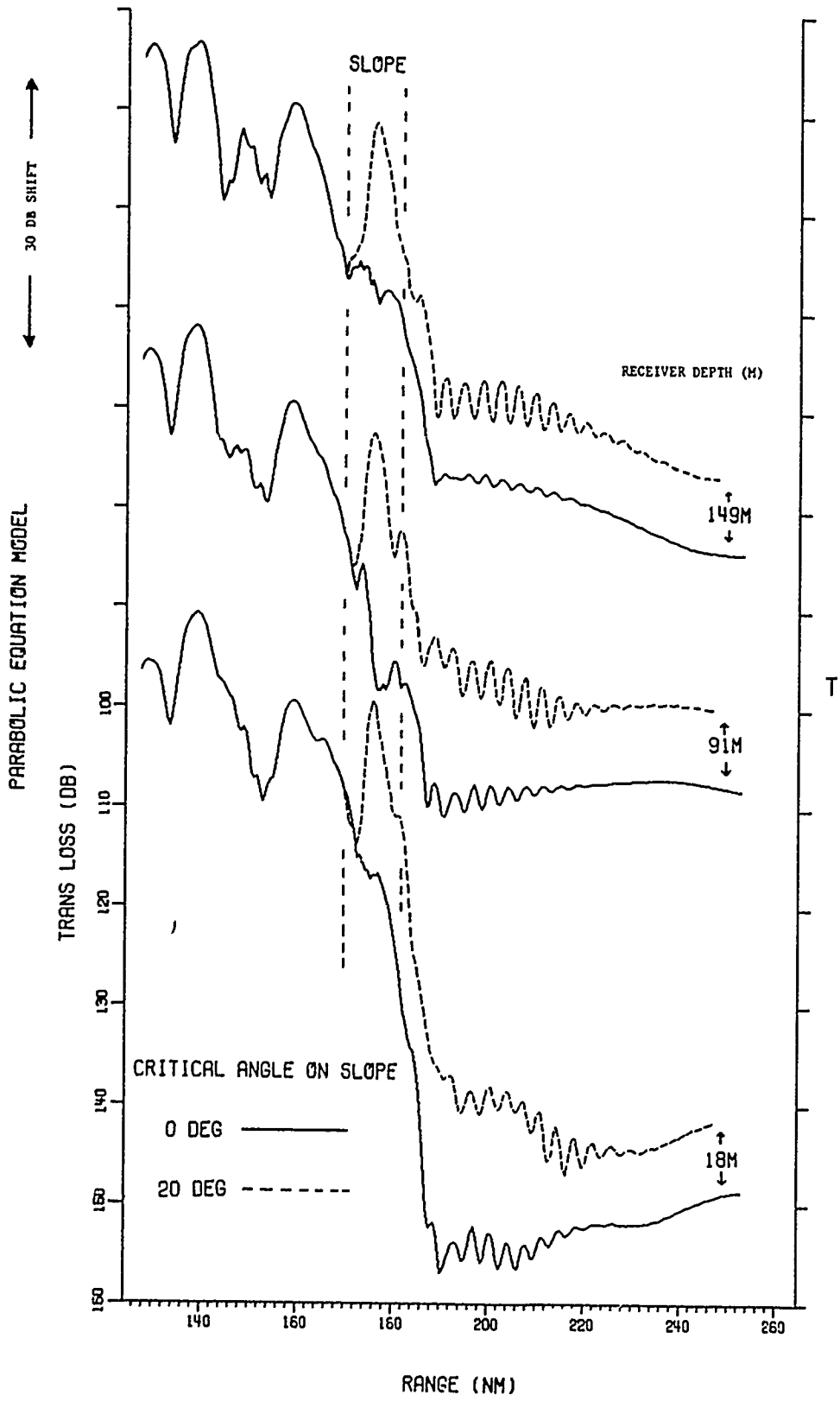

FIGURE V-16

TRANSMISSION LOSS VERSUS RANGE FOR 3-RECEIVER DEPTHS WITH A 2467m SOURCE DEPTH

BS-76-161

only a very small increase in loss beginning just beyond the top of the slope. The structure and the flattening of the curve shown by the PE model runs are not present in the TRIMAIN runs. Generally, the two models seem to be in good qualitative agreement in the parametric dependence of the enhancement on receiver depth and bottom loss critical angle on the slope. The major disagreement arises in the shallow water regime.

Continued use of such tools in sensitivity studies for sloping bottoms will serve the dual functions of revealing the capabilities and deficiencies of existing models, and of quantifying the sensitivities.

C. Other Theoretical Approaches: Feasibility Studies

In addition to the computer model approach just described, a more analytical approach was also taken. The purpose of such an effort was twofold: (1) to obtain tractable analytical tools which would yield some information about the sloping bottom problem, especially slope enhancement, without actually solving the entire problem, and (2) to provide approximate solutions, whose regime of validity is known, and to use these solutions to test more detailed computer models, such as those just discussed.

1. A Unified Approach to Propagation and Scattering Studies

An initial investigation was made of the feasibility of using the integral equation approach of Vekua[5] and Kupradze.[6] This approach uses as a fundamental solution the Green function for unbounded media and then fits the appropriate boundary conditions in a self-consistent way using integral equations. In the usual ocean geometries there would be two coupled integral equations.

A primary advantage of this approach is that the resulting dual integral equations, after exploiting all available symmetries, may be more susceptible to approximation or numerical integration than the corresponding differential equations (wave equation). Experience in other areas of physics such as many-body theory and quantum scattering theory lends credence to this belief (although nothing in such experience suggests that such a method would be simple or easily carried out).

Another virtue of this approach is that it would verify propagation theory and scattering theory in such a way that propagation over a rough bottom ocean would pass smoothly into scattering from a rough ocean bottom as the sea surface was moved away toward infinity. Such a unification would be a considerable advance as it would clear up much of the confusion about surface effects in propagation. A specific example of this type was in fact worked out: the case of water bounded above by a flat pressure release surface and below by a statistically rough pressure release surface. For vanishing roughness the usual Green function was in fact recovered, and when the water depth became unbounded the usual scattering theory results for the coherent field were obtained. Analysis of the finite depth-rough surface case led quickly into the further reaches of multidimensional Wiener-Hopf theory.

The complex nature of solutions to be used in this approach prompted us to explore other possibilities. As a general recommendation, the dual integral equation approach seems worth pursuing and with considerable effort it could result in a significant breakthrough.

2. Mode-Mode Coupling Theory

Another possibility that was investigated was the mode-mode coupling theory described formally by Pierce[1] and Milder.[2] Unlike the previous (dual integral equation) theory where mathematical underpinnings are secure and well founded, mode-mode coupling theory is essentially based on an ansatz, which, in real problems, can never be

true but may be an adequate approximation. Systematic efforts to exploit this approach, especially in the case of range variable bathymetry, are limited.

The basic idea of the approach is easily understood. With a rectangular coordinate system in which the z-axis is measured downward from the sea surface, one first presumes that at a given range location, (x,y), the depth separated wave equation can be solved for the normal modes $\varphi_n(z;x,y)$. It is then asserted that the solution to the range changing problem is given by $\varphi(x,y,z)=\psi_n(x,y)\varphi_n(z;x,y)$, where the ψ_n have yet to be determined. Upon assuming that the φ_n are orthonormal on the interval $(0,H(x,y))$, where $z=H(x,y)$ is the ocean bottom, substitution of this assumed solution of the original wave equation yields a set of coupled differential equations. In principle this formulation can treat either range changing sound speed--for which it was developed--or range changing bathymetry, or both. In subsequent discussions it will be assumed that the sound speed does not change with range since this defines the basic sloping bottom problem without additional complications.

Before considering the possible application of these ideas to the problem at hand, five important points concerning the basis of this formulation need to be discussed.

1. Concerning the fundamental ansatz, if the velocity potential φ_n satisfies the general impedance condition $\varphi_n+\gamma(\partial\varphi_n)/\partial z=0$ on $z=H$, then the φ_n form a complete set on this interval. In this case, which includes pressure release and rigid surface, the assertion about expansion of φ is trivially true since the ψ_n are nothing more than the inner product $(\varphi_n,\varphi\varphi_n)$, which is to say the coefficients in the expansion of φ in a complete set $\{\varphi_n\}$.

2. In the slightly more realistic case defined by the boundary condition $\varphi_n+\gamma(\partial\varphi_n)/\partial n=0$ on $z=H$ where $\partial/\partial n$ is the normal

derivative, the boundary condition itself is nonseparable and the partial separation effected by the product $\gamma_n\varphi_n$ cannot be carried out. In the case of a constant slope this point can be evaded by redefining γ and thereby make a return to the case considered in (1).

3. In the two fluid case there is always a continuous spectrum of eigenfunctions in addition to the discrete ones considered here. Moreover, the eigenfunctions of the two fluids taken separately are not complete in their respective domains. Even though in a range independent environment the continuous spectrum can be ignored at long range, it is not obvious that coupling between the continuous and the discrete spectra is small in a range changing environment. Physically it seems quite plausible that a single discrete mode, upon encountering a change in water depth, may couple some energy to the continuum and thereby transmit energy out of the water column.

4. In any case, if one ignores these comments and proceeds to apply the theory in a case when the bathymetry changes sufficiently slowly so that an uncoupled mode assumption is valid, then a tractable theory is obtained even in the case of a sound speed variable with depth. The equations for the ψ_n separate and the remaining equations seem to be amenable to solution by a variety of means.

5. A possible method of solution to the equations for ψ_n is to assume that in the (x,y) plane all changes are sufficiently slow to permit application of ray theory. If this is done one obtains essentially the horizontal ray theory of Weinberg and Burridge.[7]

In order to illustrate the type of problem which seems tractable using this method, we shall consider the case of a constant sound speed with both the ocean surface and bottom treated as pressure release. Extension to a locally reactive surface defined by $\varphi_n+\gamma\partial\varphi_n/\partial z=0$ is not difficult. The sea surface is considered to be at Z=0, and the bottom

is defined by $Z=H-\zeta(x,y)$. The wave equation for the Green function $(\nabla^2+k^2)G=-4\pi\delta(r-r_o)$ is assumed to have a solution of the form

$$G = \sum_n \psi_n(x,y)\ \varphi_n(z;x,y)\ \varphi_n^*(z_o;x,y) \quad , \tag{1}$$

where the φ_n satisfy the depth separated wave equation and are easily found to be

$$\varphi_n(z;x,y) = \left[2/(H-\zeta)\right]^{1/2} \sin(k_n z) \quad , \tag{2}$$

where $k_n=n\pi z/(H-\zeta)$, and $\zeta=\zeta(x,y)$. The $\{\psi_n\}$ are easily shown to satisfy the equations

$$\frac{\partial^2\psi_m}{\partial x^2} + \frac{\partial^2\psi_m}{\partial y^2} + \left(k^2-k_m^2-A_{mn}\right)\psi_m = -2\pi\delta(x-x_o)\ \delta(y-y_o) - \sum_{n\neq m}\left[A_{mn}\psi_n + B_{mn}\frac{\partial\psi_n}{\partial x} + C_{mn}\frac{\partial\psi_n}{\partial y}\right] , \tag{3}$$

where the coupling coefficients A_{mn}, B_{mn}, and C_{mn} are given by

$$A_{mn} = \int_o^{H-\zeta}\left(\varphi_m^*\frac{\partial^2\varphi_n}{\partial x^2} + \varphi_m^*\frac{\partial^2\varphi_n}{\partial y^2}\right) \quad , \tag{4}$$

$$B_{mn} = 2\int_o^{H-\zeta} dz\ \varphi_m^*\frac{\partial\varphi_n}{\partial x} \quad , \tag{5}$$

$$C_{mn} = 2\int_o^{H-\zeta} dz\ \varphi_m^*\frac{\partial\varphi_n}{\partial y} \quad . \tag{6}$$

It should be noted that, due to the completeness of the $\{\varphi_n\}$, the development is thus far exact.

If the bathymetry is sufficiently slowly varying, one might hope to ignore the mode-mode coupling terms, or at least regard such an approximation as yielding the first term in the expressions of ψ_m in powers of the slope ζ'. This approximation will now be introduced together with the more specialized geometry where ζ is independent of y, as would be the case in a treatment of a continental slope. In this case, Eq. (3) becomes

$$\frac{\partial^2\psi_m}{\partial x^2} + \frac{\partial^2\psi_m}{\partial y^2} + \left(k^2 - k_m^2 - A_{mm}\right)\psi_m = -2\pi\delta(x-x_o)\,\delta(y-y_o) \quad , \qquad (7)$$

where A_{mn} is given by

$$A_{mm}(x) = \int_o^{H-\zeta} dz\; \varphi_m^* \frac{\partial^2\varphi_m}{\partial x^2} \quad . \qquad (8)$$

This equation can be immediately reduced to an ordinary differential equation by taking a Fourier transform with respect to the y variable.

Thus,

$$\frac{d^2\psi_m(x,\gamma)}{dx^2} + \left(k^2 - k_m^2 - A_{mm} - \gamma^2\right)\psi_m = -2\pi\, e^{i\gamma y_o}\,\delta(x-x_o) \quad , \qquad (9)$$

where

$$\psi_m(x,\gamma) = \int_{-\omega}^{\omega} dy\; e^{i\gamma y}\,\psi_m(x,y) \quad , \qquad (10)$$

and where a radiation condition has been imposed for $|y| \to \infty$.

This is as far as it is possible to go with the formal development; further progress can be made only by choosing a specific form for ζ. Since it is not our purpose here to investigate any one problem in detail, but rather to comment on the applicability of this theory to a class of problems, this final step will not be carried out. It should be noted, however, that at worst we now would need to integrate Eq. (9) numerically after first computing $A_{mn}(x)$ in a specific case.

It is reasonable to ask about the modification of the foregoing development in the case that the bottom is not pressure release but rather satisfies the impedance condition $\varphi_n+\gamma(\partial\varphi_n)/\partial z=0$. This is more realistic than the previous case, since now the bottom would display a reflection coefficient variable with angle (and frequency if desired). In such a case the important problem of the interplay between ζ' and the reflection coefficient could be studied.

In the case of such an impedance condition, the only modification to the foregoing results is in the vertical eigenvalues k_n which are no longer $n\pi/H-\zeta$. In fact, the k_n are now to be determined by solving the transcendental equations $\tan k_n(H-\zeta)=-k_n\gamma$. Such an equation can be solved numerically. It is important to note that γ may be a function of x and y. In particular it would be possible to use a different reflection coefficient on the continental slope than on the deep ocean floor or in the continental shelf areas.

In short, then, to the extent that the bottom can be approximated by an impedance condition it appears that considerable progress can be made using this theory. Once the uncoupled mode solution is obtained in a particular case it is a simple matter to obtain the first-order corrections due to mode-mode coupling by perturbation theory. This line of research will be pursued in the following year.

Other work has been carried out under this contract by Claude W. Horton, Sr. This work has been chiefly directed toward obtaining a useful solution for the wedge geometry (constant slope) in the two-fluid case. Such a solution would have considerable practical utility, not so much for the wedge itself but because a wedge could be attached to a rectangular basin and thus provide a useful model of an ocean basin leading into the continental shelf. This work is summarized in Appendix D.

REFERENCES

1. Pierce, A. D., "Extension of the Method of Normal Modes to Sound Propagation in an Almost Stratified Medium," J. Acoust. Soc. Am. 37, 19 (1965).

2. Milder, D. M., "Ray and Wave Invariants for SOFAR Channel Propagation," J. Acoust. Soc. Am. 46, 1259 (1969).

3. Urick, R. J., "Sound Transmission from Deep to Shallow Water," Naval Ordnance Laboratory Report, NOLTR-72-1, 1971.

4. Roberts, B. G., Jr., "Horizontal-Gradient Acoustical Ray-Trace Program TRIMAIN, Naval Research Laboratory Report, NRL 7827, 1974.

5. Vekua, I. N., New Methods for Solving Elliptic Equations (American Elsevier Publication Company, Inc., New York, 1962).

6. Kupradze, V. D., Potential Methods in the Theory of Electricity (Israel Program for Scientific Translation, Jerusalem, 1965).

7. Weinberg, H., and R. Burridge, "Horizontal Ray Theory for Ocean Acoustics," J. Acoust. Soc. Am. 55, 63 (1974).

APPENDIX A

FINDING EIGENRAYS IN A HORIZONTALLY STRATIFIED ENVIRONMENT

In propagation problems involving interpretation of specific influences such as the magnitude of bottom interaction effects, it is often useful to decompose the propagation and identify intermediate parameters, such as bottom interaction angle, for specific eigenrays of the problem. Program RANGER is designed to find the eigenrays (rays connecting a source and receiver) for a series of receiver ranges given: a sound speed profile, a source depth, and up to six receiver depths. It assumes the ocean surface and bottom to be flat and specularly reflecting and assumes that sound speed varies only with depth. The sound speed profile points are connected by linear segments so that the sound speed gradient is constant between two depths specified in the profile. For each range, RANGER computes the minimum number of deep turning points, n, required for any ray to reach the receiver range. It then finds all the eigenrays with n, n+1, and n+2 deep turning points. For each eigenray the launch angle, bottom reflection angle (if the ray is bottom reflected), receiver angle, transit time, and general ray description (i.e., whether surface reflected, deep refracted, etc.) is printed.

RANGER can also find eigenrays which pass through the sediment. For these cases, the rays are traced downward until they reflect from the particular sediment layer interface of interest or until they turn around, by refraction, within a sediment layer.

I. SOUND SPEED PROFILE

The sound speed profile in the water column may either be read in directly as depth-speed pairs or computed from depth-temperature-salinity-latitude measurements using Leroy's formula. The sediment profile is obtained by reading in the layer thickness, speed at the top of the layer,

and the linear gradient of sound speed with depth for each layer. The depth and speed at each layer interface is then computed and added to the water profile. Whenever a sound speed mismatch at an interface occu s, an artificial, very thin (0.1 mm) layer is introduced between the two real layers. The sound speeds at the top and bottom of this artificial layer are chosen so as to eliminate the mismatch. A ray which passes through such a layer is refracted to exactly the same extent it would be if it passed directly through the sound speed discontinuity. Similarly a ray which turns around inside such a layer exits with the same angle as it entered, corresponding to a reflection from the lower (real) layer of a ray incident at less than the critical angle. These artificial layers are introduced only as a programming convenience; the usual computations for a ray traversing a layer (e.g., travel time) are suppressed except for the angle change.

After the sound speed profile is assembled it is modified slightly to account for the effect of the earth's curvature on ray paths. This is accomplished by modifying each depth-speed pair in the profile as follows:

$$z' = z(1 + z/(2R_E)) \quad , \tag{A1}$$

$$c' = cR_E/(R_E-c) \quad , \tag{A2}$$

where z is depth, c is sound speed, and R_E is the earth's radius. Also, the sound speeds are adjusted where necessary so that the sound speed difference across a layer is never less than 10^{-6} m/sec (i.e., no zero gradient layers are allowed).

Finally, new points corresponding to the source depth and up to six receiver depths are inserted in the profile. The sound speeds at these depths are obtained by linear interpolation.

II. RAY CALCULATIONS WITHIN A LAYER

For a ray traversing a layer we are interested in computing the entrance and exit angles, θ_i and θ_f, the horizontal range displacement, Δr, and the transit time (Fig. A1).

The derivations which follow are constructed to work for upgoing as well as downgoing rays, and for rays which turn around within a layer. In the latter case, $\theta_f = 0$.

The angles are related by Snell's law:

$$\frac{\cos \theta}{c} = \frac{\cos \theta_{source}}{c_{source}} \equiv p \quad . \tag{A3}$$

The ray path in a layer of constant sound speed gradient is an arc of a circle, so the range displacement can be found by

$$\Delta r = R\left|\sin \theta_f - \sin \theta_i\right| \quad . \tag{A4}$$

The layer penetration, h, is given by:

$$h = R\left|\cos \theta_f - \cos \theta_i\right| \quad , \tag{A5}$$

where R is the radius of the arc. For a nonvertexing ray, h is the layer thickness. Combining Eq. (A4) with Eq. (A5) yields

$$\Delta r = h\left|\frac{\sin \theta_f - \sin \theta_i}{\cos \theta_f - \cos \theta_i}\right| \quad . \tag{A6}$$

Computationally, this is a poor formula because cancellation errors occur when $\theta_i \sim \theta_f$. However, it can be rewritten with the aid of trigonometric identities in the form:

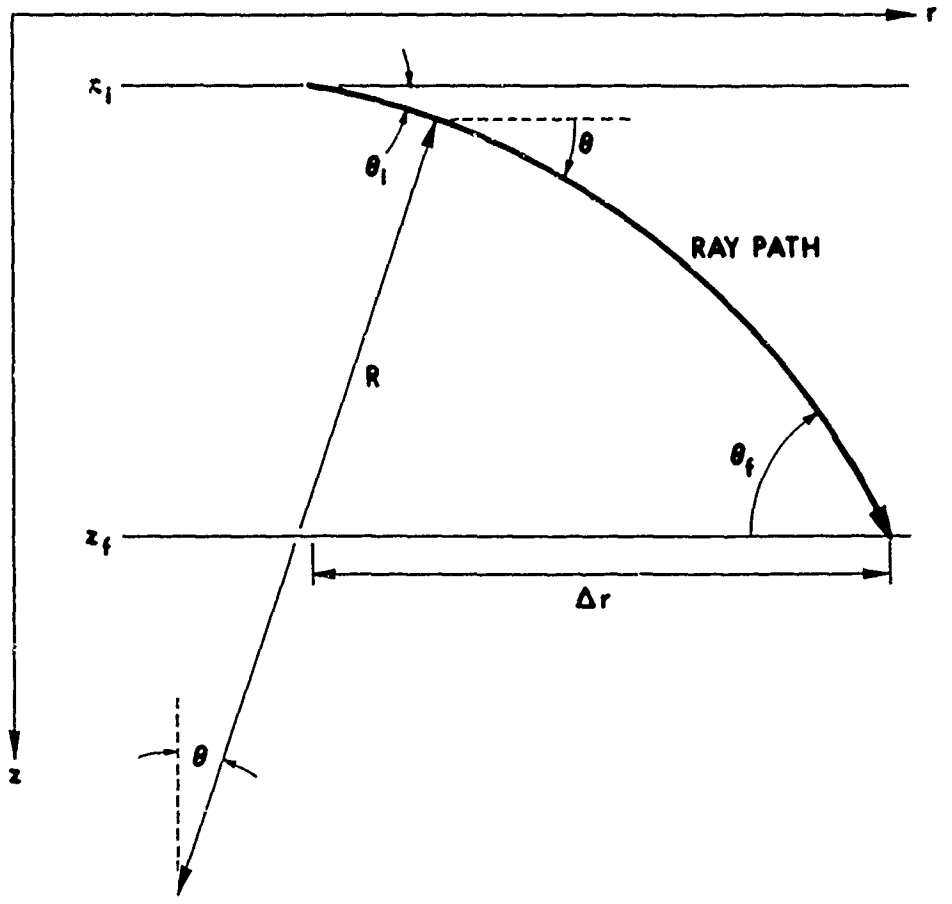

FIGURE A1
RAY PARAMETERS IN A SINGLE LAYER
OF LINEAR SOUND SPEED GRADIENT

ARL - UT
AS-76-122
ALA - DR
2 - 12 - 76

$$\Delta r = h\left|\frac{\cos\theta_i + \cos\theta_f}{\sin\theta_i + \sin\theta_f}\right| \quad , \tag{A7}$$

which is the formula used in RANGER. The transit time, Δt, is given by

$$\Delta t = \int_o^s \frac{ds}{c(s)} = \int_o^h \frac{dz}{c(z)|\sin\theta(z)|} \quad , \tag{A8}$$

where s is the pathlength. But, by Eq. (A3),

$$|\sin\theta| = \sqrt{1 - c^2p^2} \quad . \tag{A9}$$

Combining Eqs. (A8) and (A9) yields

$$\Delta t = \int_o^h \frac{dz}{c(z)\sqrt{1 - c^2(z)p^2}} \tag{A10}$$

$$c(z) = c_i + g(z-z_i)$$

$$dc = gdz$$

$$\Delta t = \left|\frac{1}{g}\int_{c_i}^{c_f} \frac{dc}{c\sqrt{1 - c^2p^2}}\right|$$

$$= \left|\frac{1}{g}\,\ell n\left(\frac{c_f}{c_i}\,\frac{1 + \sqrt{1 - c_i^2p^2}}{1 + \sqrt{1 - c_f^2p^2}}\right)\right|$$

$$\Delta t = \left|\frac{1}{g}\,\ell n\left(\frac{c_f}{c_i}\,\frac{1 + |\sin\theta_i|}{1 + |\sin\theta_f|}\right)\right| \quad , \tag{A11}$$

where g is the sound speed gradient in the layer.

III. RAY CLASSIFICATION

Since the number of possible eigenrays for a given configuration of source, receiver, sound speed profile, and receiver range may be infinite, it is necessary to classify them so that the ones of real interest can be selected. RANGER classifies rays according to the formula

$$r(\theta_s) = nD_c(\theta_s) \pm D_1(\theta_s) \pm D_2(\theta_s) \quad ,$$

which defines the ray range r in terms of the number of deep turning points, n, the cycle distance D_c, the source angle, θ_s, and the source and receiver range segments, D_1 and D_2. D_1 and D_2 are simply the range displacements associated with those segments of the ray which lie above the source and receiver (see Fig. A2). To calculate D_c, D_1, and D_2 the ray is first traced through a half cycle, from the point at which it reflects or refracts at or near the surface to the point at which it reflects or refracts at or near the ocean bottom (or one of the reflecting sediment layer interfaces). The range displacement, Δr, for each layer penetrated is computed and tabulated. Then D_c, D_1, and D_2 are computed according to the following expressions (see Fig. A3):

$$D_c = \sum_{i=I_T}^{I_B} \Delta r_i \qquad \text{(A12)}$$

$$D_1 = \sum_{i=I_T}^{I_{SRCE}-1} \Delta r_i \qquad \text{(A13)}$$

$$D_2 = \sum_{i=I_T}^{I_{RCVR}-1} \Delta r_i \quad . \qquad \text{(A14)}$$

The total range for given n and given signs of D_1 and D_2 is calculated for specified angles of the source subject to the following definitions and restrictions.

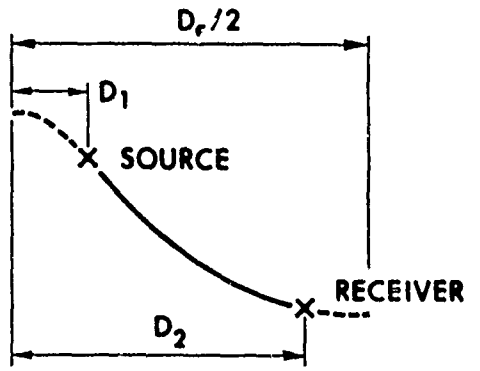

$r = -D_1 + D_2$

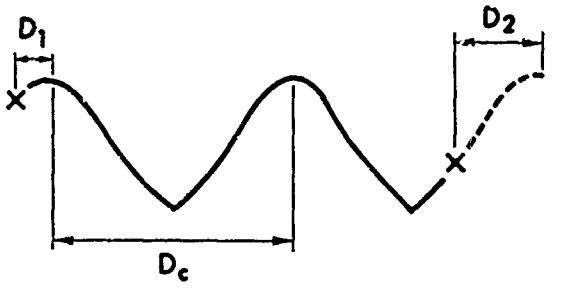

$r = 2D_c + D_1 - D_2$

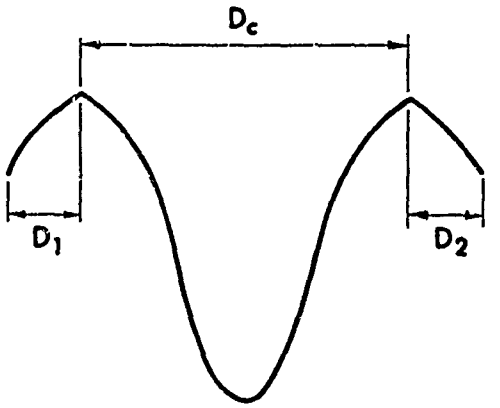

$r = D_c + D_1 + D_2$

FIGURE A2
DEFINITION OF RAY CYCLE SEGMENTS

ARL - UT
AS-76-123
ALA - DR
2 - 12 - 76

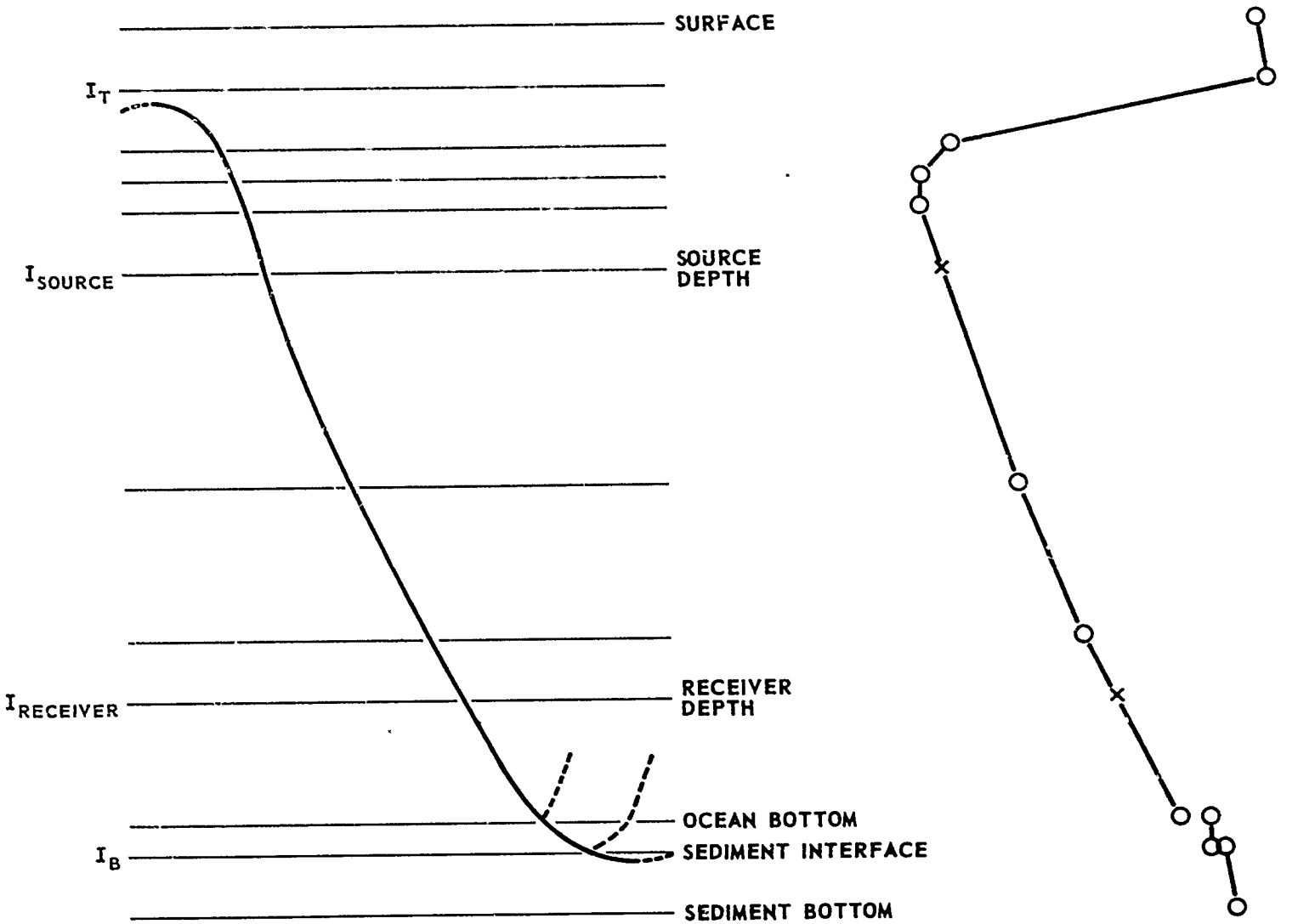

FIGURE A3
BOTTOM PENETRATING EIGENRAYS

ARL - UT
AS-76-124
ALA - DR
2 - 12 - 76

1. A deep turning point refers to either a reflection or a refraction. The depth of penetration is limited to the depth of a given reflecting layer. The ocean bottom or deepest subbottom layer is always considered reflecting.

2. The range could be negative if n=0 for some combinations of the signs of D_1 and D_2; this is physically meaningless and so these combinations are disallowed.

3. The range is undefined (and not computed) for rays which do not penetrate to the receiver depth.

This total range, when computed for several angles of departure of the rays at the source, can be used to construct range versus source angle curves (r-θ curves).

IV. RANGE-ANGLE CURVES

Shown in Fig. A4 is a set of r-θ curves for the profile of Fig. A5 with n=2, a source at 410 m depth and a receiver at 1200 m depth. The eigenrays are given by the intersections of the curves with the receiver range line. Note that

1. only positive θ_s are used; the sign of D_1 determines the true sign of the launch angle;

2. for all angles less than 5.4410° r is undefined because the rays don't reach the receiver depth for smaller angles;

3. the discontinuities in the r-θ curves (Fig. A4) at 8.0442° and 11.5765° are caused by features A and B in the sound speed profile (Fig. A5);

4. the peak at 14.3522°, where the r-θ curve is continuous but its first derivative changes sign, is caused by feature C in the profile. When eigenrays found just to the right of the peak in the r-θ curve are used for intensity calculations they produce false caustics. This problem is an artifact of the straight line segment approximation; and

5. the slope change at 21.2800° shows the effect on the r-θ curves when the rays begin to reflect from the bottom. For larger angles, r decreases steadily until, at θ_s=90°, r=0.

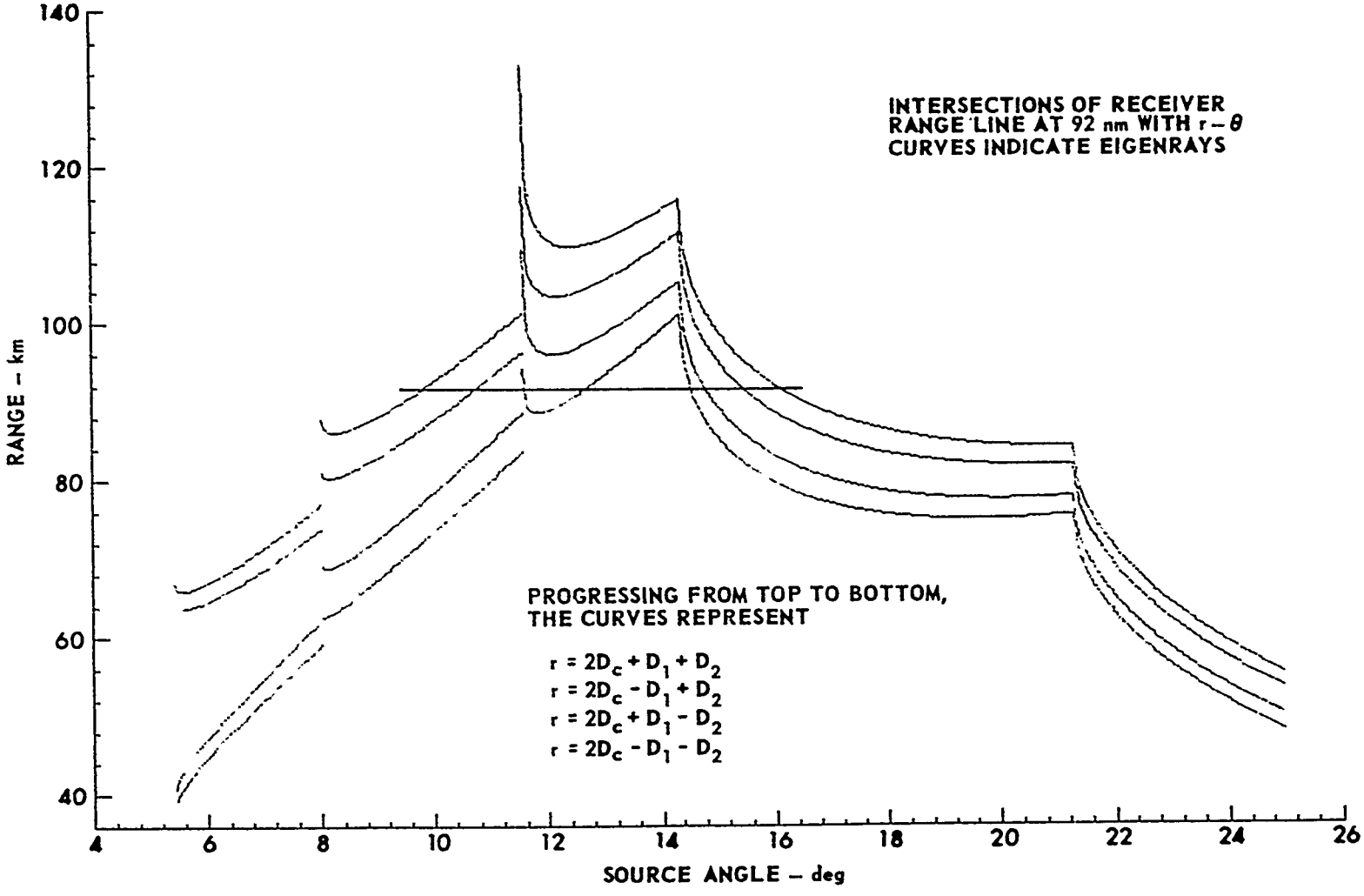

FIGURE A4
RANGE VERSUS SOURCE ANGLE PLOT

ARL - UT
AS-76-126
ALA - DR
2 - 12 - 76

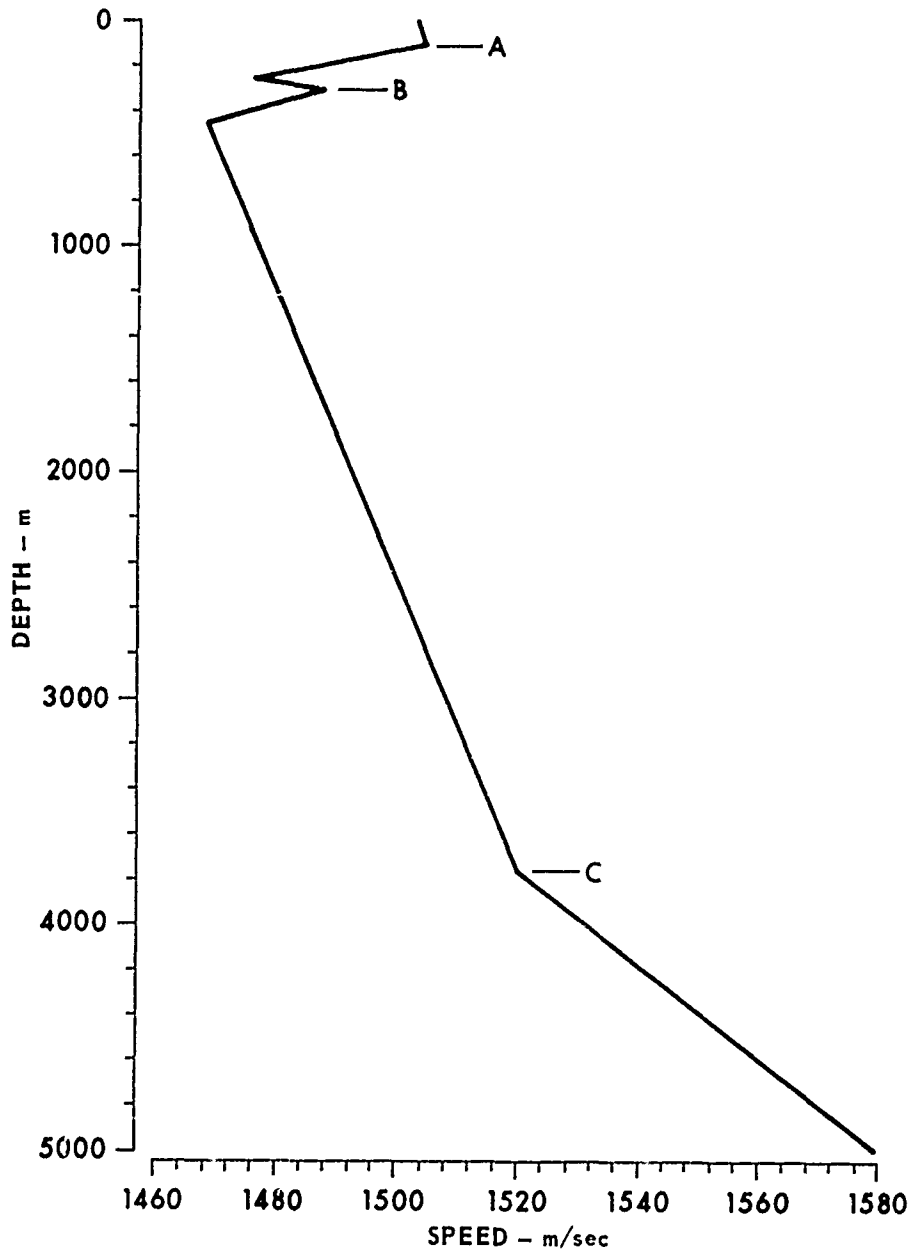

FIGURE A5
SOUND SPEED VERSUS DEPTH PROFILE

ARL - UT
AS-76-125
ALA - DR
2 - 12 - 76

V. CRITICAL ANGLES

As described above, certain features in the sound speed profile can cause discontinuities and peaks to appear in the r-θ curves. These irregularities in the r-θ curves must be taken into account when searching for eigenrays since they are found by locating intersections of the r-θ curves with the receiver range. Fortunately, the angles at which discontinuities occur can always be found easily. This is not quite the case with peaks (range maxima): though the angles at which they might occur are easily found, it is not easy to eliminate false alarms. For this reason RANGER treats all candidate peak angles alike, resulting in a slight loss in speed.

To find ray angles at the source which are associated with discontinuities or maxima (peaks) in the r-θ curve, RANGER starts at the source depth and works down, searching for a sound speed, c_M, which is greater than any which have occurred previously. When such a depth-speed pair is found, the associated angle is computed by

$$\cos \theta_M = c_{SRCE}/c_M \quad . \tag{A15}$$

By Snell's law, this is exactly the angle at the source that is required to cause a ray to turn around at the depth at which c_M occurs. Whether this angle (θ_M) corresponds to a discontinuity or a possible peak is determined by examining the next depth-speed pair. If the speed there is less than c_M, there is a discontinuity. Otherwise, θ_M is classified as a possible peak angle. After examining all profile points below the source depth the process is repeated, this time starting at the source depth and working toward the surface. The resulting set of angles (θ_M) are printed out and are designated as critical angles (not to be confused with the critical angle associated with reflection from an interface).

VI. RAY DESIGNATION

If a ray reflects from the ocean's surface, the ray is designated SR; if it refracts near the surface it is designated SR*. Similarly, ocean bottom reflection and refraction designations are BR and BR*, respectively. Rays which penetrate the bottom and enter the sediment are designated BP rather than BR or BR*.

VII. EIGENRAYS

Before any eigenrays can be found, the sound speed profile must be assembled and the critical angles (θ_M) found. Then, since RANGER is completely automated, it must determine which ray classifications at least have the possibility of containing eigenrays. This determination is made by computing the minimum number of deep turning points required for a ray to reach the receiver range. Mathematically, this can be written

$$n_{MIN}\, D_{c_{MAX}} + D_{1_{MAX}} + D_{2_{MAX}} \geq \text{receiver range} \quad , \tag{A16}$$

where $D_{c_{MAX}}$ is the largest cycle distance the profile allows and $D_{1_{MAX}}$ and $D_{2_{MAX}}$ are the source and receiver incremental distances associated with $D_{c_{MAX}}$. The maximum cycle distance, $D_{c_{MAX}}$, is found by computing D_c for every critical angle (for discontinuities, two angles near and on either side of the critical angle are used) and by taking the largest D_c encountered as $D_{c_{MAX}}$. The minimum number of deep turnings, n_{MIN}, is obtained by rounding

$$\frac{\text{receiver range} - D_{1_{MAX}} - D_{2_{MAX}}}{D_{c_{MAX}}} \quad , \tag{A17}$$

up to the next higher integer. There is no guarantee that eigenrays exist for n_{MIN}, but this is the minimum number of deep turnings for a ray to

potentially be an eigenray. RANGER finds the eigenrays which do exist for n_{MIN}, $n_{MIN}+1$, and $n_{MIN}+2$ and all allowed sign combinations of D_1 and D_2.

The method used to find the eigenrays of a given classification relies on the fact that the r-θ curves are always concave upward. The range at each pair of adjacent critical angles (θ_n) is computed (for break angles, angles very near the critical angle are used). If the two ranges obtained are both less than the receiver range then there are no eigenrays between these two angles and RANGER moves on to the next pair of critical angles. If one range is less than the receiver range and the other is greater then there is precisely one eigenangle between the critical angles and a standard root-finding subroutine is invoked to find it. If both ranges exceed the receiver range then there are either no eigenangles between the critical angles or there are two. An angle is chosen roughly halfway between the two critical angles and the range is computed at that angle. If this range also exceeds the receiver range, then RANGER concludes there are no eigenangles in the interval. However, if the range is less than the receiver range then the root-finding routine is invoked twice to find both eigenangles.

Table A1 is the output from RANGER showing the eigenrays for the configuration described in Section IV. Figure A6 is a ray trace of the eigenrays which were found by RANGER for n=2.

```
   DOUBLE AXIS PROFILE

 S DEPTH  R DEPTHS
   410.00   1200.00

INPUT PROFILE IN WATER COLUMN (DEPTH/SPEED OR DEPTH/TEMP-SAL-LATITUDE)
        0   1503.00
   100.00   1504.00
   250.00   1476.00
   300.00   1488.00
   450.00   1468.00
  3750.00   1520.00
  5000.00   1580.00

SEDIMENT PROFILE (LAYER THICKNESS/SPEED-DEN)

MODIFIED PROFILE (DEPTH/SPEED)
        0   1503.00
   100.00   1504.02
   250.01   1476.06
   300.01   1488.07
   410.03   1473.43
   450.03   1468.10
  1200.23   1480.10
  3752.21   1520.90
  5003.93   1581.24

CRITICAL ANGLE   TYPE
         0       *
      5.4410     0
      8.0442     1
     11.5765     1
     14.3522     0
     21.2800     0
     90.0000     *

RECEIVER RANGE (NM): 49.676
   RECEIVER NO. 1
      NO. DEEP TURNING POINTS:  2
         REFLECTING LAYER NO.: 1
            SRCE ANGLE:  11.5875  RCVR ANGLE: -10.2460  RAY ANGLE:**********  TIME (S): 62.032138  SR  BR*
            SRCE ANGLE:  12.7888  RCVR ANGLE: -11.5822  RAY ANGLE:**********  TIME (S): 62.025537  SR  BR*
            SRCE ANGLE:  14.5383  RCVR ANGLE: -13.4935  RAY ANGLE:**********  TIME (S): 62.044752  SR  BR*
         REFLECTING LAYER NO.: 1
            SRCE ANGLE: -14.7683  RCVR ANGLE: -13.7903  RAY ANGLE:**********  TIME (S): 62.159337  SR  BR*
         REFLECTING LAYER NO.: 1
            SRCE ANGLE:  10.8364  RCVR ANGLE:  9.3858  RAY ANGLE:**********  TIME (S): 62.301519  SR* BR*
            SRCE ANGLE:  15.3977  RCVR ANGLE:  14.4261  RAY ANGLE:**********  TIME (S): 62.436322  SR  BR*
         REFLECTING LAYER NO.: 1
            SRCE ANGLE:  -9.9234  RCVR ANGLE:  8.3112  RAY ANGLE:**********  TIME (S): 62.351443  SR* BR*
            SRCE ANGLE: -14.0197  RCVR ANGLE:  15.0902  RAY ANGLE:**********  TIME (S): 62.561308  SR  BR*
      NO. DEEP TURNING POINTS:  3
         REFLECTING LAYER NO.: 1
            SRCE ANGLE:   7.9260  RCVR ANGLE:  -5.7727  RAY ANGLE:**********  TIME (S): 62.357618  SR* BR*
            SRCE ANGLE:  22.3562  RCVR ANGLE: -21.7160  RAY ANGLE:   7.0145  TIME (S): 64.658978  SR  BR
         REFLECTING LAYER NO.: 1
            SRCE ANGLE:  -7.6261  RCVR ANGLE:  -5.3515  RAY ANGLE:**********  TIME (S): 62.370158  SR* BR*
            SRCE ANGLE: -22.5720  RCVR ANGLE: -21.9397  RAY ANGLE:   7.7881  TIME (S): 64.854818  SR  BR
         REFLECTING LAYER NO.: 1
            SRCE ANGLE:   5.9311  RCVR ANGLE:  2.3444  RAY ANGLE:**********  TIME (S): 62.493841  SR* BR*
            SRCE ANGLE:  22.9954  RCVR ANGLE:  22.3765  RAY ANGLE:   8.9248  TIME (S): 64.269138  SR  BR
         REFLECTING LAYER NO.: 1
            SRCE ANGLE: -23.2526  RCVR ANGLE:  22.6415  RAY ANGLE:   9.5982  TIME (S): 64.471407  SR  BR
      NO. DEEP TURNING POINTS:  4
         REFLECTING LAYER NO.: 1
            SRCE ANGLE:   5.4572  RCVR ANGLE:  -0.4205  RAY ANGLE:**********  TIME (S): 62.494429  SR* BR*
            SRCE ANGLE:  26.1764  RCVR ANGLE: -25.6438  RAY ANGLE:  15.6118  TIME (S): 66.010109  SR  BR
         REFLECTING LAYER NO.: 1
            SRCE ANGLE: -24.4914  RCVR ANGLE: -25.9465  RAY ANGLE:  14.1601  TIME (S): 66.242749  SR  BR
         REFLECTING LAYER NO.: 1
            SRCE ANGLE:  27.0753  RCVR ANGLE:  26.5436  RAY ANGLE:  17.1451  TIME (S): 66.725236  SR  BR
         REFLECTING LAYER NO.: 1
            SRCE ANGLE: -27.4066  RCVR ANGLE:  26.8961  RAY ANGLE:  17.4791  TIME (S): 66.966191  SR  BR

 I FIND 0060 STOP
```

TABLE A1
RANGER OUTPUT

ARL - UT
AS-76-127
ALA - LR
2 - 12 - 76

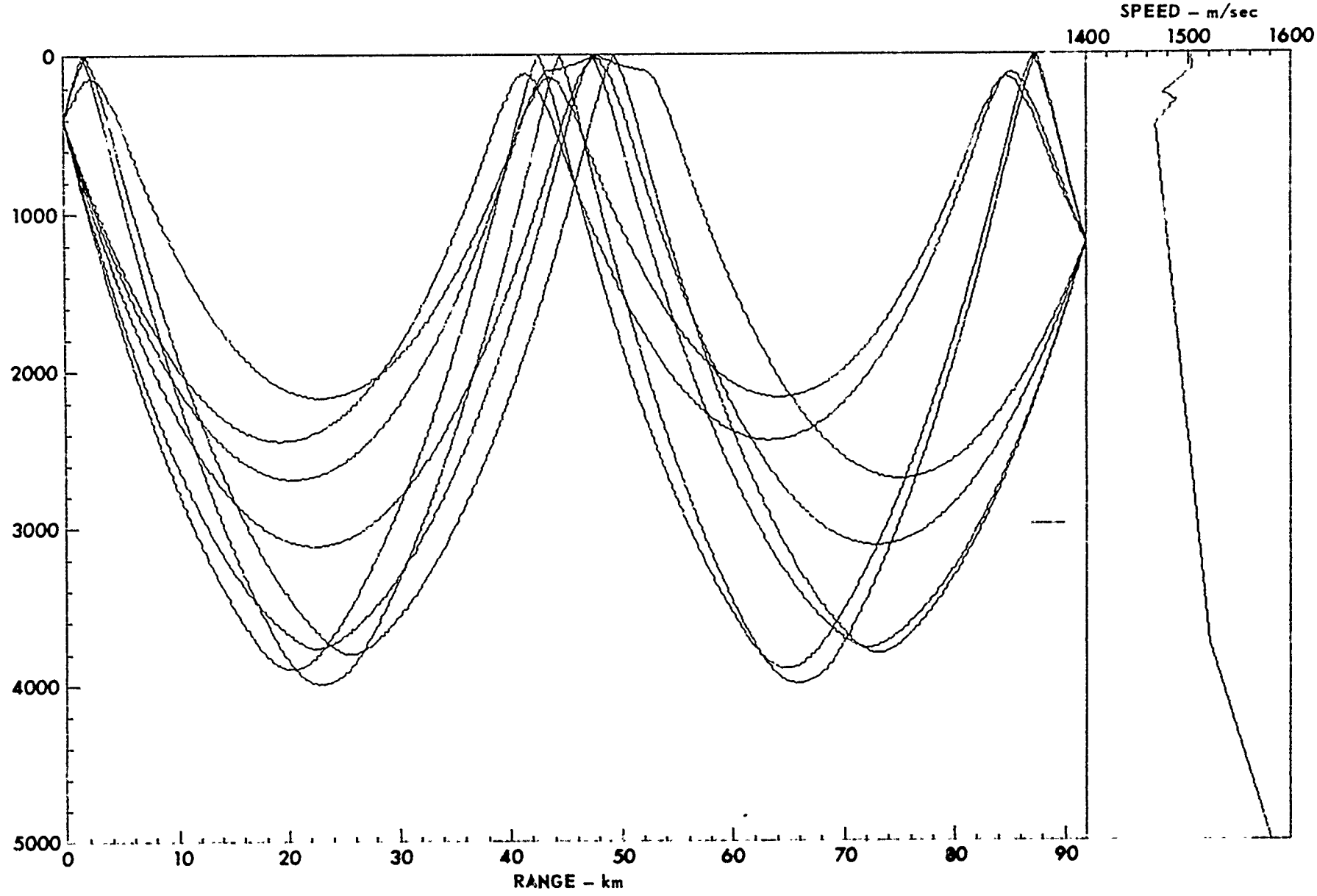

ARL - UT
AS-76-128
ALA - DR
2 - 12 - 76

FIGURE A6
DOUBLE AXIS PROFILE EIGENRAYS

APPENDIX B

A BOTTOM LOSS MODEL BASED ON NUMERICAL INTEGRATION

This appendix describes a bottom loss (plane wave reflection coefficient) model based on a direct numerical integration of the depth separated wave equation. The important advantages of such an approach are fourfold:

1. essentially arbitrary sound speed profiles can be tested;
2. inclusion of a continuously variable density is trivial;
3. values of the sound field throughout the sediment layers are always available for use as an additional diagnostic tool; and
4. numerical errors are relatively easily controlled.

After first discussing the mathematical basis for the model, a brief description of the computer code is given. A more detailed explanation of the code and algorithms used will be given in a later report.

A. Mathematical Model

The basic model (Fig. B-1) consists of an arbitrary number of (fluid) sediment layers overlying a semiinfinite substrate which can be either fluid or solid. The sediment layers may have arbitrary sound speed and density profiles; however, the substrate is treated as completely homogeneous.

The sound pressure field in the overlying water is assumed to be

$$P_o = A_o\left[e^{ik_o \sin\theta z} + R\, e^{-ik_o \sin\theta z}\right] e^{-i\omega t}\, e^{+i\kappa_o x} \quad . \tag{B1}$$

where $k_o = \omega/c_o$, $\kappa_o = k_o \cos\theta$, and θ is the grazing angle. Within each sediment layer, say the jth, the sound pressure satisfies

$$\frac{d^2 P_j}{dz^2} - \frac{\rho_j'(z)}{\rho_j(z)} \frac{dP_j}{dz} + \left[k_j^2(z) - \kappa_o^2\right] P_j = 0 \quad , \tag{B2}$$

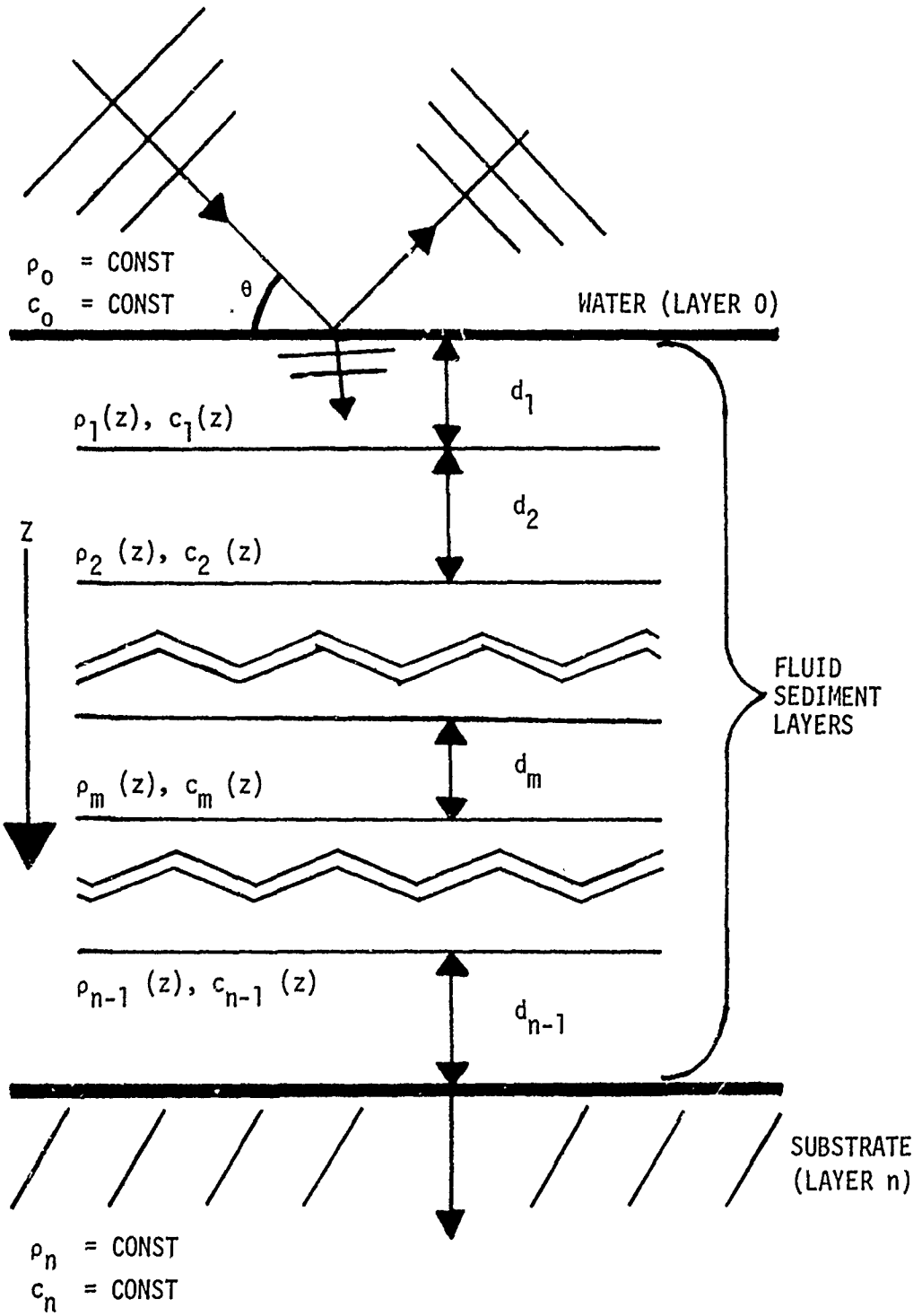

FIGURE B-1

LAYER NUMBERING CONVENTION

AS-76-142

where the density is $\rho_j(z)$, and the wavenumber $k_j(z)$ may be complex to account for absorption. The second term in Eq. (B2) accounts for the (possibly) variable density in the case when the direct effect of the gravitational field is ignored (see Bergmann[1]). In the substrate, there are two fields, compressional and shear, which are most conveniently described by the velocity potentials $\varphi_n(z)$ and $\psi_n(z)$ satisfying

$$\frac{d^2\varphi_n}{dz^2} + \left(k_n{}^{c2} - \kappa_o{}^2\right)\varphi_n = 0 \quad , \tag{B3}$$

and

$$\frac{d^2\psi_n}{dz^2} + \left(k_n{}^{s2} - \kappa_o{}^2\right)\psi_n = 0 \quad , \tag{B4}$$

where $k_n{}^c = \omega/c_n{}^c$, $k_n{}^s = \omega/c_n{}^s$, and $c_n{}^c$ and $c_n{}^s$ are the compressional and shear wave speeds in the substrate, the nth layer. With the time dependence $e^{-i\omega t}$ and the z-axis measured as increasing downward, φ_n and ψ_n are determined by the radiation condition to be

$$\varphi_n = A_n\, e^{i\kappa_n{}^c z}\, e^{+i\kappa_o x}\, e^{-i\omega t} \quad , \tag{B5}$$

$$\psi_n = B_n\, e^{i\kappa_n{}^s z}\, e^{+i\kappa_o x}\, e^{-i\omega t} \quad , \tag{B6}$$

with $\kappa_n{}^c = \left[k_n{}^{c2} - \kappa_o{}^2\right]^{1/2}$, $\kappa_n{}^s = \left[k_n{}^{s2} - \kappa_o{}^2\right]^{1/2}$ and, as before, $k_n{}^c$ and $k_n{}^s$ may be complex.

At a fluid-fluid interface the well known continuity conditions apply:

$$\left.\begin{aligned} \rho_i{}^{-1} P_i{}' &= \rho_{i+1}{}^{-1} P_{i+1}{}' \\ P_i &= P_{i+1} \end{aligned}\right\} \text{ at the interface} \quad . \tag{B7}$$

Upon applying these conditions at the water-sediment interface, taken as z=0, the incident amplitude A_o can be eliminated and the reflection coefficient, R, is found to be given by

$$R = \left. \frac{ik_o \sin\theta - \frac{\rho_o}{\rho_1}\frac{\varphi_1'}{\varphi_1}}{ik_o \sin\theta + \frac{\rho_o}{\rho_1}\frac{\varphi_1'}{\varphi_1}} \right|_o \quad . \tag{B8}$$

It is clear that only $\varphi_1'(o)/\varphi_1(o)$ is now required in order to compute R. This ratio may be determined by solving the wave equation in each layer and applying the continuity conditions plus a radiation condition in the lower half space. If all n layers, including the substrate, were fluids, there would be 2n unknown constants and 2n continuity conditions.

Before discussing how the wave equation is to be solved in each layer, it is necessary to examine the continuity conditions for a fluid-solid interface. These are continuity of the normal component of velocity, continuity of normal stress, and continuity of tangential stress. Since the tangential stress in the liquid vanishes, so must the tangential stress in the solid. These conditions are given, for example, by Brekhovshikh.[2] It will be convenient to deal with the pressure in the fluid layers and the two velocity potentials in the substrate. Denoting the shear and compressional field by ψ_s and φ_s, we have

$$v_z^{\text{fluid}} = \frac{-1}{i\omega\rho}\frac{\partial p^{\text{fluid}}}{\partial z} = v_z^{\text{solid}} = \frac{\partial \varphi_s}{\partial z} + \frac{\partial \psi_s}{\partial z} \quad , \tag{B9}$$

$$\sigma_{zz}^{\text{fluid}} = -p^{\text{fluid}} = \sigma_{zz}^{\text{solid}} = \frac{-1}{i\omega}\left\{\lambda_s \nabla^2 \varphi + 2\mu_s\left(\frac{\partial^2 \varphi_s}{\partial z^2} + \frac{\partial^2 \psi_s}{\partial x \partial z}\right)\right\} \quad , \tag{B10}$$

$$\sigma_{zx}^{\text{fluid}} = 0 = \sigma_{zx}^{\text{solid}} = 2\frac{\partial^2 \varphi_s}{\partial x \partial z} + \frac{\partial^2 \psi_s}{\partial x^2} - \frac{\partial^2 \psi_s}{\partial z^2} \quad , \tag{B11}$$

where σ is the stress tensor, and λ_s and μ_s are the usual Lame' constants.

Upon reintroducing our layer numbering convention (water: φ_o, sediment: $P_1,\ldots,P_{n-1}$, substrate: φ_n, ψ_n) and using Eqs. (B5) and (B6), then Eq. (B11) may be solved for ψ_s and thereby eliminate ψ_s, and its derivatives, from the problem. After some simple algebra, one finds

$$P_{n-1} = \left(-i\omega Q\varphi_n\right)\left(P\rho_n\right) \quad , \tag{B12}$$

$$\frac{P_{n-1}'}{\rho_{n-1}} = \kappa_n{}^c\omega\left(Q\varphi_n\right) = -i\omega Q\varphi_n \quad , \tag{B13}$$

where P and Q are given by

$$Q = \frac{k_n{}^{s\,2}}{\kappa_n{}^{s\,2} - \kappa_o{}^2} \quad , \tag{B14}$$

$$P = \frac{\left(\kappa_n{}^{s\,2} - \kappa_o{}^2\right)^2 + 4\kappa_o{}^2\kappa_n{}^s\kappa_n{}^c}{k_n{}^{s\,4}} \quad . \tag{B15}$$

It should be noted that if $c_n{}^s=0$, that is, the substrate is a fluid, then $Q=P=1$, and upon using $-i\omega\rho_n\varphi_n=p_n$ and $-i\omega\varphi_n'=p_n'/\rho_n$, one obtains the usual continuity conditions involving the pressure.

This completes the specification of the mathematical model and its boundary conditions.

B. The Numerical Integration Bottom Loss Model

The basic idea behind the numerical integration model is now easily grasped. Having obtained boundary conditions in the form given in Eqs. (B12) and (B13), one simply assumes $\varphi_n=1$ and thereby obtains ρ_{n-1}

and ρ_{n-1}' at the bottom of the lowest sediment layer. Knowledge of $\rho_{n-1}(H_{n-1})$ and $\rho_{n-1}'(H_{n-1})$ together with the differential equation, Eq. (B2), specifies an initial value problem which may be readily solved numerically on a finite interval. This procedure is repeated upward through all sediment layers until finally $\varphi_1(o)$ and $\varphi_1'(o)$ are obtained. The reflection coefficient R and the bottom loss $-20 \log_{10} |R|$ are then easily computed using Eq. (B8).

Program BOTLOSS (Fig. B-2) was implemented on a CDC 3200 computer. It reads in physical parameters which completely specify the system, computes reflection coefficients for specified grazing angles, and then produces printer or Calcomp plots of reflection coefficient versus angle on either a linear or logarithmic (dB) scale. A printed tabulation of calculated values is also generated. BOTLOSS can also print out the wavefield throughout the sediment layers for any specified grazing angle.

At the time of this writing BOTLOSS can use any of the following depth dependent functions.

$$\rho(z) = \begin{cases} \rho(0) \\ \rho(0) + g_\rho z, \text{ where } g_\rho \text{ is a constant gradient} \end{cases}$$

$$c(z) = \begin{cases} c(0) \\ c(0) + g_c z, \text{ where } g_c \text{ is a constant gradient} \\ c(0)/\sqrt{1 - 2g_c/c(0)} \end{cases} .$$

The program is structured so that the extension of this repertoire of functions is easily carried out.

The method used to solve the differential equation is a Runge-Kutta scheme devised by E. Fehlberg. This variation on the classical fourth order scheme is a relatively slow but stable method which is capable of

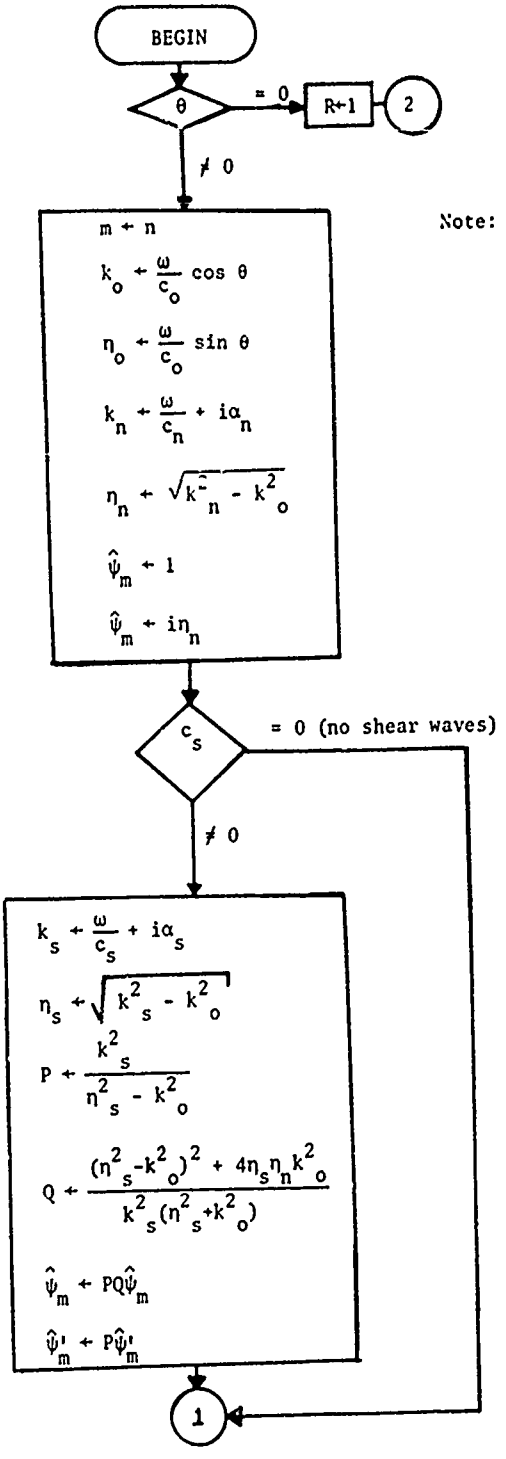

FIGURE B2

FLOW DIAGRAM OF THE PROCEDURE USED TO COMPUTE REFLECTION COEFFICIENTS

BS-76-568

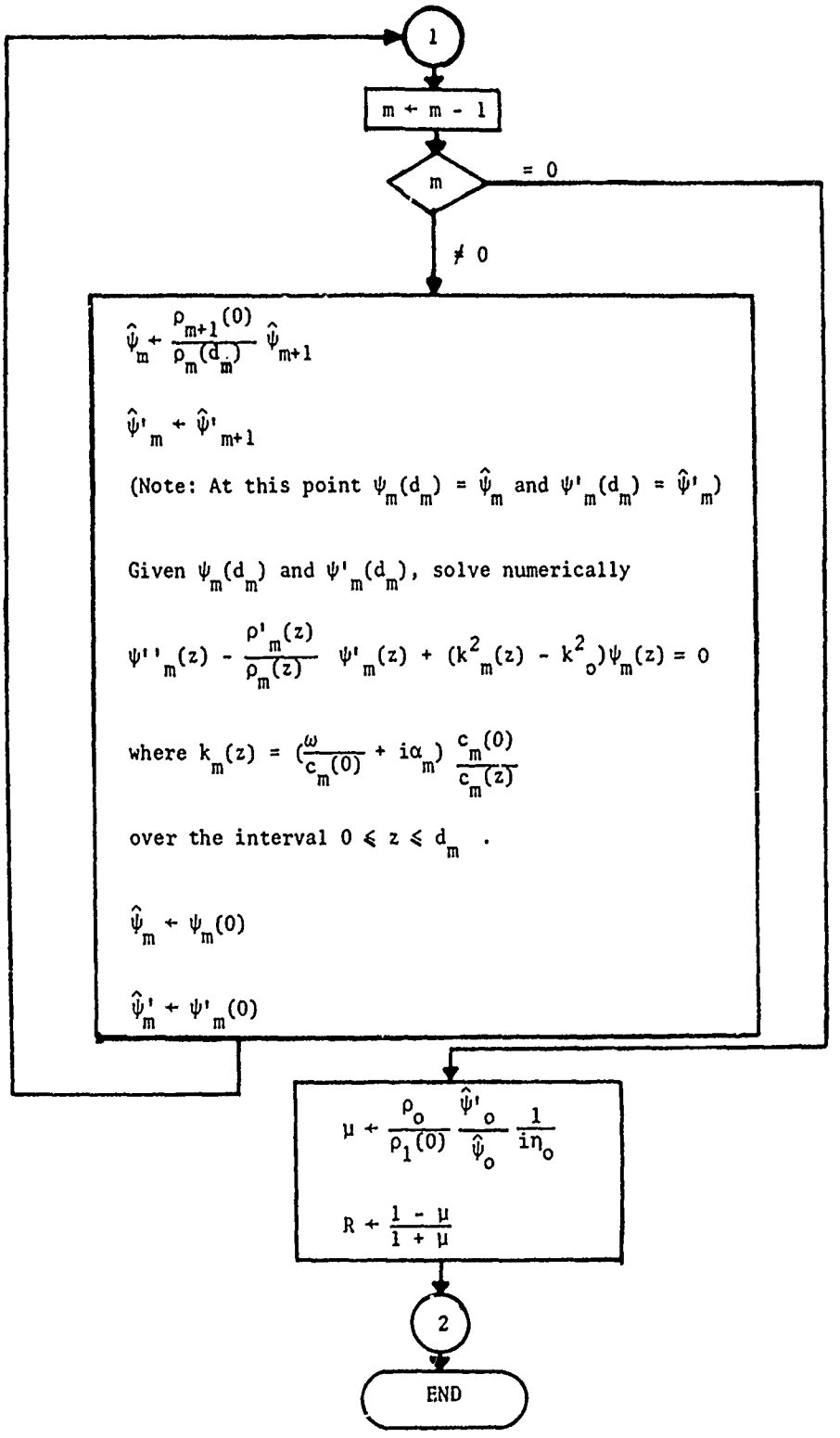

FIGURE B2 (Cont'd)

BS-76-569

continually adjusting the integration step size to meet specified local (one step) error requirements (see Shampine and Allen). Error incurred during the integration process is the dominant source of error in the calculation of the reflection coefficient, so it is vital that a sufficiently stringent local error requirement be specified to guarantee an acceptably small total error. Since the global error is determined by the local error (finite word size roundoff error is expected to be negligible in this problem), it may be possible to provide a running estimate of total error. If so, then future versions of this program will provide estimates of the global error in the tabulated output.

Verification of the model has centered on comparison of its predictions with those made by models which assume $\rho(z)$ = constant, and $c(z)$ = constant or, $c(z)=c(0)\left[1-2g_c/c(0)\right]^{-1/2}$ (the pseudolinear model)--assumptions which make exact solutions possible. No discrepancies greater than a few hundredths of a decibel have been observed. In any case, since the global error is controlled, it is always possible to obtain a desired overall accuracy simply by requiring a sufficiently small local error.

An ultimate limit to this procedure is imposed by finite word size and resultant roundoff error, but it is not expected that this limit will play a role in present applications. This linkage between local and global error has been explicitly verified in comparisons between a numerical solution and a numerical evaluation of an analytical solution for the cases of a constant sound speed and the pseudolinear model.

An important shortcoming of this model is the long integration time required to solve the differential equation. This effectively limits use of the model to sediments no thicker than about 50 to 100 wavelengths. Critical sections of the code are being converted to assembly language, but this will not reduce execution time enough to allow investigation of significantly higher frequencies or thicker sediments.

A hybrid numerical/WKB technique, now under investigation, may significantly reduce execution time.

Additional improvement will include adding the capability for specifying $c(z)$ and $\rho(z)$ by a sequence of discrete points $\left(\rho_i(z_i), c_i(z_i), z_i\right)$, rather than through an assumption of a functional form. This modification will then permit examination of cases when $c(z)$ and $\rho(z)$ are only approximately linear due to the distance required to establish a constant gradient.

REFERENCES

1. Bergmann, P. G., "The Wave Equation in a Medium with a Variable Index of Refraction," J. Acoust. Soc. Am. 17, 329 (1946).

2. Brekhovskikh, L. M., Waves in Layered Media (Academic Press, New York, 1960).

3. Shampine, L. F., and R. C. Allen, Jr., Numerical Computing: An Introduction (W. B. Saunders Company, Philadelphia, 1973).

APPENDIX C

HIDDEN DEPTHS: ACCEPTABLE IGNORANCE ABOUT OCEAN BOTTOMS

by

A. O. Williams, Jr.

Normal-mode analysis of underwater-sound propagation in principle requires knowledge of pertinent physical parameters at all depths in the water and the bottom material--an unattainable omniscience. We present a method for determining the maximum depth to which this knowledge is necessary in order to hold the fractional errors in mode eigenvalues to prescribed limits. Let h_n represent a vertical distance below the lower turning point of the nth-mode solution. Insertion or removal of a horizontal plane reflector, at this depth, alters the mode eigenfunction and therefore the eigenvalue E_n. The fractional error $\Delta E_n/E_n$ is a calculable function of h_n; this error being stipulated, h_n can be found. The calculation need be made only for the highest mode that contributes significantly. Conversely, if all parameters are known to depth h, the consequent errors can be found. Two examples are analyzed, with simplifying restrictions: deep isovelocity water; low frequencies; many modes; bottoms that are isovelocity (the Pekeris case) or have a positive gradient of sound speed. For fractional errors of 10^{-4}--10^{-6}, h is a few acoustic wavelengths. In each example, bottom absorption has little effect on the result.

Introduction

In principle, wave-theoretical analyses of underwater sound propagation require complete knowledge of sound speed, absorption coefficient, and density everywhere in the water column and the bottom material. This is true even when standard simplifying restrictions are imposed: (1) a CW point source of single frequency; (2) cylindrical symmetry about the vertical axis through the source; (3) constant water depth; (4) parameters varying only with depth; (5) no scattering; and (6) neglect of the near field (described by a continuous set of modes or a branch-line integral). Each of these restraints can be relaxed, but the problem thus restricted is usually a good starting point, and we adhere to it throughout this discussion.

Satisfactory data may often be available for the water column, but certainly not for the whole bottom material. We therefore seek a criterion for a depth, in the water or the bottom, below which the physical parameters of the "hidden depths" affect the solution negligibly. A general approach is presented and two examples are discussed.

I. The normal-mode solution

Given the restrictions listed above, the acoustic velocity potential $\phi(r,z)$--the factor $\exp(-i\omega t)$ being suppressed--or equally well the acoustic pressure can be written in cylindrical coordinates r,z:

$$\phi(r,z) = \text{const. } r^{-1/2} \sum_{n=1}^{N} k_n^{-1/2} \, Z_n(d) \, Z_n(z) e^{ik_n r} \quad . \qquad (1)$$

The mode eigenfunctions Z_n, at source depth d or field-point depth z, satisfy the equation

$$d^2Z_n/dz^2 + [k^2(z) - k_n^2] Z_n = 0 \quad , \tag{2}$$

at all depths in the water and the bottom. Here N is the number of the highest discrete mode; k(z) is $\omega/c(z)$ with ω the angular frequency and c(z) the sound speed. The constants k_n^2 are the eigenvalues (k_n, ω/k_n, x_n as defined by Pekeris[1], or x_n^2 can be so regarded, instead). Equation 1 embodies the asymptotic expression for a Hankel function of $k_n r$, as is almost always safe when the near field is neglected.

If at any depth z the sound speed and/or the density change practically discontinuously, acoustic boundary conditions must be applied at the interface. The net result of all such steps is an eigenvalue equation from which k_n^2 can be calculated. The effects of absorption can be incorporated by assigning a suitable imaginary part to k(z).

Equation 2 always has two independent solutions that depend in detail upon the local properties of $[k^2(z) - k_n^2]$. Linear combinations of the two solutions can be chosen to make Z_n vanish at the sea surface (taken here as at z = 0, with z increasing downward), and at $z = \infty$.

It is widely accepted that unconsolidated bottom materials display sound speeds increasing with depth; far enough down, moreover, the material

must be hard dense rock. Hence in any given problem we can assume that for each mode there exists a depth $z = \zeta_n$--the lower turning point of Eq. 2--at which $c(z)$ has become large enough to make $[k^2(z) - k_n^2]$ turn from positive to negative and remain negative for $z > \zeta_n$. Then $Z_n(z)$ for $z > \zeta_n$ is convex toward the axis, and to satisfy the radiation condition at infinite depth we choose the unique form of Z_n that monotonically approaches zero as $z \to \infty$. For values of $z < \zeta_n$ (with localized exceptions, as in the barrier underlying an acoustic duct), $[k^2(z) - k_n^2]$ remains positive; Z_n is concave toward the axis and in general is an oscillatory function, a standing wave. Incidentally, ζ_n may lie in the water column.

II. Locating the "hidden depths"

Just above $z = \zeta_n$, let ρ_1 be the density and u_n be the properly chosen Z_n for Eqs. 1 and 2. Just below ζ_n, let ρ_2 be the density and v_n, w_n be two independent solutions of Eq. 2, so chosen that, monotonically as $z \to \infty$, $v_n \to 0$ and $w_n \to \infty$. Ordinarily v and w vary exponentially or faster, with increasing z.

At $z = \zeta_n$, as at any other interface, the acoustic conditions are continuity of two quantities: (a), the acoustic pressure, and therefore $\rho\phi$, and therefore each Z_n; (b) the z-component of acoustic particle velocity, and therefore each $Z_n' = dZ_n/dz$. Because w_n does not satisfy the radiation condition at infinity, we write the acoustic conditions in terms of u_n and

v_n, at $z = \zeta_n$. Upon taking the ratios of the two equations, we obtain

$$(u_n/u_n')_{\zeta_n} = \delta(v_n/v_n')_{\zeta_n} \quad , \tag{3}$$

with $\delta = \rho_2/\rho_1$ (which might be unity). To a degree, Eq. 3 is only symbolic, although correct. The form of u_n appearing therein depends on physical parameters everywhere above ζ_n, and of v_n on those below ζ_n. It will sometimes be preferable (Sec. IV) to express Eq. 3 at some $z < \zeta_n$. However, the general procedure will be unaltered.

Next, we consider some greater depth, $z = \zeta_n + h_n$, at which a horizontal pressure-release plane can be inserted or removed. With this reflecting plane inserted, $Z_n(\zeta_n + h_n)$ has to vanish. Therefore, $v_n(z)$ for $z > \zeta_n$ must be replaced by $v_n + \eta w_n$, with η chosen to ensure that

$$(v_n + \eta w_n)_{\zeta_n + h_n} = 0 \quad . \tag{4}$$

What happens to the other Z_n's is of no concern at the moment. Equation 3 is replaced by

$$(u_n/u_n')_{\zeta_n} = \delta[(v_n + \eta w_n)/(v_n' + \eta w_n')]_{\zeta_n} \quad . \tag{5}$$

Because of the behaviors of v and w below ζ_n, proper choice of h_n will make η as small as may be desired. Then Eq. 5 approaches, similarly closely, the form

$$(u_n/u_n')_{\zeta_n} = \delta[1-\eta\, W(v_n, w_n)/(v_n v_n')]_{\zeta_n} (v_n/v_n')_{\zeta_n} \quad . \tag{6}$$

W is the Wronskian of the independent functions v_n and w_n. It can be seen that v_n and w_n need not be normalized.

A rigid plane, upon which Z_n' vanishes, could be used in place of the pressure-release plane. The value of η would be altered, but the new η can also be made arbitrarily small, and Eq. 6 still holds. With either plane, of course, the value of (u_n/u_n') at ζ_n differs from that satisfying Eq. 3.

Equation 3 leads to an eigenvalue--e.g., k_n^2--and Eq. 6 to another eigenvalue, slightly altered by a multiplying factor $(1 + \Delta_n)$, in which Δ_n depends upon η and other quantities in Eq. 6. This relationship connecting Δ_n and η can be found; the fact that η is very small may ease the task. To complete the formal problem, we specify a numerical value for Δ_n, expressing the greatest acceptable fractional error in the eigenvalue. The known or estimated precision of available physical data may guide the choice of Δ_n. From Δ_n we find η, and finally h_n from Eq. 4. It is convenient although without physical significance to regard $\delta[1-\eta \ . \ . \ . \ ]$ in Eq. 6 as an altered density ratio. This artifice allows δ to serve as a "tracer" of $[\ . \ . \ . \ ]$, in the process of relating Δ_n and η.

There is no need to find $\zeta_n + h_n$ for all modes. If the modes are numbered in the usual fashion, so that k_n^2 decreases as n increases, v_n and w_n change most slowly, with increasing z, for the highest mode, numbered N. Consequently, $\zeta_N + h_N$ is an upper bound on the depth that we want to find. In many cases, the acoustic absorption coefficient for mode n increases with n. Sometimes it can be estimated confidently that all modes with $N > n > n_o$

are attenuated too rapidly to contribute significantly at the horizontal ranges of interest. Then $\zeta_{n_o} + h_{n_o}$ is a safe upper bound.

The whole calculation could be done in reverse. If the necessary physical parameters are known to some depth $z_o > \zeta_n$, but not below, this procedure can be used to find the maximum error in the eigenvalue of the nth mode.

We now explore two simple examples, in each one treating the water column as isovelocity, the bottom material as a fluid, and the water and bottom densities as constants. In Example A, the bottom sound speed is a constant exceeding that in the water--the standard Pekeris case[1], although not necessarily limited to shallow water and low frequency. In Example B, instead, there is a positive gradient of sound speed in the bottom. Effects of absorption are discussed in Sec. V.

III. Example A: isovelocity bottom

The water column, of depth H, has constant sound speed c_w and density ρ_w; the bottom material, a fluid half-space, has constant $c_b > c_w$ and $\rho_b > \rho_w$. We define two positive dimensionless quantities:[1,2]

$$x_n = H(k_w^2 - k_n^2)^{1/2}; \quad x_c = H(k_w^2 - k_b^2)^{1/2} \quad . \tag{7}$$

In this example, ζ_n equals H, for all n. The functions u, v and w can be expressed thus:[1,2]

$$u_n(z) = \sin(x_n z/H),\ 0 \leq z \leq H; \tag{8}$$

$$v_n,\ w_n = \exp[\mp(x_c^2 - x_n^2)^{1/2}\ (z-H)/H],\ z \geq H. \tag{9}$$

The negative sign goes with v, the positive with w. With no reflecting plane, the eigenvalue Eq. 3 is[1,2]

$$x_n^{-1} \tan x_n = -\delta(x_c^2 - x_n^2)^{-1/2} \quad . \tag{10}$$

By using Eqs. 4 and 9, we find that

$$\eta = -\exp[-2(x_c^2 - x_n^2)^{1/2}(h_n/H)] \quad , \tag{11}$$

and that [1-η . . .] in Eq. 6 is (1 + 2η).

We consider only many-mode cases and modes for which $n \approx N >> 1$. The modes are so ordered that $x_{n+1} > x_n$. Equations 7 and 10, together with the Appendix of Ref. 2, show that x_n is an angle in the second, fourth, . . . quadrant, starting in quadrant 2 for the lowest mode (n = 1) and increasing by somewhat less than π for each Δn = +1. Hence, successively larger x_n's "back up," clockwise, in the pertinent quadrants, toward an odd multiple of π/2. The largest x_n, x_N, cannot exceed x_c; if by chance the physical parameters yield $x_N = x_c$, x_N also equals $(N - 1/2)\pi$. The normalization constant for Z_N can then be shown to vanish identically[1,2]. (An equivalent phrasing is that such a mode is not the highest in a discrete set but the lowest in a continuous set of modes, which collectively affect only the near field.)

Therefore, x_N for the highest nonvanishing mode can be expressed as

$$x_N = (N - 1/2)\,\pi + \nu, \quad 0 < \nu < \pi/2 \quad , \tag{12}$$

with N the largest integer satisfying $x_n < x_c$. For many-mode cases, ν is much less than $\pi/2$. Consequently, we can make these approximations in Eq. 10: $x_N^{-1} \simeq [(N - 1/2)\pi]^{-1}$; $\tan x_N \simeq -1/\nu$; $(x_c^2 - x_N^2)^{1/2} \simeq (2x_c)^{-1/2}\,(x_c - x_N)^{-1/2}$. The result is

$$\nu \simeq [2 - (2N-1)(\pi/x_c)]^{1/2}/\delta \quad , \tag{13}$$

which with Eq. 12 yields x_N.

When the pressure-release reflector is inserted at $z = H + h_N$, δ of Eq. 13 is replaced by $\delta(1 + 2\eta)$; ν is changed by $\Delta\nu = \Delta x_N$:

$$\Delta\nu = \Delta x_N \simeq -2\eta\nu; \quad |\Delta x_N| << \pi \quad . \tag{14}$$

At this point, a choice of eigenvalue must be made; we adopt x_n^2, which is simpler for calculations and more conservative in its results than k_n^2. The outcome is

$$\Delta_N = \Delta(x_N^2)/x_N^2 \simeq 2\Delta(x_N)/x_N \simeq -(4\nu/N\pi)\eta \quad , \tag{15}$$

with ν obtainable from Eq. 13. In magnitude, Δ_N is smaller than $(2/N)|\eta|$. Once the greatest acceptable numerical value of Δ_N is specified, h_N is found from Eqs. 11, 13, and 15. For a rough assessment of h_N, we make additional approximations. First, $x_c - x_N$ can range from just above zero to somewhat less than π; as an average, we take $x_c - x_N \simeq \pi/2$, and use it in Eqs. 11 and 13. Secondly, in (h_N/H) of Eq. 11, we use the empirical relation $H \simeq N\lambda_w$, with the λ_w the acoustic wavelength in the water.

Then h_N/λ_w can be calculated for various values of N and Δ_N. Pairs of numbers, in the order $(\Delta_N, h_N/\lambda_w)$, were found for N = 25, 50, and 100 and were then averaged over N to yield $(10^{-4}, 3)$; $(10^{-5}, 6)$; $(10^{-6}, 8)$.

If k_N^2 is chosen as the eigenvalue, converted from x_N^2 by use of Eq. 7, the equation corresponding to Eq. 15 is somewhat more complicated. For the same three numerical values of Δ_N, the values of h_N/λ_w are smaller by 15--30%.

As was suggested above, it may sometimes be desired to find h_{n_o} for $n_o < N$. If $N - n_o << N$, Eq. 13 is probably still valid with n_o replacing N. If $n_o \leq N/2$, a different approximate solution of Eq. 10 is available[3].

IV. Example B: bottom material with positive gradient

The water column retains the properties of Sec. III. The bottom material, still fluid and of constant density ρ_b, now has a positive gradient of sound speed; a typical value is +1 sec^{-1}. We use a standard pseudo-linear gradient,

$$k^2(z) = k_w^2[1-\beta(z-H)], \quad z \geq H \quad . \tag{16}$$

The value $\beta \simeq 1.3 \times 10^{-3}$ m^{-1} approximates a constant gradient $dc/dz \simeq 1$ sec^{-1}, provided that z - H remains considerably smaller than $1/\beta$. Equation 16 must be treated with caution, for, at $(z-H) = 1/\beta$, c(z) becomes infinite and for greater z, imaginary. For the present we assume that a satisfactory $\zeta_n + h_n$ lies well above $z - H = 1/\beta$. k_w^2 in Eq. 16 could realistically be replaced by a value a few percent different, but this complicates the analysis without adding to the illustrative effect.

In the water column, Z_n is still given by Eq. 8 with x_n as in Eq. 7. For $z > H$, we substitute Eq. 16 in Eq. 2, and change variable from z to y_n:

$$y_n = -M^{-2/3}[k_w^2 - k_n^2 - M(z-H)], \quad z \geq H \quad ; \tag{17}$$

$$M = k_w^2 \beta \quad . \tag{18}$$

Equation 2 takes the form

$$d^2Z_n/dy_n^2 - y_n Z_n = 0 \quad , \tag{19}$$

which has as independent solutions the Airy functions[5], $Ai(y_n)$ and $Bi(y_n)$.

Since $k_n^2 < k_w^2$ always, y_n is negative at $z = H$ and for some distance below; y_n vanishes at $z = \zeta_n$ and is positive at all greater depths:

$$\zeta_n - H = M^{-1}(k_w^2 - k_n^2) = (MH^2)^{-1} x_n^2 \quad . \tag{20}$$

The proper solution of Eq. 19 is $Ai(y_n)$. This function[5] oscillates for $y_n < 0$ and falls monotonically toward zero as $+y_n \to \infty$ and therefore as $z \to \infty$. Hence the depth ζ_n given by Eq. 20 agrees with its definition in Sec. I. Also, $Ai(y_n)$ is continuous with continuous derivative dAi/dz, thereby satisfying the acoustic conditions at $z = \zeta_n$ (where δ is unity). Since Eq. 3 is automatically satisfied in this example, we find the eigenvalue equation by applying the acoustic conditions at $z = H$, not at ζ_n. The result is

$$Hx_n^{-1} \tan x_n = \delta M^{-1/3} Ai(-y_H)/Ai'(-y_H) \quad ; \tag{21}$$

$$y_H = |y_n|_{z=H} = M^{-2/3}(k_w^2 - k_n^2) = Bx_n^2 \quad ; \tag{22}$$

$$B = (Mi^3)^{-2/3} \quad . \tag{23}$$

In standard notation, Ai' in Eq. 21 is dAi/dy_n; $M^{1/3}Ai'$ is dAi/dz, which is needed in the acoustic conditions. Evidently, for all $z > H$ both u_n and v_n of Sec. II equal $Ai(y_n)$. The independent solution is $Bi(y_n)$, which oscillates for $z < \zeta_n$ and diverges toward + infinity as $z \to \infty$.

In Sec. III, N and x_N were set by the physical parameters, but that is not so, here. We must establish meaningful values for N and x_N. In particular, they must correspond to an acoustic field restricted to depths z in which Eq. 16 still approximates a constant dc/dz, to agree with geophysical facts. We start by arguing that, given a many-mode field in deep water, at least the lower eigenvalues must approximate those of the Pekeris problem in Sec. III. This is perhaps most easily seen by temporarily setting $\delta = 1$ and applying the WKB method[6]. The Bohr-Sommerfeld integral that establishes k_n^2 is

$$\int_0^{\zeta_n} [k^2(z) - k_n^2]^{1/2} dz = (n - 1/4)\pi; \; n = 1, 2, \ldots . \tag{24}$$

It turns out that $(\zeta_n - H) << H$ for n not too large, and therefore Eq. 24 is little changed by using H for the upper limit, which then gives the WKB solution of the Pekeris problem. It follows from Eqs. 7 and 24 that $x_n \simeq n\pi$. We therefore try $N = H/\lambda_w$, which is approximately true in the Pekeris problem, and $x_N \simeq N\pi$. Equation 20 yields

$$\zeta_N - H \simeq (4\beta)^{-1} \simeq 190 \text{ m} \quad , \tag{25}$$

which when put into Eq. 16 leads to $c(\zeta_N)/c_w \simeq 1.15$--a physically reasonable value and one only 2 or 3% above the linear approximation. This choice of N appears to be quite satisfactory.

The same values, used in Eq. 23, show that $y_H = Bx_N^2 \geq 4.6$ for acoustic frequencies not less than 25 Hz. Consequently, asymptotic forms of the Airy functions[5] can be substituted in Eq. 21, with an error no more than 2 to 3%. The outcome is

$$\tan x_N = -\delta \tan(\psi_N + \pi/4); \quad \psi_N = 2(Bx_N^2)^{3/2}/3 \quad . \tag{26}$$

Seeking an approximate solution of Eq. 26, we write

$$x_N = n_1\pi - \varepsilon; \quad \tan x_N = -\tan \varepsilon \quad , \tag{27}$$

with $0 < \varepsilon < \pi$ and n_1 an integer ($n_1 \leq N$). Although ε's of 0, $\pi/2$, or π might satisfy the eigenvalue equation, these exact values are highly unlikely, because any one of them would require a precise combination of several physical parameters.

Approximate solutions of Eqs. 26, 27 are fairly easily derived for ε near 0, $\pi/4$, $\pi/2$, $3\pi/4$, or π. We indicate the procedure for $\varepsilon^2 << \pi^2/4$, the most plausible surmise when $(\zeta_n - H) << H$, and state results for the other special cases. After $\tan x_N$ in Eq. 26 is approximated by $-\varepsilon$, ψ_N can be found:

$$\psi_N \simeq (n_2 - 1/4)\,\pi + \varepsilon/\delta \simeq (n_2 - 1/4)\,\pi\,[1 + \frac{\varepsilon}{\delta(n_2 - 1/4)\pi}], \; n_2 = 1,2\ldots \; . \tag{28}$$

From Eqs. 26 and 28, we calculate x_N, using the binomial theorem for powers of [ ]:

$$x_N \simeq B^{-1/2}[(3\pi/2)(n_2 - 1/4)]^{1/3}\,[1 + \frac{\varepsilon}{3\delta(n_2 - 1/4)\pi}] \quad . \tag{29}$$

With the pressure-release plane inserted at $z = \zeta_N + h_N$, δ in Eq. 29 is to be replaced by $\delta[\ldots]_H$, as in Eq. 6 (except that H now replaces ζ_N).

In [...], W is π^{-1}; $v_N v_N'$ is $(AiAi')_{II}$, and asymptotic forms[5] can be used as they were to obtain Eq. 26. The result is that $(1/\delta)$ in Eq. 29 is to be multiplied by $[1 - 2\eta \csc(2\psi_N + \pi/2)]$, which (from Eq. 28) is $(1 - \eta\delta/\epsilon)$. Comparison of this result with Eq. 29 leads to

$$\Delta x_N \simeq B^{-1/2}[(3\pi/2)(n_2 - 1/4)])^{1/3}[(\eta/3\pi)/(n_2 - 1/4)]$$

$$\simeq \eta\, x_N/[3\pi(n_2 - 1/4)] \quad . \tag{30}$$

Then with $\Delta_N = \Delta(x_N^2)/x_N^2$ we have

$$\Delta_N \simeq 2\eta/[3\pi(n_2 - 1/4)] \leq 0.1\,\eta \quad ; \tag{31}$$

the inequality holds because $n_2 \geq 2$ for $f \geq 25$ Hz, as is found by calculating Bx_N^2. The same result, $\Delta_N \leq 0.1\eta$, also holds for ϵ near π, ϵ near $\pi/2$, $|\epsilon - \pi/4| \leq 0.25$ and $|\epsilon - 3\pi/4| \leq 0.25$. These approximations cover much of the range of ϵ, and there is no reason to expect markedly different results for any other value of ϵ.

Equation 4, with Ai and Bi for v and w, and with asymptotic values of the Airy functions, gives

$$\eta = -1/2 \exp(-4\, y_h^{3/2}/3) \quad ; \tag{32}$$

y_h is y_N at $z = \zeta_N + h_N$, which from Eqs. 17 and 20 means that $y_h = M^{1/3}h_N$. Using M from Eq. 18, we obtain

$$h_N/\lambda_w \simeq 2.7\, y_h\, \lambda_w^{-1/3} \ (\lambda \text{ in meters}) \quad . \tag{33}$$

With Δ_N taken as 0.1η and with the numerical values of Δ_N prescribed in Section III, we find at f = 25 Hz the combinations $(10^{-4}, 1.9)$, $(10^{-5}, 2.4)$, $(10^{-6}, 2.8)$. The second entry in each parenthesis is h_N/λ_w; this quantity increase slowly with frequency, as $f^{1/3}$. Comparison with tabulated

values[5] shows that even for the smallest y_h encountered here (about 2.8) the asymptotic form of Ai/Bi used to obtain Eq. 32 is in error by less than 5%, a completely negligible discrepancy in view of our various approximations.

Two points of difference from Example A must be kept in mind. First, in this example we have defined N, the number of the highest mode to be considered, as $N = H/\lambda_w$--a reasonable but not inevitable choice. Second, h_N is measured down from depth ζ_N, not H. Equation 25 shows that the top of the "hidden depths" lies below the bottom interface by a distance Δz:

$$\Delta z = z - H \simeq 190 \text{ m} + h_N \quad . \tag{34}$$

At 25 Hz, for example, Δz is 5 or 6 times λ_w, with the numerical values of $|\Delta_N|$ used as illustrations. At higher frequencies, $\Delta z/\lambda_w$ of course increases, but Δz itself decreases toward about 190 m; i.e., toward $\zeta_N - H$.

V. Effect of including absorption

At the low frequencies emphasized here, and even at much higher frequencies, absorption in the water column is too small to affect our discussion. In this same low-frequency range, however, absorption coefficients in unconsolidated bottom materials are much larger, and it appears that they increase approximately as the first power of the frequency. Hence their possible effects should be considered. Sections I and II remain essentially unchanged, except for the fact that bottom absorption leads to complex eigenvalues.

Returning to Eq. 7, we treat k_w as real and incorporate bottom absorption in Example A by writing

$$k_b = k_{br} + i\alpha_b ; \; \alpha_b^2 << k_{br}^2 \quad . \tag{35}$$

The inequality is justified by experimental results. Kornhauser and Raney[7] have analyzed the consequences; k_n must also be complex:

$$k_n = k_{nr} + i\alpha_n ; \; \alpha_n^2 << k_{nr}^2 \quad . \tag{36}$$

Except very near cut-off, α_n is much smaller[7] than α_b. Using Eqs. 35 and 36 in Eq. 2, with $k^2(z) = k_b^2$ in the bottom, we find $v_n(z)$:

$$v_n(z) \approx \exp[-(k_{nr}^2 - k_{br}^2)^{1/2} (z - H)]$$

$$\times \exp[-i \frac{(k_{nr}\alpha_n - k_{br}\alpha_b)}{(k_{nr}^2 - k_{br}^2)^{1/2}} (z - H)] \quad . \tag{37}$$

$w_n(z)$ has the same form, but with positive exponentials (see Eq. 9). It is always true that $k_w > k_{nr} > k_{br}$; also, k_w rarely exceeds k_{br} by more than, say, 20%, but α_b exceeds α_n by a much greater amount. Examination of the complex exponential term in Eq. 37 shows that it has a positive argument for $z > H$. That is, Eq. 37 represents an exponentially damped progressive wave, directed downward; the presence of bottom absorption has destroyed total reflection at the bottom interface. In contrast, w_n represents a progressive wave directed upward, its amplitude diverging exponentially as $z \to \infty$.

Use of these expressions for v_N and w_N, with the help of Eqs. 4 and 7, shows that η still has the magnitude indicated in Eq. 11 (except that the real parts of x_c and x_N are to be used). The only change is that η now has a phase factor of unit magnitude. The remainder of Sec. III can be repeated, with only the real parts of all complex quantities--including the new η--and no appreciable change in h_N/λ_w is to be expected.

It may be surprising to see no absorption of the downgoing wave, but this results from our neglect of quadratic terms in α_n and α_b. The vertical attenuation of v_n, shown in Eqs. 9 and 37, will ordinarily far exceed true absorptive effects. The main influence of α_b is, via α_n, an attenuation of each mode in the factors $\exp(ik_n r)$ of Eq. 1.

Example B(Sec. IV) yields a similar result. We replace the real k_w in Eq. 16 by $k_{br} + i\alpha_b$, with $k_{br} \approx k_w$ and $\alpha_b^2 << k_{br}^2$; y_n of Eq. 17 becomes complex. The Airy functions $Ai(y_n)$ and $Bi(y_n)$ continue to be solutions[5] of Eq. 2 after $k^2(z)$ and k_n^2 become complex. Also, the asymptotic expressions for the Airy functions remain unchanged when y_n is complex. Therefore η is still given by Eq. 32, although now y_h is complex with an unaltered real part and an imaginary part related to α_b and α_n. The outcome is the same as in Example A: η is practically unchanged in magnitude but acquires a phase that depends on h_N.

For z sufficiently exceeding ζ_n, it is readily shown from the asymptotic expressions used to obtain complex η that Ai represents a rapidly damped wave progressing downward, whereas Bi corresponds to a wave progressing upward but with an amplitude that diverges as $z \to \infty$.

VI. Summary

A method has been presented for naming a depth, in the water or the bottom material, below which physical parameters need not be known because they would have negligible effects upon the normal-mode expressions for underwater-sound propagation. "Negligible effect" is defined by specifying the

maximum acceptable values of the fractional errors in mode eigenvalues. Provided that the near field is not considered, the calculation need be made only for the highest discrete mode or, in some cases, perhaps for a single lower mode.

Two illustrative examples have been analyzed. Each assumed isovelocity water; in one example the bottom was isovelocity, and in the other it had a positive gradient of sound speed. For several acceptable errors, the pertinent depths were calculated, in acoustic wavelengths, below the turning point of the mode eigenfunction. Only many-mode cases, at low frequencies in deep water, were treated, although the general method is not thus restricted. The effects of bottom absorption were also considered and were found to be quite small, in both examples.

Acknowledgement

This work was supported by Naval Electronic Systems Command, Department of the Navy, Washington, D. C., under Contract N00039-75-C-0171.

List of Footnotes

*Permanent address: Brown University, Providence, Rhode Island 02912.

1. C. L. Pekeris, Geol. Soc. Am., Mem. 27 (1948).

2. A. O. Williams, Jr., J. Acoust. Soc. Am. 32, 363-371 (1960).

3. Reference 2, Appendix.

4. Reference 2, Sec. VI.

5. M. Abramowitz and I. Stegun, Eds., Handbook of Mathematical Functions (National Bureau of Standards, Washington, D. C., 1965), pp. 446-478.

6. L. I. Schiff, Quantum Mechanics (McGraw-Hill, New York, 1955), 2nd ed., pp. 184-193.

7. E. T. Kornhauser and W. P. Raney, J. Acoust. Soc. Am. 27, 689-692 (1955).

APPENDIX D

A FORMAL SOLUTION TO THE PROBLEM OF WAVE PROPAGATION IN A HALF SPACE OF TWO FLUID MEDIA SEPARATED BY AN INCLINED PLANE

by*

C. W. Horton, Sr.

I. INTRODUCTION

In the case of constant sound speed, the wave equation is of course separable in a multitude of coordinate systems. Of these, only the wedge seems to offer promise of immediate applicability to relevant propagation problems. It is well known that the wedge problem with perfectly reflecting boundaries is exactly solvable in terms of Bessel functions. However, in the case of one wedge boundary separating two fluids (i.e., the bottom-water interface) the problem has never been solved. This appendix outlines a formal solution to this rather practical problem and suggests a method for carrying the calculation forward toward a specific numerical evaluation.

Before dealing with the two-fluid problem, it will be useful to briefly review the simpler case of a single fluid medium. We suppose a wedge geometry in which, for the present, the pressure is assumed to vanish on the plane $\varphi=\alpha$ as well as on the boundary $\varphi=0$. The coordinate system is cylindrical with the z-axis normal to the plane of the figure. The wave

$$\left[\frac{1}{r}\frac{\partial}{\partial r}\left(r\frac{\partial}{\partial r}\right) + \frac{1}{r^2}\frac{\partial^2}{\partial \varphi^2} + \frac{\partial^2}{\partial z^2} + k^2\right] p = 0 \quad ,$$

*This appendix is based on an informal report by C. W. Horton, Sr., to which the present authors added a brief introduction.

is separated in all three coordinates by the solution

$$p = R(r)\ \sin(\alpha_n \theta)\ e^{ik_z z} \quad ,$$

where $\alpha_n = n\pi/\alpha$ and $R(r)$ satisfies the equation

$$\left[\frac{1}{r}\frac{d}{dr}\left(r\frac{d}{dr}\right) + k^2 - k_z^2 - \frac{\alpha_n^2}{r^2}\right] R(r) = 0 \quad ,$$

which is just Bessel's equation. In the case that the source is located at $(r_o, \theta_o, 0)$, the Green function is given by

$$G = \frac{1}{2i\alpha} \sum_{n=0}^{\infty} \left\{ \sin(\alpha_n \theta)\ \sin(\alpha_n \theta_n) \int_{-\infty}^{\infty} dk_z \right.$$

$$\left. \left[J_{\alpha_n}(k_x r_<)\ H^{(1)}_{\alpha_n}(k_x r_>)\ e^{ik_z z} \right] \right\} \quad ,$$

where $k_x^2 = k^2 - K_z^2$ and $r_{\lessgtr} = \left\{ \begin{matrix} \max \\ \min \end{matrix} \right\} r_1 r_o$. This solution was obtained, and is discussed in detail, by Bradley and Hudiman.[1]

The much more interesting and potentially useful problem defined by imposing an impedance condition, $p + \gamma(\partial p)/\partial n = 0$, on one or both wedge boundaries, has never been considered in detail with reference to underwater acoustic applications. The theory of this problem, as well as related integration techniques, is discussed by Felsen and Marcuvitz,[2] Ch. 6. As before, such a boundary condition defines a problem midway between the case of perfectly reflecting boundaries and the two-fluid problem. It would seem desirable to explore this problem thoroughly with view to the application to practical propagation problems.

Recently a different attack on wedge problems has been proposed by Uberall and co-workers, see for example, Graves, Nagle, Uberall, and Zarur.[3] These authors consider a mode-mode coupling approach where the unperturbed problem is taken to be the rectangular ocean. Only perfectly reflecting boundaries were considered by these authors.

With these background comments in mind, a method for treating the two-fluid wedge problem will be outlined.

II. THE TWO-FLUID WEDGE PROBLEM

Suppose fluids 1 and 2 are located in the wedges $0 \leq \varphi \leq \alpha$ and $\alpha \leq \varphi \leq \pi$, respectively. The plane surface $\varphi = (0, \pi)$ is a pressure release surface. We wish to write down an expression for waves whose periodic source is at the origin and which satisfies the boundary conditions at $\varphi = \{0, \alpha, \pi\}$ and also the Sommerfeld radiation condition at infinity. Presumably the solution to this problem will be sums or integrals over ν of expressions such as

$$\text{Medium No. 1.} \qquad \sin \nu\varphi H_\nu^{(1)}(k_1 r) \quad , \tag{1}$$

$$\text{Medium No. 2.} \qquad \sin \mu(\pi-\varphi)\, H_\mu^{(1)}(k_2 r) \quad . \tag{2}$$

It is clear that the basic problem is the matching of the Hankel functions along the ray $\varphi = \alpha$. It was thought that a viable technique could be obtained by using "multiplication theorem" from Erdeli, Vol. II, p. 66, which states

$$J_\nu(\lambda z) = \lambda^\nu \sum_{n=0}^{\infty} \left[\frac{z(1-\lambda^2)}{2}\right]^n J_{\nu+n}(z)\, \frac{1}{n!} \quad .$$

Unfortunately, when applied to Hankel functions there is no obvious way to proceed.

S. Banerji[5] proposes a similar problem for the wedge and suggests, in effect, expanding $H_\nu^{(1)}(k_2 r)$ in a Taylor series in (k_2-k_1). He does not carry out this idea, and it does not seem promising since the nth term in the Taylor's series is proportional to $r^n H_\nu^{(1)}(k_1 r)$.

There is a more recent report by Karp and Sollfrey[6] who solve a similar problem by using a perturbation theory expressed as a power series in a parameter p defined as $p=k_2^2-k_1^2$. Now, for the ocean bottom a normalized value of p will be near 0.4, so that 4 terms in the expansion will be necessary for 2% accuracy. Nevertheless, their method will be pursued in some detail.

Suppose we modify the wedge geometry by indenting the vacuum surface $\varphi=(0,\pi)$ into a semicircle of radius a (to be determined later). In expressions 1 and 2 select only those values of ν and μ such that $H_\nu^{(1)}(k_1 a)=0$ and $H_\mu^{(1)}(k_2 a)=0$. There is a countably infinite set of these values.

Each of these sets is complete and orthogonal in the sense that

$$\int_a^\infty dr\, r^{-1} H_{\nu_i}^{(1)}(k_1 r)\, H_{\nu_j}^{(1)}(k_1 r) = N_i\, \delta_{ij} \quad , \tag{3}$$

$$\int_a^\infty dr\, r^{-1} H_{\mu_i}^{(1)}(k_2 r)\, H_{\nu_j}^{(1)}(k_2 r) = M_i\, \delta_{ij} \quad . \tag{4}$$

See the paper by Cohen[7] for an extensive discussion of the completeness of these functions and of the convergences of expansions in terms of these functions.

Thus any function $H_{\mu_i}^{(1)}(k_2 r)$ in the second medium can be expressed as a linear sum of functions $H_{\nu_i}^{(1)}(k_1 r)$ suitable for the first medium, and vice versa.

The difficulty with this suggestion is that a large number of integrals of the form

$$\int_a^\infty dr\, r^{-1} H_{\nu_i}(k_1 r)\, H_{\mu_j}^{(1)}(k_2 r) \tag{5}$$

must be evaluated to give the coefficients of matrices that must be inverted. It does not seem that a closed expression for this integral exists. This is, of course, a computational difficulty only, though a serious one.

Now suppose that over the surface

$$r = a \quad , \quad 0 \leq \varphi \leq \alpha \quad , \tag{6}$$

there is a simple source

$$p = p_o \sin \nu\varphi\, H_\nu^{(1)}(k_1 a)\, e^{-i\omega t} \quad . \tag{7}$$

Then we can find two sets of coefficients $\{A_i\}$ and $\{B_j\}$ so that the pressure fields in media 1 and 2 (omitting $e^{-i\omega t}$) are

$$p_1 = p_o \sin(\nu\varphi)\, H_\nu^{(1)}(b,r) + \sum_{i-1}^{\infty} A_i \sin(\nu_i\varphi)\, H_{\nu_i}^{(1)}(k_1 r) \tag{8}$$

$$p_2 = \sum_{j=1}^{\infty} B_j \sin(\mu_j\varphi)\, H_{\mu_j}(\lambda_2 r) \quad , \tag{9}$$

respectively, and such that

$$\left.\begin{aligned} p_1 &= p_2 \\ \rho_1^{-1}\frac{\partial p_1}{\partial \varphi} &= \rho_2^{-1}\frac{\partial p_2}{\partial \varphi} \end{aligned}\right\} \text{on} \quad \varphi = \alpha \qquad (10), (11)$$

where ρ_1, ρ_2 are the densities of the media.

The coefficients of the two expansions can be determined as follows. Substitute Eqs. (8-9) into Eq. (10), multiply by $(1/r)H_{\nu_\rho}^{(1)}(k_1 r)$, and integrate from a to ∞. This gives

$$p_o \sin(\nu\alpha) \int_a^\infty dr\, r^{-1} H_\nu(k_1 r)\, H_{\nu_p}^{(1)}(k_1 r) + A_p N_p \sin(\nu_p \alpha) \qquad (12)$$

$$= \sum_{j=1}^{\infty} \sin\left[\mu_1(\pi-\alpha)\right] C_{pj} B_j$$

where

$$C_{pj} = \int_a^\infty dr\, r^{-1} H_{\nu_p}^{(1)}(k_1 r)\, H_{\mu_j}^{(1)}(k_2 r) \quad . \qquad (13)$$

N_p is defined in Eq. (3) above.

Equation 11 can be treated in a similar way to give a second equation for A_p. When A_p is eliminated from these two equations, we get one infinite set of inhomogeneous equations for the sequence of unknown coefficients $\{B_j\}$. This analysis is entirely formal and questions of the existence of solutions to the infinite set of equations must be answered, questions of the convergence of the series 8 and 9 must be answered, and a tremendous amount of numerical work must be done. Finally, there is a question about the significance of the size of a, which is so far arbitrary.

The entire analysis can be repeated using instead of the ν_i and μ_i defined above the different set given by roots of

$$\frac{\partial}{\partial r} H_\nu^{(1)}(k_1 r)\Big|_{r=a} = 0 \quad .$$

Further progress in the direction outlined here will depend upon obtaining a useful evaluation of the integral in Eq. 13. Possibly, depending on the size of $k_1 a$ and $k_2 a$, an asymptotic evaluation would be adequate. Alternatively, a direct numerical evaluation, though cumbersome, might be a viable method.

REFERENCES

1. Bradley, D., and A. A. Hudmac, "The Propagation of Sound in a Wedge Shaped Shallow Water Duct," Naval Ordnance Laboratory Report NOLTR 70-235, NOL, 1970.

2. Felsen, L. B., and N. Marcuvitz, Radiation and Scattering of Waves (Prentice-Hall, Englewood Cliffs, New Jersey, 1973).

3. Graves, R. D., A. Nagle, H. Uberall, and G. L. Zarur, "Range Dependent Normal Modes in Underwater Sound Propagation: Application to the Wedge-Shaped Ocean," J. Acoust. Soc. Am. 58, 1171-1177 (1975).

4. A. Erdelyi, Higher Transcendental Functions (McGraw-Hill Book Company, New York, 1953).

5. S. Banerji, "On the diffraction of light by a transparent wedge," Calcutta Math. Soc. Bull. 10, 199-206 (1919).

6. S. Karp, and W. Sollfrey, "Diffraction by a dielectric wedge with application to propagation through a cold front," New York University Mathematics Research Group, Research Report No. EM-23, October 1950.

7. D. S. Cohen, "Eigenfunction expansions and non-selfadjoint boundary value problems," Commun. on Pure and Appl. Math. 17, 23-34, (1964).

APPENDIX E

PARAMETERS OF RAYS IN A SEDIMENT LAYER

Several ray parameters are often useful for diagnostic purposes in examining the results of calculations such as the reflection coefficient of the ocean bottom. For example, for a ray penetrating into the bottom, if the sediment sound speed is described by a positive linear gradient of sound speed with depth, the parameters of interest include: (1) the depth of penetration of the ray below the water sediment interface (turnaround depth), (2) the length of the arc of the ray in the sediment, (3) the horizontal displacement of the ray at the water sediment interface (horizontal distance between the point of ray penetration into the bottom and the point where the ray reemerges into the water), and (4) the time the ray spends in the sediment.

Results of calculations of these parameters are shown in Figs. E1 through E5. For these figures, the sound speed versus depth z_s below the water sediment interface is described by the expression

$$c(z_s) = c_s + gz_s \quad ,$$

where c_s = the sound speed in the sediment just below the water sediment interface and g is the constant gradient of sound speed with depth. The grazing angle specified in the figures is the angle in the water between the ray and the water-sediment interface. In Fig. E1, the ray penetration depth is shown versus grazing angle for several realistic values of g for the situation where sound speed at the top of the sediment column is equal to sound speed in the overlying water. For the remaining figures (E2 to E4) the ray parameters are shown for several values of the ratio of sound speed at the top of the sediment to that of the overlying water (c_s/c_w), but always for a gradient of one (g=1).

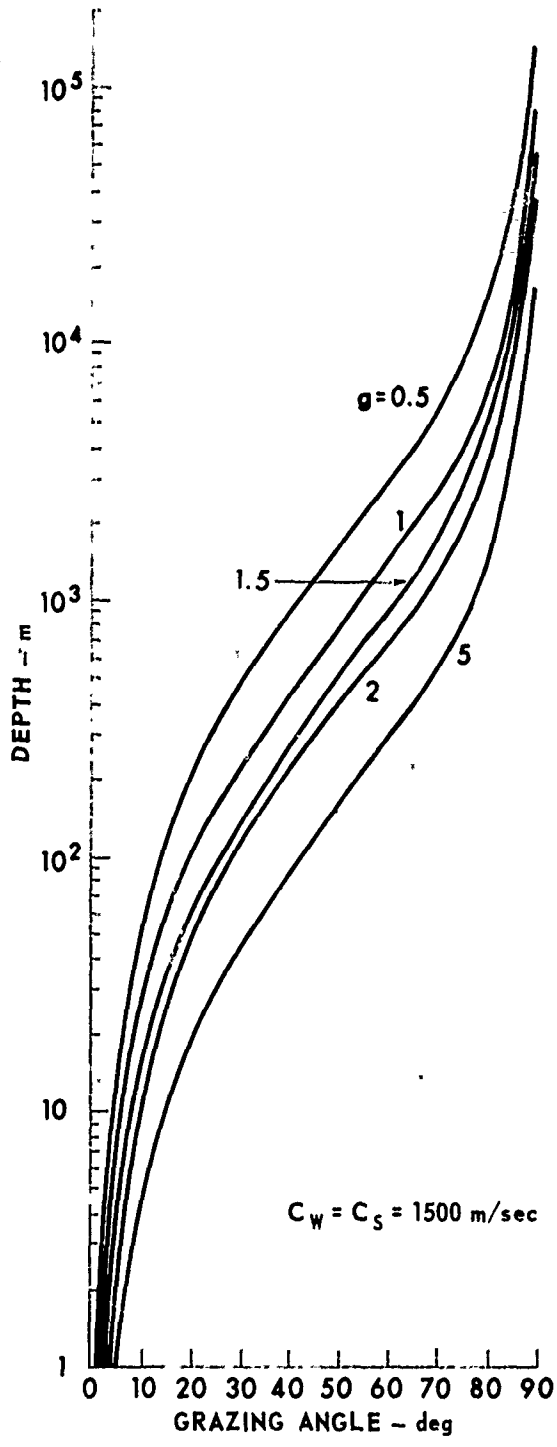

FIGURE E 1
PENETRATION DEPTH VERSUS GRAZING ANGLE
AS A FUNCTION OF THE GRADIENT

ARL - UT
AS-76-174
ALA - DR
2 - 20 - 76

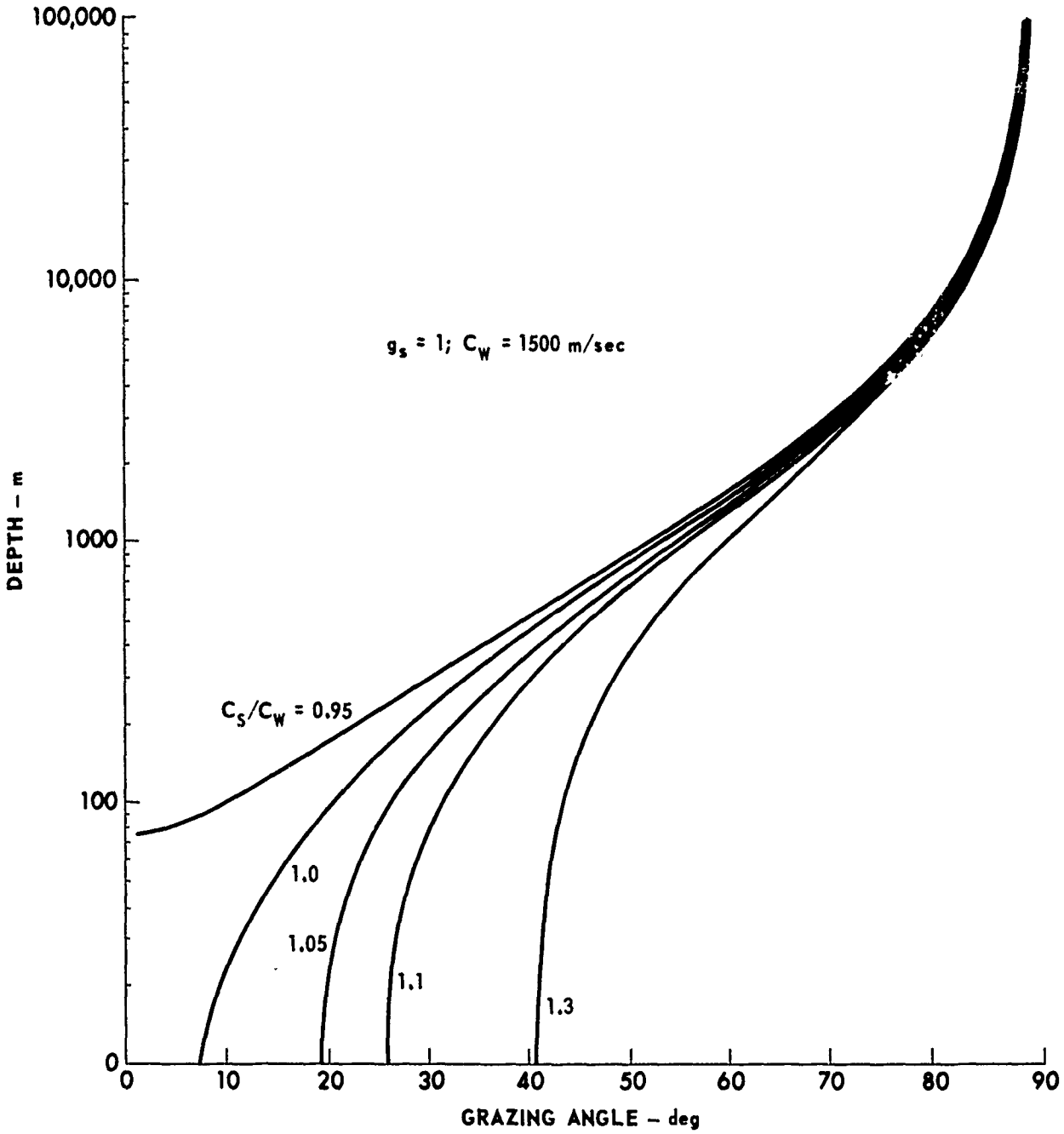

FIGURE E2
PENETRATION DEPTH VERSUS GRAZING ANGLE AS A FUNCTION OF C_S/C_W

ARL - UT
AS-76-177
ALA - DR
2 - 20 - 76

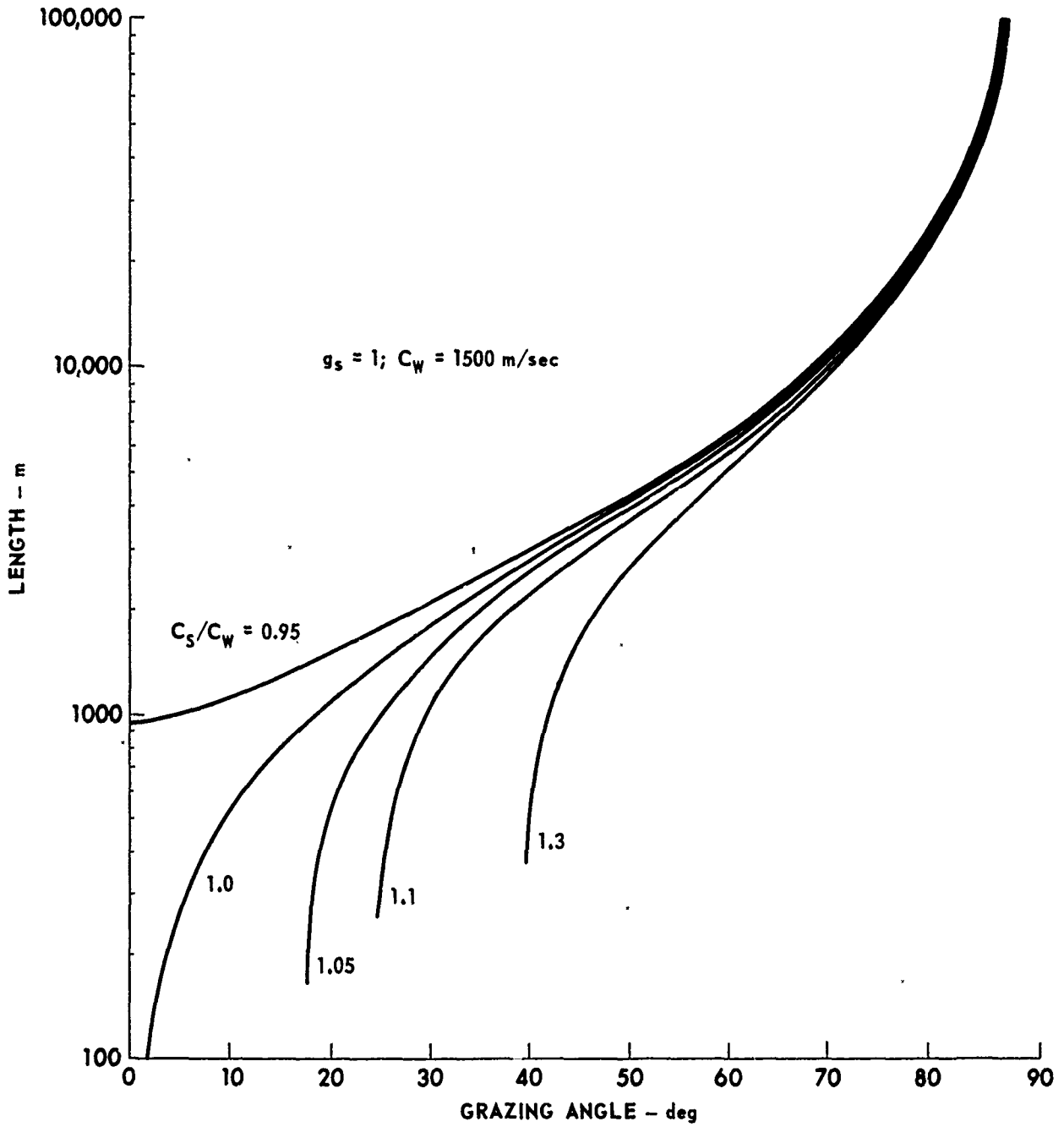

FIGURE E3
LENGTH OF ARC VERSUS GRAZING ANGLE AS A FUNCTION OF C_S/C_W

ARL - UT
AS-76-175
ALA - DR
2 - 20 - 76

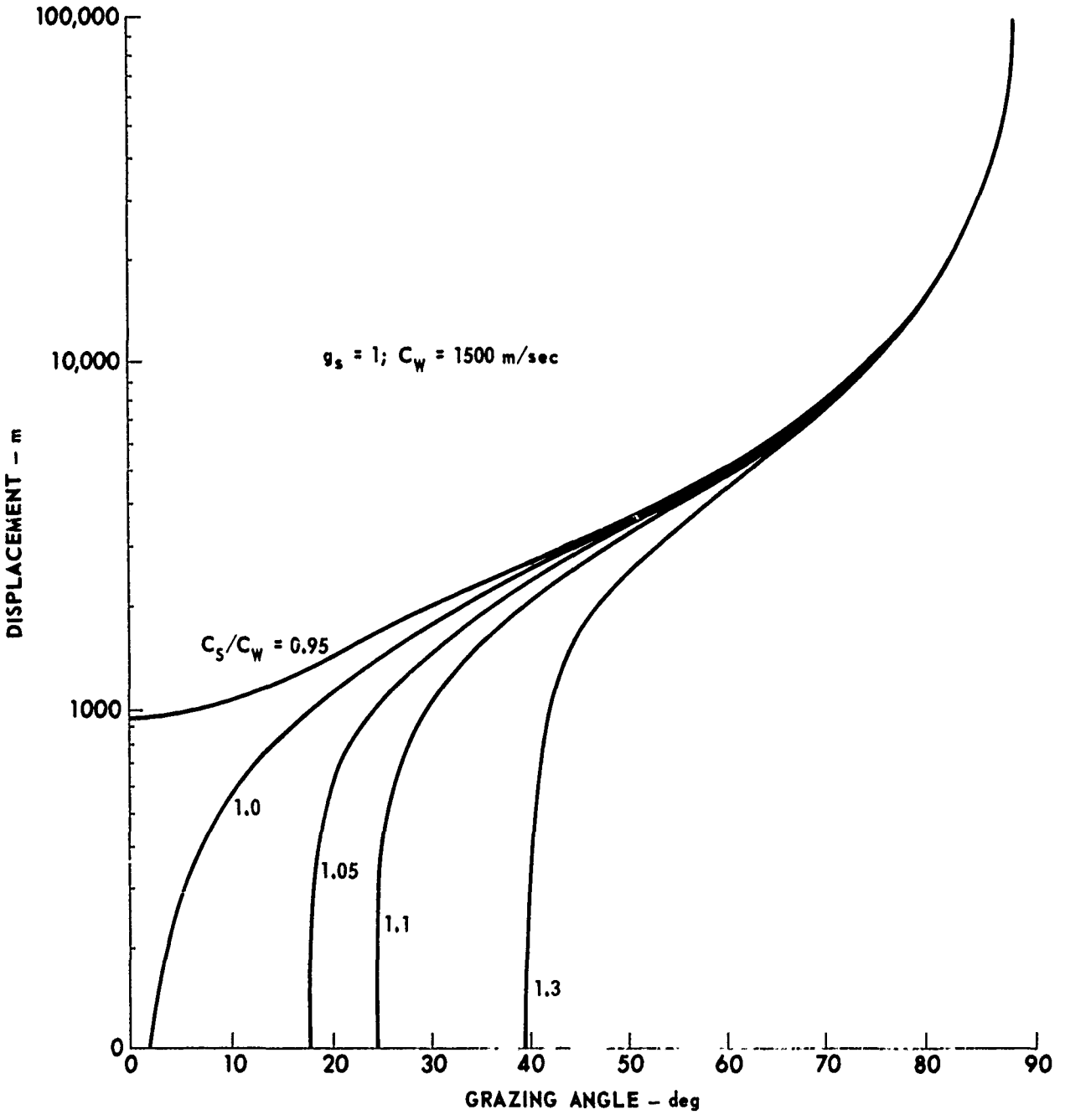

FIGURE E 4
HORIZONTAL RAY DISPLACEMENT VERSUS GRAZING ANGLE
AS A FUNCTION OF C_S/C_W

ARL - UT
AS-76-176
ALA - DR
2 - 20 - 76

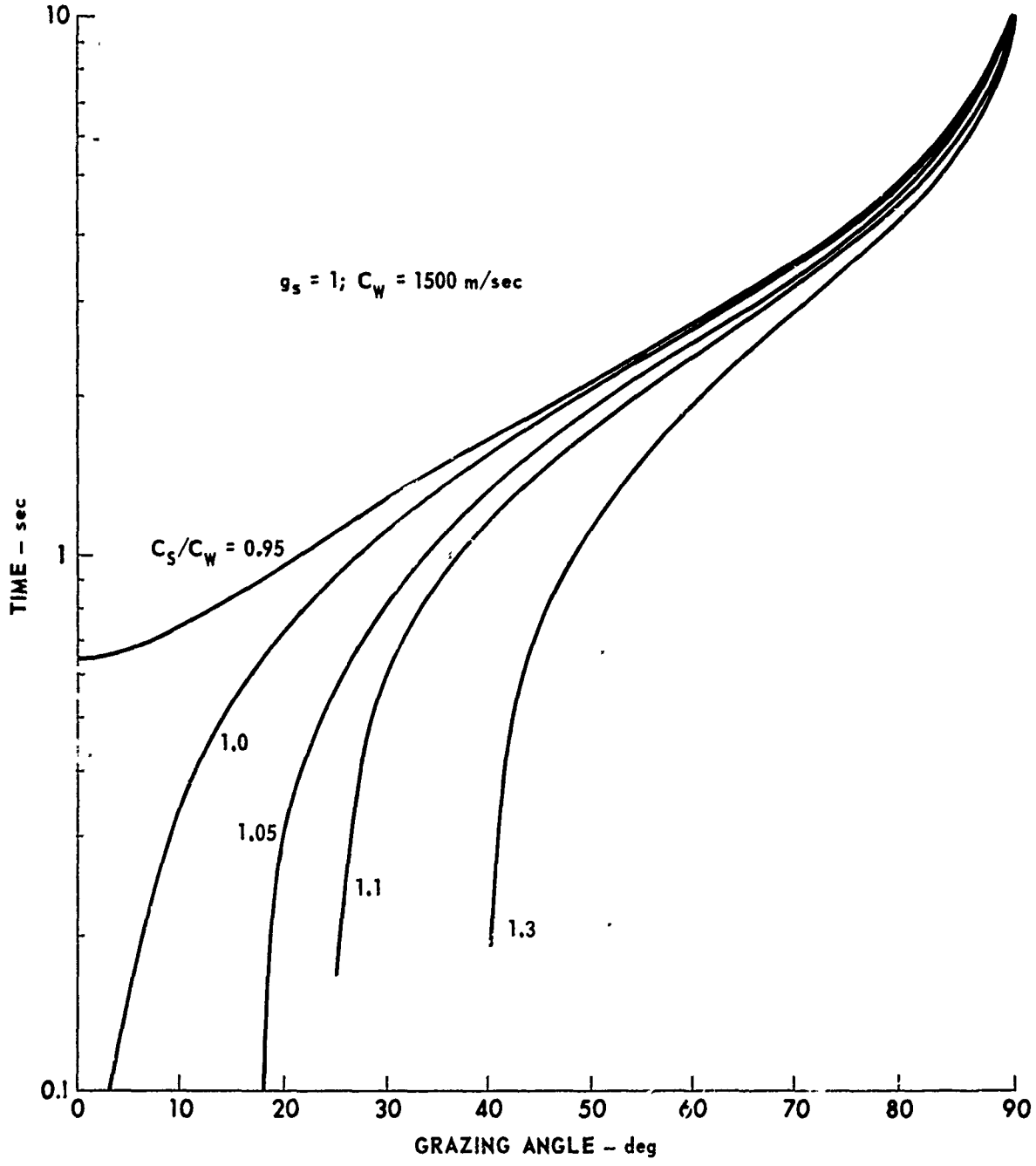

FIGURE E5
TRANSIT TIME VERSUS GRAZING ANGLE AS A FUNCTION OF C_S/C_W

ARL - UT
AS-76-178
ALA - DR
2 - 20 - 76

6 April 1976

DISTRIBUTION LIST FOR
ARL-TR-76-14
FINAL REPORT UNDER CONTRACT N00039-75-C-0171
1 December 1974 - 30 November 1975

Copy No.	
1 - 5	Commanding Officer Naval Electronic Systems Command Department of the Navy Washington, D. C. 20362
6	Commander Naval Sea Systems Command Department of the Navy Washington, D. C. 20362 Attn: Mr. A. P. Franceschetti
	Commander Naval Oceanographic Research and Development Activity Department of the Navy Washington, D. C. 20362
7	Attn: CDR E. T. Young (Code 32) Numerical Modeling Division
8	Dr. Roy Gaul (Code 22)
9	Code 34
10	Code 36
	Commanding Officer Office of Naval Research Department of the Navy Ballston Tower No. 1 800 N. Quincy Street Arlington, VA 22217
11	Attn: Dr. A. Malahoff (Code 480)
12	Dr. H. Bezdek
13	Commanding Officer Office of Naval Research Arlington, VA 22217 Attn: Dr. J. B. Hersey (Code 102-OS)
	Commander Naval Undersea Center Department of the Navy San Diego, CA 92132
14	Attn: Mr. M. A. Pedersen (Code 307)
15	Dr. R. R. Gardner
16	Dr. Ed Hamilton
17	Dr. Homer P. Bucker (Code 409)

Distribution List for ARL-TR-76-14 under Contr N00039-75-C-0171 (Cont'd)

Copy No.

Director
Naval Research Laboratory
Department of the Navy
Washington, DC 20375
18 Attn: Mr. B. G. Hurdle
19 Mr. R. H. Ferris

Naval Oceanographic Office
Department of the Navy
Washington, DC 02373
20 Attn: Mr. W. H. Geddes
21 Mr. K. V. Mackenzie

22 Commanding Officer
Naval Ocean Research and Development Activity
Liaison Office
Arlington, VA 22217
Attn: Mr. R. S. Winoker

Commander
Naval Air Development Center
Department of the Navy
Warminster, PA 18974
23 Attn: M. Bartberger
24 P. Haas

Commander
Naval Underwater Systems Center
New London Laboratory
Department of the Navy
New London, CT 06320
25 Attn: F. R. DiNapoli
26 S. R. Santaniello
27 R. L. Deavenport

28 Commanding Officer
Naval Coastal Systems Laboratory
Panama City, FL 32401
Attn: Dr. E. G. McLeroy, Jr.

29 - 30 Superintendent
Naval Postgraduate School
Monterey, CA 93940

Distribution List for ARL-TR-76-14 under Contr N00039-75-C-0171 (Cont'd)

Copy No.

Woods Hole Oceanographic Institution
Woods Hole, MA 02543
31 Attn: Dr. John Ewing
32 Dr. Earl E. Hays

33 Mar Associates, Inc.
1335 Rockville Pike
Rockville, MD 20852
Attn: Dr. Morris Schulkin

34 Bolt Beranek and Newman, Inc.
50 Moulton Street
Cambridge, MA 02138
Attn: Mr. Preston W. Smith, Jr.

35 Science Applications, Inc.
1651 Old Meadow Road
McLean, VA 22101
Attn: Dr. John Hanna

36 Applied Research Laboratory
Pennsylvania State University
P. O. Box 30
State College, PA 16801
Attn: Dr. D. C. Stickler

37 Underwater Systems, Inc.
3121 Georgia Avenue
Silver Spring, MD 20910
Attn: Dr. Marvin S. Weinstein

38 Geophysics Laboratory
Marine Science Institute
The University of Texas
700 The Strand
Galveston, TX 77550
Attn: Dr. J. L. Worzel, Director

39 TRACOR, Inc.
1601 Research Boulevard
Rockville, MD 20850
Attn: Dr. R. J. Urick

40 The Catholic University of America
6220 Michigan Avenue, NE
Washington, DC 20017
Attn: Dr. H. M. Uberall

Distribution List for ARL-TR-76-14 under Contr N00039-75-C-0171 (Cont'd)

Copy No.

41	Lamont-Doherty Geological Observatory Palisades, NY 10964 Attn: Mr. Henry R. Kutschale Mr. John E. Nafe
42 - 53	Commanding Officer and Director Defense Documentation Center Defense Services Administration Cameron Station, Building 5 5010 Duke Street Alexandria, VA 22314
54	Office of Naval Research Resident Representative Room 582, Federal Building Austin, TX 78701
55	Computer Sciences Division, ARL/UT
56	Marine Sciences Division, ARL/UT
57	Aubrey L. Anderson, ARL/UT
58	Glen E. Ellis, ARL/UT
59	Karl C. Focke, ARL/UT
60	Terry L. Foreman, ARL/UT
61	Kenneth E. Hawker, ARL/UT
62	Loyd D. Hampton, ARL/UT
63	Stephen K. Mitchell, ARL/UT
64	Reuben H. Wallace, ARL/UT
65	Library, ARL/UT
66 - 90	ARL/UT Reserve